

*Critical evaluation of isolation and
characterization techniques of breast
cancer exosomes*

Frøydis Sved Skottvoll



Thesis for the Master's degree in chemistry

60 ECTS credits

Department of Chemistry

Faculty of Mathematics and Natural Sciences

UNIVERSITY OF OSLO

22.05.2017

**Critical evaluation of isolation and
characterization techniques of breast
cancer exosomes**

Copyright Frøydis Sved Skottvoll

2017

Critical evaluation of isolation and characterization techniques of breast cancer exosomes

Frøydis Sved Skottvoll

<http://www.duo.uio.no>

Trykk: Reprosentralen, Universitetet i Oslo

Abstract

Exosomes represent a distinct class of extracellular vesicles of endocytic origin secreted by multiple cell types, including tumour cells. An increased release of exosomes, which appears to be a rich source of biomarkers, has been reported from tumour cells. However, current strategies concerning the isolation (and characterization) of exosomes from fluids differ significantly and no consensus method is established.

The goal of this work was to evaluate two different exosome isolation methods with two different breast cancer cell lines in culture: differential ultracentrifugation and commercial isolation kit. Evaluation was done using a bicinchoninic acid assay (protein concentration), transmission electron microscopy (morphology), dynamic light scattering (hydrodynamic size), western blotting (targeted protein exosome markers) and nano liquid chromatography tandem mass spectrometry (comprehensive protein identification).

The characterization techniques confirmed the isolation of exosomes with both isolation kit and ultracentrifugation. However, the isolated samples did contain contaminations, and there was a clear difference in the protein amount, particle size and populations identified with the two isolation methods. In addition, the majority of the characterization techniques provided poor repeatability, reproducibility and/or demanded extensive optimization.

The evaluation showed that the exosome isolation procedures used in this thesis appear to be far from mature. Additionally, the majority of the characterization techniques used in this study provided challenges.

Preface

The work presented in this thesis was performed at the research section for Bioanalytical Chemistry at the Department of Chemistry, University of Oslo, as well as at the unit for Cell Signalling, Oslo University Hospital. I would like to thank my supervisors for the great support, motivation and guidance through this work; PhD student Henriette Sjønes Berg, Dr. Kaja Lund, Dr. Hanne Røberg-Larsen, Associate Professor Steven R.H. Wilson and Professor Elsa Lundanes.

During my work, I have had the pleasure of cooperating with a number of students and academic staff, across different disciplines. First of all, I would like to thank my fellow student Kamilla Bjørseth for the collaboration on the project on exosome isolation, sharing both experiences and worries. I would also like to thank Professor Norbert Roos (Department of Biosciences) for greatly helping me out with issues related to immunogold labelling and TEM-imaging. His patience and company is highly appreciated. Dr. Sara Bekhradnia and Professor Bo Örjan Gunnar Nyström have provided much appreciated support, being responsible for the DLS-measurements and providing interesting discussions. I would like to express my gratitude to Axl Neurauter and Ketil Winther Pedersen from Thermo Fisher; for assisting with SW480 samples, exosomes and great guidance regarding the challenges of exosome isolation and characterization.

Also, I would like to thank the entire Bioanalytical chemistry group and the unit for Cell Signalling for providing a great academic and social environment. And among them, to Christine Olsen and PhD student Ole Kristian Brandzæg for the inspiring, albeit smaller, side project on testing trypsin reactors.

I would like to thank my family; including but not limited to Bente, Eldbjørg and Frode, and my boyfriend Johan, for being incredibly caring and supportive. At last, this thesis is dedicated to the memory of my loving mother.

Oslo, Norway, May 2017

- Frøydis Sved Skottvoll

Abbreviations

ABC	Ammonium bicarbonate
ACN	Acetonitrile
AGC	Automatic gain control
ALIX	Programmed cell death 6 interacting protein
ATCC	American Type Culture Collection
BCA	Bicinchoninic acid
Bis-Tris	2-bis (2-hydroxyethyl) amino-2-(hydroxymethyl) propane-1, 3-diol
BSA	Bovine serum albumin
CD	Cluster of differentiation
dd	Data dependent
ddMS/MS	data dependent tandem mass spectrometry
DLS	Dynamic light scattering
DMSO	Dimethyl sulfoxide
DNA	Deoxyribonucleic acid
DTT	Dithiothreitol
ECL	Enhanced chemiluminescence
EDTA	Ethylenediaminetetraacetic acid
ELISA	Enzyme-linked immunosorbent assay
EM	Electron microscopy
ER	Endoplasmic reticulum
ESI	Electrospray ionization
EVs	Extracellular vesicles
FA	Formic acid
FAR	Fixed angle rotor
Fab	Fragment antigen binding
Fc	Fragment crystallisable
FDR	False discovery rate
FBS	Fetal bovine serum
FSG	Cold water fish skin gelatin
GAPDH	Glyceraldehyde 3-phosphate dehydrogenase
GE	Gel electrophoresis
GO	Gene ontology

HCD	Higher energy collisional dissociation cell
HDL	High density lipoprotein
HPLC	High performance liquid chromatography
HRP	Horseradish peroxidase
HSA	Human serum albumin
Hsp	Heat shock proteins
IAM	Iodoacetamide
IEX	ion exchange chromatography
ID	Inner diameter
IAM	Iodoacetamide
Ig	Immunoglobulin
IgG	Immunoglobulin G
LDL	Low density lipoprotein
LC	Liquid chromatography
LC-MS	Liquid chromatography mass spectrometry
MES	2-(N-morpholino) ethanesulfonic acid
MIK	Department of Microbiology, UOS
MOPS	3-Morpholinopropane-1-sulfonic acid
MP	Mobile phase
MS	Mass spectrometry
MS/MS	Tandem mass spectrometry
MVEs	Multivesicular endosomes
NA	Numerical aperture
NP-40	Nonyl phenoxy polyethoxy ethanol
NMR	Nuclear magnetic resonance
NTA	Nanoparticle tracking analysis
OUS	Oslo University Hospital
PAG	Protein A gold
PBS	Phosphate buffered saline
PEG	Polyethylene glycol
PS	Phosphatidylserine
P/S	Penicillin/ streptomycin
PSM	Peptide spectral matches
RCF	Relative centrifugal force

RIPA	Radioimmunoprecipitation assay
RNA	Ribonucleic acid
RP	Reversed phase
RPM	Revolutions per minute
RPMI	Roswell Park Memorial Institute
RT	Room temperature
SBI	System Biosciences
SDS-PAGE	Sodium dodecyl sulphate – polyacrylamide gel electrophoresis
SP	Stationary phase
SPE	Solid phase extraction
SW	Swinging bucket rotor
TBS-T	Tris buffered saline in polyoxyethylene (20) sorbitan monolaurate
TEM	Transmission electron microscopy
TFA	Trifluoroacetic acid
Tris	2-amino-2-(hydroxymethyl) propane-1,3-diol
TSG101	Tumour susceptibility gene 101 protein
UiO	University of Oslo
UC	Ultracentrifugation
WB	Western blot

Definitions

Antigen	Organic molecules (most often proteins) capable of binding to an antibody.
Cancer	Heterogeneous group of diseases that feature abnormal cell division and the ability to promote malignancy in other tissues.
Cell	The basic biological unit of all living organisms.
Cell lysis	Disruption of the cell membrane.
Cell confluency	An estimation of the number of cells (in %) covering the surface of the flask they are grown in.
Endosome	Intracellular sorting vesicle. Exist as early, late and recycling endosome.
Immunolabeling	A biochemical technique used for the labelling of a specific biological target (antigen) using an antibody.
Lipoproteins	Protein complex particles transporting hydrophobic molecules through body fluids.
Passage	The number of times a cell line in culture has been harvested and reseeded.
Selective estrogen receptor modulator	Components that have the ability to interact with an estrogen receptor.
Vesicle	Membrane-bound organelle enclosing fluid inside cells.

Table of contents

1	Introduction.....	1
1.1	The biogenesis and characteristic of exosomes	2
1.2	Exosomes in intercellular communication.....	4
1.2.1	Clinical relevance of cancer exosomes and the purification issue.....	5
1.3	Cell culturing prior to exosome isolation.....	5
1.4	Current isolation techniques; ultracentrifugation and others	6
1.4.1	Ultracentrifugation.....	6
1.4.2	Other isolation methods	9
1.5	Characterization techniques.....	10
1.5.1	Colometric measurement of the protein concentration	10
1.5.2	Dynamic light scattering (DLS) and nanoparticle tracking analysis (NTA)	12
1.5.3	Transmission electron microscopy; principle and sample preparation.....	14
1.6	Protein characterization.....	19
1.6.1	Immunoblotting with western blot.....	19
1.6.2	Bottom-up an top-down proteomics	23
1.6.3	Sample preparation prior to analysis.....	24
1.6.4	Liquid chromatography	27
1.6.5	Electrospray ionization (ESI).....	30
1.6.6	Mass spectrometry.....	31
1.6.7	Protein identification	33
2	Aim of study	35
3	Materials and methods	36
3.1	Cell culturing and exosome isolation	36
3.1.1	Cell splitting.....	37
3.1.2	Cryopreserving	37
3.1.3	Cell culturing prior to exosome isolation	38
3.1.4	Exosome isolation by ultracentrifugation	39
3.1.5	Exosome isolation by isolation kit.....	39
3.1.6	Cell and exosome lysis.....	39
3.2	Determination of protein concentrations with BCA assay.....	40
3.3	Western Blot	41
3.3.1	Sample preparation.....	41
3.3.2	Gel electrophoresis	41
3.3.3	Protein transfer	42
3.3.4	Immunolabeling and visualizing	42
3.4	Sample preparation and TEM of exosomes	44
3.5	DLS.....	45
3.6	Sample preparation prior to LC-MS analysis.....	45
3.6.1	Protein digestion in-solution with peptide desalting.....	46
3.6.2	Protein digestion in-gel	47
3.7	LC-MS settings	49
3.7.1	LC-MS settings with analyses in house.....	49
3.7.2	LC-MS settings with analyses by the Thiede group.....	51
3.8	Data procession and protein identification with gene ontology annotation	52

4	Results and discussion	55
4.1	Cell culturing	55
4.1.1	Cell morphology	55
4.1.2	Cell confluency	56
4.2	Isolation of exosomes	58
4.2.1	Time considerations	58
4.2.2	Technical considerations	58
4.3	Measurement of the protein amount of the isolated exosomes by BCA assay	60
4.4	Size distribution with DLS	62
4.5	Targeted proteomics; Western Blot	64
4.5.1	WB of protein exosome markers with cell lysates	64
4.5.2	WB of protein exosome markers with isolated lysates	66
4.6	TEM with immunogold labelling	68
4.6.1	Immunogold labelling with MCF-7 exosomes	68
4.6.2	Immunogold labelling with MDA-MB-231 exosomes	71
4.6.3	Immunogold labelling with blank	75
4.7	Protein characterization with the use of nanoLC-MS/MS	76
4.7.1	Protein identification with external analyses further reproduced in house	76
4.7.2	Protein identification with protein exosome markers and annotation to cellular location	78
4.7.3	Proteins identified in blank	85
5	Conclusion	86
5.1	Future outlook	87
6	References	88
7	Appendix	98
7.1	Experimental supplementary	98
7.1.1	Isolation with the isolation kit	98
7.1.2	Example on measurements and calculations of protein concentration	99
7.2	Experimental considerations and discussions	100
7.2.1	Experiences with CD63 antibodies	100
7.2.2	Experimental considerations and observations of membrane structures with TEM	101
7.2.3	Immunogold labelling optimization with TEM	102
7.2.4	Immunogold labelling of MCF-7 isolated samples (UC), rejected	111
7.2.5	Experimental considerations when reproducing the nanoLC-MS/MS protein analyses performed externally	113
7.2.6	Protein identification with MCF-7 isolated exosomes	116
7.2.7	Protein identification with MDA-MB-231 isolated exosomes	118
7.3	Raw data and calculations (tables)	119
7.3.1	cell culturing confluency and	119
7.3.2	UV-measurements	120
7.3.3	DLS measurements	121
7.4	WB	122
7.4.1	WB-raw files	122
7.4.2	TEM raw files	129
7.5	LC-MS raw files	130
7.5.1	Protein identification	131
7.5.2	GO annotation of proteins	132

1 Introduction

Exosomes represent a distinct class of extracellular vesicles (EVs); small membrane-bound bodies secreted as a part of the endocytic pathway (**Box 1**), by various cell types. They were initially described by Trams et al. in 1981 [1], followed by Pan et al. and Harding et al. (1983-1985) observing the secretion of these exosomes by the use of electron microscopy [2-4].

Box 1: An outline of the endocytic pathway.

The endocytic pathway

The endocytic pathway is a part of the sorting system of the cell, and mainly concerns the recycling and degradation of cell compartments (e.g. proteins and ribonucleic acids (RNA)) (**Figure A**) [5]. The early endosome (fused with transport vesicles containing membrane proteins and other cell components, arriving from the plasma membrane or the Golgi-network) decides whether these components can be recycled or degraded. When degraded, the early endosome turns into late endosome and fuses with a lysosome (i.e. vesicle that holds digestive enzymes). The endocytic pathway also concerns the secretion of vesicles (Not shown in the **Figure A**).

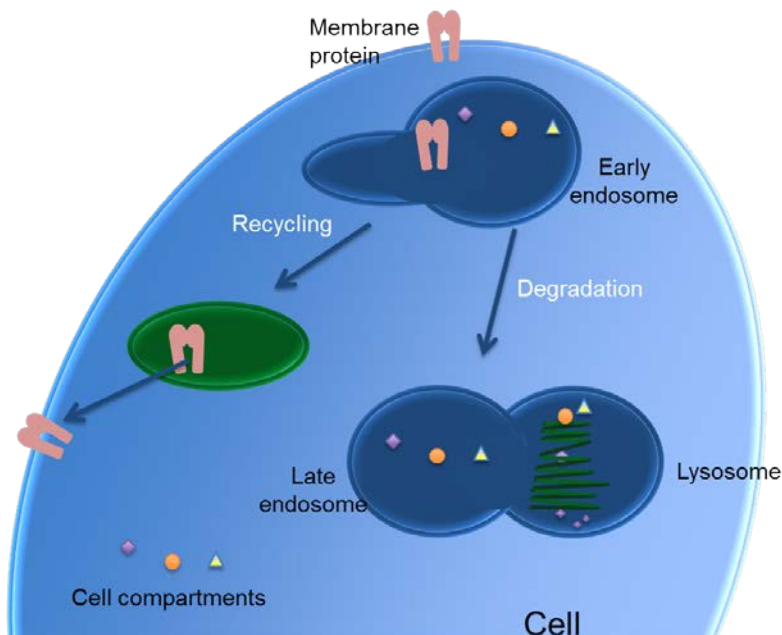


Figure A: The main routes of the endocytic transport with the early endosome deciding the destiny of its content. The recycling pathway of a membrane protein is green and the degradation pathway of cell compartments is blue. When deciding to degrade its content, the early endosome turns into a late endosome fusing with a lysosome holding digestive enzymes. Adapted from [5].

Based on the early findings, exosomes were first thought to contain components that the cell could not degrade itself, however this perception changed when researchers started to observe their involvement in immune responses [6-8]. Today, exosomes are found to be secreted by most cell types, and their contribution to diseases as cancer has caused an expanding interest.

1.1 The biogenesis and characteristic of exosomes

As shown in **Figure 1**, these vesicles are firstly formed by invaginations of the endosomal membrane, enclosing portions of cytosolic content (i.e. cell compartments) [9]. This is one of the processes of the maturation of early endosomes into late endosomes, which are similarly called multivesicular endosome (MVEs) [10, 11]. The exosome release is one out of three possible outcomes for the MVEs; lysosomal degradation, recycling or secretion of these vesicles into extracellular matrix [12].

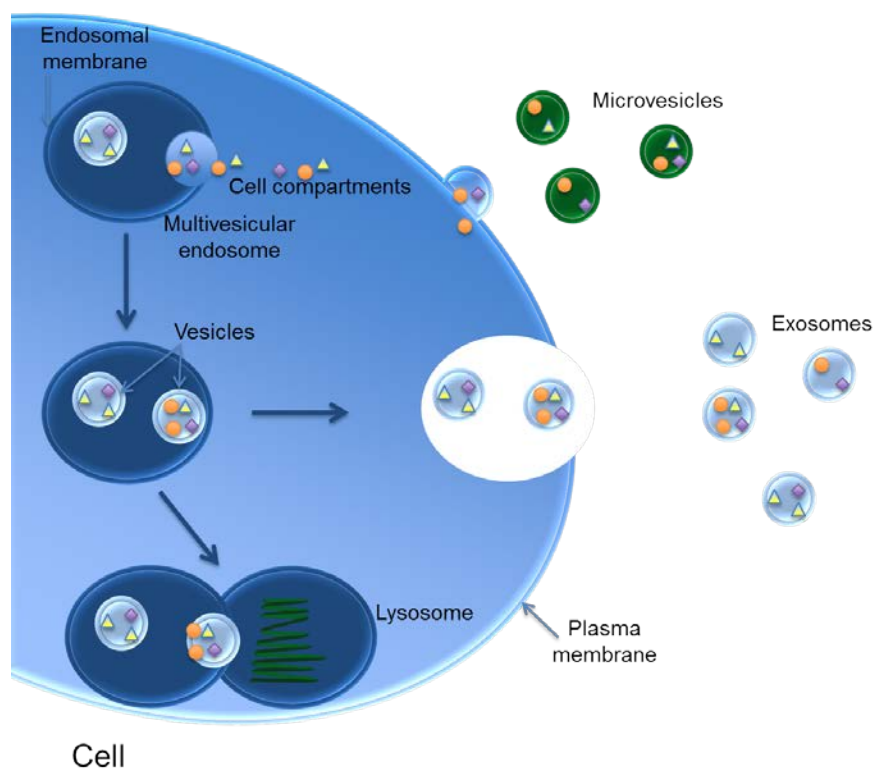


Figure 1: The biogenesis of exosomes: Invaginations of the endosomal membrane encloses portions of cell compartments and form vesicles inside the endosomes, which is now called multivesicular bodies (MVE). The fusion of MVE with the lysosome for degradation of its content is one outcome, another is the release of exosomes through the fusion of MVE with the plasma membrane of the cell. Adapted from [13].

The released exosomes are said to range in size between 30-100 nm in diameters [14], yet they can have a broader size range [15, 16]. The double membrane enfolded lumen holds a diverse mixture of proteins, lipids and nucleic acids [17], however the composition is

depending on the cell of origin and the mechanism of biogenesis [9, 14] (See **Figure 2** for composition of an exosome). Exosomes commonly contain proteins involved in membrane transport and fusion (such as annexins, G-proteins and flotillin), adhesion proteins such as integrins and tetraspanins (e.g. CD9, CD63, CD81. and CD82) and heat shock proteins (Hsp). In addition the cytoskeletal proteins actin, myosin, tubulin and syntenins are similarly present together with proteins involved in MVEs biogenesis (such as programmed cell death 6 interacting protein (ALIX) and TSG101) [9, 11]. Lipid related proteins, phospholipases, metabolic enzymes, signal transduction proteins, albumin and antigens are also to be present [9]. Furthermore the exosomes contain cargo from genetic material such as DNA, microRNA (i.e. a small, non-coding RNA, functions in RNA silencing and post regulation of gene expression) and mRNA [18].

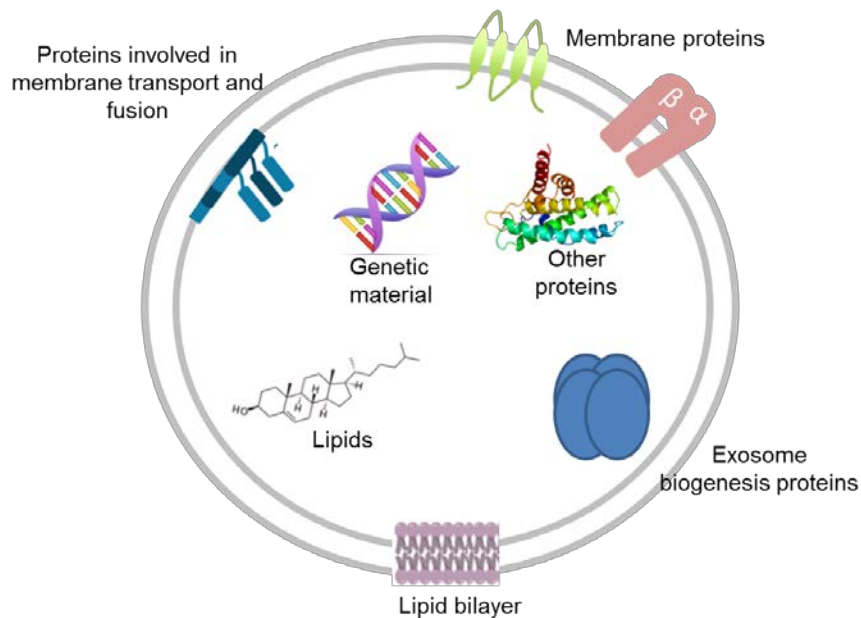


Figure 2: Schematic illustration of common content of the exosomes: a double membrane , other lipids, genetic material, proteins involved in membrane transport an fusion, membrane proteins, exosome biogenesis proteins and other proteins. Adapted from [19].

The exosome membrane consist of two membrane leaflets enriched in lipids such as different cholesterols, and dissimilar types of phospholipids [9]. The lipid composition of the exosome membrane confers rigidity of the exosomes; consequently provides the stability of exosomes in biological fluids and cell culture media [17, 20].

1.2 Exosomes in intercellular communication

The main function of the exosomes seems to be the transportation of bioactive molecules between parental- and recipient cell, hence they participate in intercellular communication [21, 22]. However the agreement of their biological function is still debated [23]. As illustrated in **Figure 3**, three possible mechanisms of the uptake of exosomes by target cells are shown; the fusion of exosome membrane with the plasma membrane of the cell releasing the exosome content into cytoplasm, endocytosis (with invaginations of the plasma membrane to form a vesicle around the exosome) and the receptor mediated endocytosis where the exosomes are enfolded by an endosome [12]. Ligand-receptor interaction also occurs and causes the receptor to change its conformation inducing a cell response.

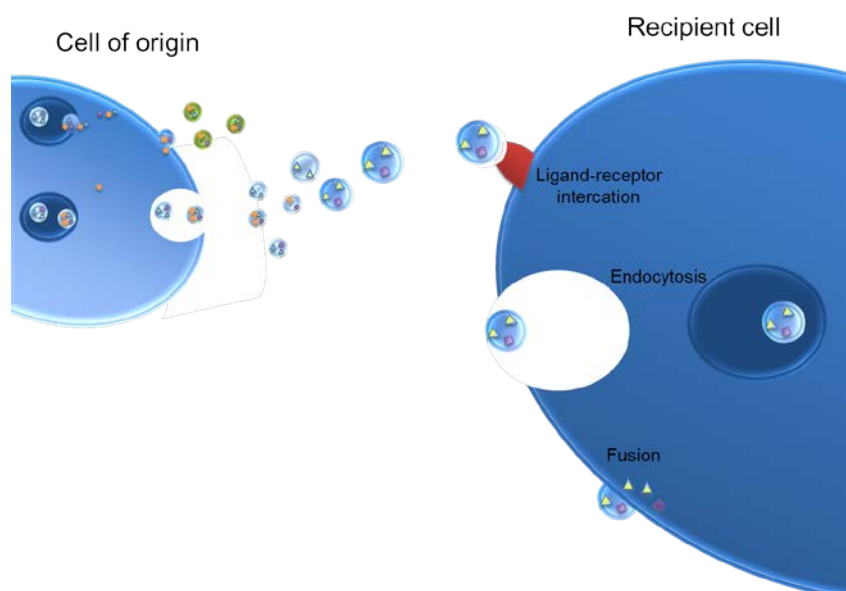


Figure 3: Illustration of the intercellular communication between cells with the use of exosomes: The exosomes are secreted from the cell of origin and passes through extracellular matrix, blood and other body fluids. When reaching the recipient cell, the sharing of information can occur through ligand-receptor interaction, endocytosis or fusion. Adapted from [13].

Such sharing of information as the ones above, leads to an activation of intracellular signalling networks and can affect the behaviour of the target cell in different ways [24-26]. This is additionally representative to tumour derived exosomes containing tumour related cargo [27], which could impact the development and progression of cancer. Cancer cells have been found to release more exosomes than stromal cells [28, 29], and they have a great capability of merging with and transfer parental cell cargo to recipient cells by reaching biological fluids [17]. This results in the potential of being a rich source of biomarkers which provide information on a specific pathological condition [10].

1.2.1 Clinical relevance of cancer exosomes and the purification issue

The role of tumour derived exosomes related cancer diagnostics is of escalating interest; Melo et al. found an enrichment of the protein (glypican-1) in cancer exosomes detecting early pancreatic cancer [30], Taylor et al. detected microRNA exclusively in exosomes from ovarian cancer [31] and microRNA was also detected in exosomes from glioblastoma patients [32]. In addition increased levels of 27-hydroxycholesterol (a potential biomarker for some breast cancers) was found in estrogen receptor positive breast cancer exosomes (from MCF-7 cell line) [33].

However, the scientific community has not fully taken advantage of the potential of exosomes which may be due to a lack of a standardized purification method. One reason to this can be related to their small size and amount released, in addition to the complexity of the biological material they are isolated from.

1.3 Cell culturing prior to exosome isolation

Not all types of cells release the same amount exosomes at all time. The rate of secretion most probably depends on the general cell properties; what are their main functions? Are they stem cells or cancer cells, are they grown from tumour tissues or from immortalized cell lines (cells customized to grow for prolonged periods in vitro)? The rate of secretion also most likely depends on the influence from the microenvironment (i.e. culturing conditions); the type and amount of growth medium (the liquid the exosomes are released into), cell density or flask size. Several papers claim to enhance exosome release by culturing (i.e. growing cells) under hypoxia (under 21 % O₂) [34], acidic microenvironment (pH 4) [35] or by using a culture system originally designed for large scale production of antibodies (i.e. CELLLine Culture System) [36]. There is little literature on optimized culturing conditions for each cell line, as it seems to be a common practice for keeping the cell-conditioned media from 24-48 hours after the cells have reached a confluency of 50-100 % [37], even though there is no specific evidence on the benefits of this related to all kinds of cell types. Others tend to seed out a specific number of cells (e.g. 10⁶–10⁹ cells for a period of 5-7 days) [36, 38].

1.4 Current isolation techniques; ultracentrifugation and others

As these possible exosomes are secreted from the cell, they are present in the cell culture media surrounded by other types of released membranous vesicles and cell debris [39]. Hence a suitable exosome isolation method is needed to obtain a more homogenous sample for further analysis. Although there are several protocols suggested for the isolation of exosomes [37, 40-42], there is a lack of consensus between the laboratories as the methods for rigorous isolation are still largely empirical.

1.4.1 Ultracentrifugation

The most commonly used technique for exosome isolation is the use of preparative ultracentrifugation (UC). Centrifugation is a method separating components with different masses by spinning the sample around an axis at a defined velocity (affected and separated by the centrifugal forces). The centrifugal force (F_s) on a particle is given based on three factors (*Equation 1*);

$$F_s = m\omega^2r$$

Equation 1

where m is the mass of the particle (in grams), ω is the angular speed (given by revolutions/rounds per minute (RPM)) and r is the distance of the migrating particles from the rotor axis. RPM or the relative centrifugal force (RCF) (also termed g or g -force) are “units” (RPM is not a SI unit) commonly used to term the velocity of the centrifugation. RPM describes how fast the centrifuge (rotor) is going, RCF (g) describes the centrifugal force applied to the contents of the rotor and varies with the distance from the rotor axis.

An ultracentrifuge is a centrifuge optimized to operate at very high speed (up to 2000 000 g or more) [43, 44]. Such high velocity demands a system with vacuum to hinder frictional heating. There are two types of rotors frequently used for exosome isolation; the swinging bucket (SW) rotor which stands out horizontally from the rotational axis during rotation, and the fixed angle (FAr) rotor which is held at a constant angle during the whole centrifugation (**Figure 4**) [45].

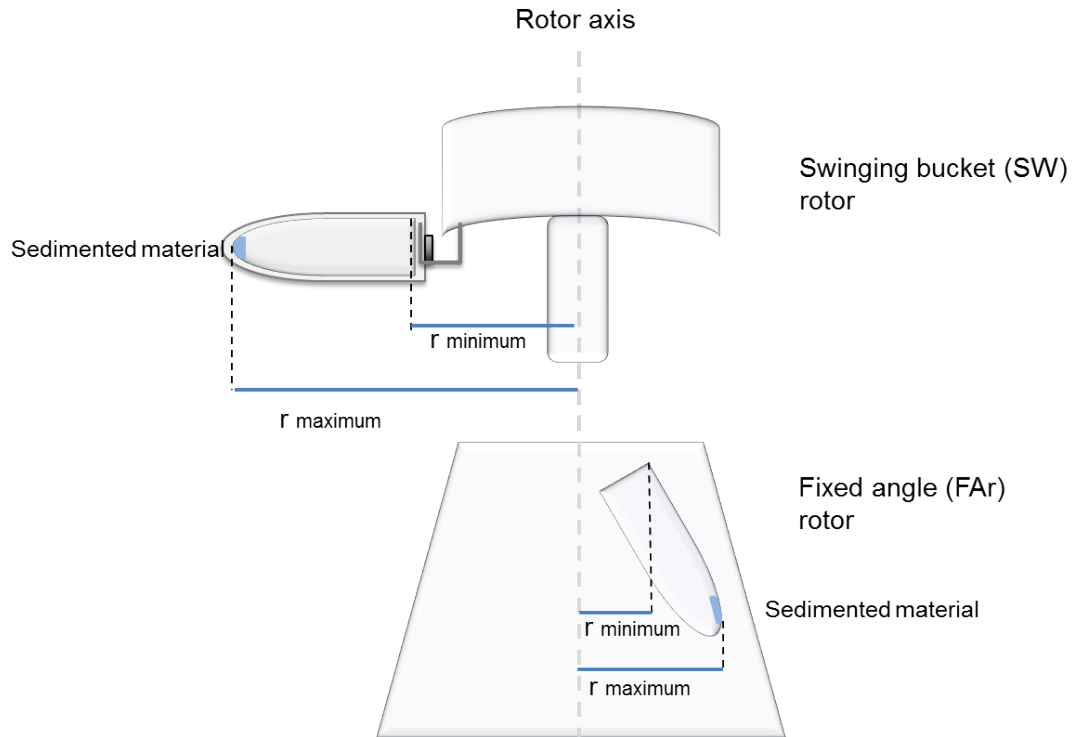


Figure 4: Schematic illustration of the different rotors with the position of sedimented material and different distance from the rotor axis (i.e. radius, r): The swinging bucket (SW) rotor has longer sedimentation path length ($r_{\text{maximum}} - r_{\text{minimum}}$) than the fixed angle (FAR) rotor. Shorter sedimentation path length means particles have less distance to travel before pelleting against the tube wall. Adapted from [46]

With the shorter sedimentation path length (i.e. $r_{\text{maximum}} - r_{\text{minimum}}$) of the Far rotor, the particles have less distance to travel before pelleting against the tube wall. And as the sedimentation path length of the SW rotor is longer, this can result in a lower pelleting efficiency if not compensated by prolonged centrifugation duration. On the other hand the SW rotor can offer greater resolution of the particles. When conversion between different rotors is needed, this is not fully straight forward. The k-factor (clearing factor, k) is the relative pelleting efficiency of a specific centrifuge rotor at maximum rotation speed, and is based on several variables as shown in *Equation 2*.

$$\text{k-factor} = \frac{2.533 \cdot 10^5 \left[\ln \left(\frac{r_{\text{maximum}}}{r_{\text{minimum}}} \right) \right]}{\left(\frac{\text{RPM}}{1000} \right)^2} \quad \text{Equation 2}$$

r_{maximum} and r_{minimum} is the maximum- and minimum radius of the rotor (in mm) respectively, and RPM is the maximum speed of the rotor (in RPM). With decreasing k-factor, the rotor efficiency increases. Next the sedimentation coefficient, s , is to be calculated and is based on Stokes law. The sedimentation coefficient describes the movement of the particles through a solution (*Equation 3*).

$$s = \frac{m}{6\pi\eta r}$$

Equation 3

Where m is the mass of the particle (kg), η terms the viscosity of the solution (kg/ms) and r is the radius of the particles. s is the sedimentation coefficient, expressed in svedberg, where one S is corresponding to 10^{-13} seconds. In literature, sedimentation coefficients are often referred to sedimentation in water at 20°C. Larger particles (larger radius) sediment faster and have higher s -values. Based on the k -factor and the sedimentation coefficient (s), the time (t , in hours) required to pellet a particle can be calculated (*Equation 4*).

$$t = \frac{k\text{-factor}}{s}$$

Equation 4

Conversion of a centrifugal condition from one rotor to another can be done according to *Equation 5*,

$$\frac{t_1}{k_1} = \frac{t_2}{k_2}$$

Equation 5

where t_1 and t_2 are the run time (in hours) of the two different rotors, and k_1 and k_2 are the different k -factors of the two different rotors.

Ultracentrifugation is regarded as the “gold” standard of exosome isolation, and the most commonly used protocol was presented by Théry et al. in 2006 [37], isolating the exosomes by differential ultracentrifugation of the fluid. In addition this method can be supplied by differential filtration and/or gradient sedimentation with sucrose [47]. There are several parameters to control when working with ultracentrifugation (FAr or SW rotor, temperature, duration of the centrifugation, RCF, k -factor [45] and solution viscosity [48]). The number of parameters to control can cause difficulties when the reproducibility is to be investigated using different rotors and k -factors. However, the number of parameters also enables the possibility to achieve high purity exosomes. Nevertheless, ultracentrifugation is a time consuming process which requires a large starting volume (up to 70 mL for one sample). According to Théry et al. [37], the yield increases with the starting volume, however there is no literature confirming this.

1.4.2 Other isolation methods

Alternative methods have been developed to overcome the drawbacks of ultracentrifugation. A selection of the different methods is briefly described in **Table 1**; density gradient separation with ultracentrifugation, size exclusion chromatography, filtration, polymer-based precipitation, immunoaffinity capture and flow field-flow fractionation.

Table 1: A selection of other methods applied in the isolation of exosomes, with short description of the separation principle and literature on the field related to exosomes.

Method	Separation principle	Literature
Density gradient separation with UC	Based on the densities of the exosomes (1.1-1.19 g/mL), with the use of sucrose (or synthetically made) density gradients. The low-density exosomes are floating upward, while higher-density contaminants remain on the bottom.	[6] [49, 50]
Size exclusion chromatography	Using the hydrodynamic radius of the exosomes to separate them from larger contaminants by the use of a column packed with heteroporous beads.	[51-53]
Filtration	Isolation based on size with the use of filtration membranes.	[54, 55]
Polymer-based precipitation	Precipitation of exosomes by the use of polymers as polyethylene glycol (PEG) and centrifugation at low velocity.	[42, 56]
Immunoaffinity capture	Isolation by employing magnetic beads coated with monoclonal antibodies that reflects specific exosomal membrane protein.	[40, 57, 58]
Flow field-flow fractionation	Separation of exosomes by hydrodynamic size with the combination of a cross- and laminar flow.	[59]

Density gradient separation combined with ultracentrifugation generates a cleaner isolate than differential UC. However this method does not discriminate other vesicles or viruses that have the same buoyant density. In addition certain vesicles need up to 62-90 hours to reach equilibrium [49]. If the separation duration is too short or the tube is too long, contaminating aggregates may not reach the bottom. Size exclusion chromatography was the preferred method over ultracentrifugation when isolating exosomes from human and rat blood plasma [60]. In addition, this method does not use force or other factors that might

affect the biological activity and structure of the exosomes isolated. However making uniform pore sizes is a challenge. The use of filtration to extract exosomes is little used alone as exosomes can adhere to the membrane, additionally filtration does not completely remove the smaller components. Lately, several commercial isolation kits have been developed to offer a less time consuming method, in addition to the demand of a smaller volume for isolation. The content of these kits is not disclosed; however they most likely use PEGs and/or salts to precipitate the vesicles. Little equipment is needed, and the isolation is rapidly performed. The use of PEG is not compatible with further analytical techniques, as an liquid chromatography mass spectrometry (LC-MS). In addition co-isolation of non-vesicular contaminants as lipoproteins (e.g. high density lipoproteins (HDL) and low density lipoproteins (LDL)), RNA and proteins are frequently observed. Immunoaffinity capturing with anti-EpCAM (a transmembrane protein) showed to be the preferred method (displayed the highest purity) for the isolation of exosomes from a human colon cancer cell line [61] when compared with density gradient ultracentrifugation, and ultracentrifugation. But as previously mentioned; the exosomal population is heterogeneous, hence does not always display the same amount/type of membrane protein.

1.5 Characterization techniques

No standard procedure for the characterization of exosomes is agreed upon and this lead to an article written by the International Society for Extracellular vesicles (Lötval et al.) proposing the minimal experimental requirements to discriminate EVs from non EVs components [62]. Lötval et al. proposes commonly used characterization methods for this purpose [62], which mostly covers methods used in this work. The specific techniques with possibilities and drawbacks are described in the following sections.

1.5.1 Colometric measurement of the protein concentration

Even though there is not much mentioned about characterization with protein quantification using bicinchoninic acid assay (BCA assay, [63]) in the article written by Lötval et al. [62], this is a widely used method in the field of exosome characterization. The protein concentration (often stated as $\mu\text{g}/\text{mL}$ isolated sample) gives a rough idea on the recovery of the isolation method, while the ratio of particles to proteins (particle measurements is done by either dynamic light scattering or nanoparticle tracking analysis) is often compared to give an approximation on the purity of the isolated samples [37, 41, 64, 65].

The BCA assay combines the protein-induced “biuret reaction” [66], originally the reduction of Cu^{2+} to Cu^{1+} with the presence of biuret (2-imidodicarbonic diamide) in the presence of an alkaline environment. The chemical structure of biuret (**Figure 5**) is similar to that of peptides with three or more amino acid residues, hence they are able to complex with copper (II) and reduce it to copper (I) with the same principles as with biuret.

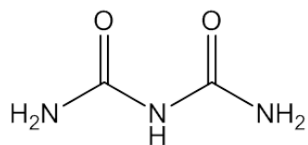


Figure 5: The chemical structure of 2-imidodicarbonic diamide, also termed biuret. The chemical structure is similar to the one of a peptide with three or more amino acid residues.

When BCA is added, two molecules of BCA reacts with one copper (I) ion, creating a BCA-copper complex absorbing wavelengths of 562 nm (i.e. purple coloured sample) (**Figure 6**).

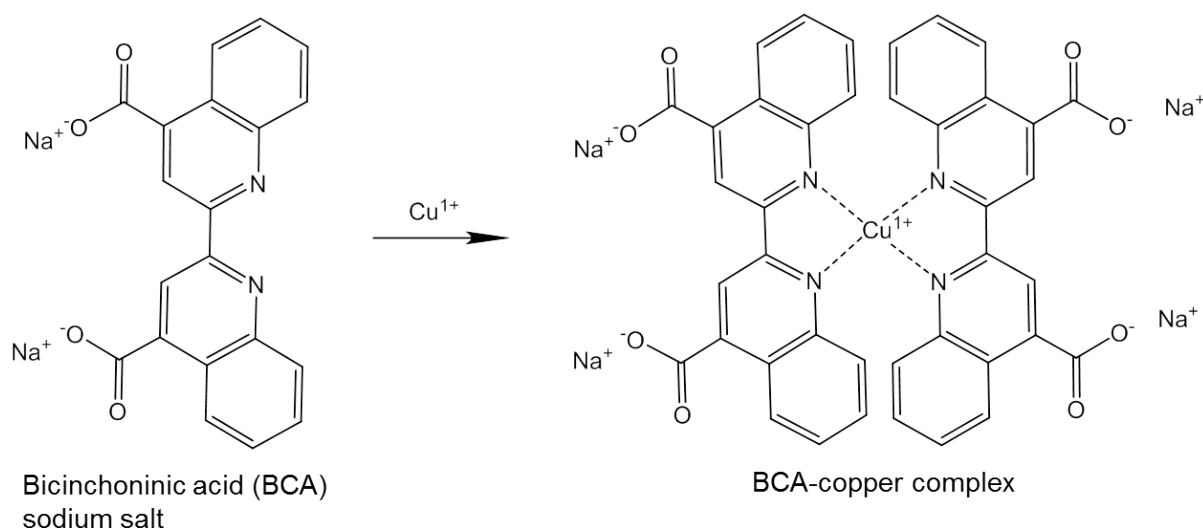


Figure 6: Reaction of two BCA sodium salts with the reduced copper (I) creating a BCA-copper complex absorbing light at 562 nm.

The absorbance (A) of the sample is given by Beer-Lambert law (*Equation 6*);

$$A = \epsilon bc$$

Equation 6

where ϵ is the molar absorptivity (L/mol/cm), b is the path length of the sample (cm) and c reflects the concentration of the sample (mol/L). When preparing standard protein concentrations in parallel to the unknown samples, the protein concentration is calculated from the calibration curve obtained with the standard protein concentration.

1.5.2 Dynamic light scattering (DLS) and nanoparticle tracking analysis (NTA)

Lötvall et al. [62] discuss the importance of characterizing EVs with the use of a size distribution technique, providing information about the different size range of the particles present in the samples. To achieve accurately determination of the small sizes of the particles present, hence the ability to see possible contaminants (i.e. lipoproteins), high sensitivity techniques (i.e. measure particles of sizes ≤ 30 nm) are required. Hereby two techniques are described; DLS and NTA.

DLS is a method used for determination of the size distribution of particles or molecules dissolved in a liquid, ranging in size from 1 nm to 6 μm . As shown in

Figure 7, monochromatic light (electromagnetic radiation at a given wavelength (λ)) from a laser is directed towards particles in suspension. Particles in suspension continuously move in random directions and collide with solvent molecules. This causes a random motion of particles called Brownian motion, resulting in intensity fluctuations of the scattered light. Large particles move at low velocity, thus the intensity fluctuates slowly too. This is contrary for small particles which move at high velocity, and therefore yields in high intensity fluctuation. Next, these intensity fluctuations of light are detected by a fast photon detector at a known scattering angle (θ).

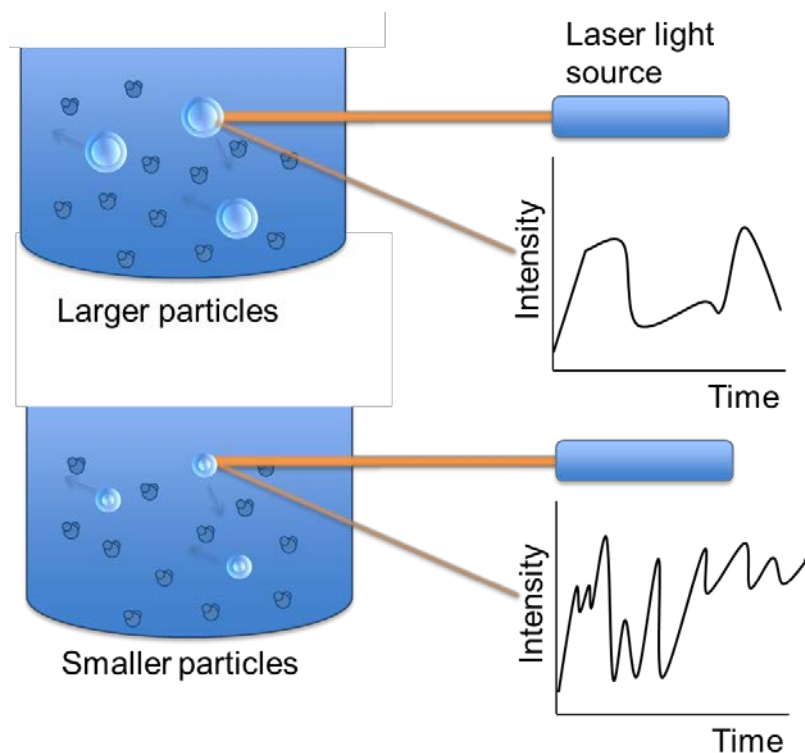


Figure 7: Schematic DLS of two samples with particles of different sizes, and their related auto-correlation function. Large particles move slowly, thus the intensity fluctuates slowly too. This is contrary for small particles which move rapidly, and yields in high intensity fluctuation. Further, using an auto-correlation function and the Stokes-Einstein equation the hydrodynamic radius of the particle is determined. All objects are not drawn to scale with respect to each other. Adopted from [67].

The time scale of the scattered light intensity fluctuations is analysed by an auto-correlation function, which reports how quickly on average the light intensity changes with time. This yields the diffusion coefficient, D (m^2/s), and the hydrodynamic diameter, d , of the particles are determined using the Stokes-Einstein equation (*Equation 7*),

$$d_H = \frac{kT}{3\pi\eta D} \quad \text{Equation 7}$$

where d_H is the hydrodynamic diameter (m), k is the Boltzmann constant (approximately 1.3806×10^{-23} J/K), T is the temperature (K) and η is the solvent viscosity (kg/ms).

Even though this technique works well for monodisperse samples (equally sized particles in solution), it has been reported that DLS measurements are less suitable when polydisperse samples are to be measured (i.e. particles of different sizes in a solution) [68-70]. One other commonly used technique which copes with these issues is NTA (**Figure 8**), first commercialized in 2006. This technique visualizes and records the trajectories of the scattering particles (illuminated by a laser beam) under a microscope, and the software is able to identify and track the particles observing their Brownian motion. This software relates their movement to the hydrodynamic diameters using a derived equation from the Stokes-Einstein equation (*Equation 7*).

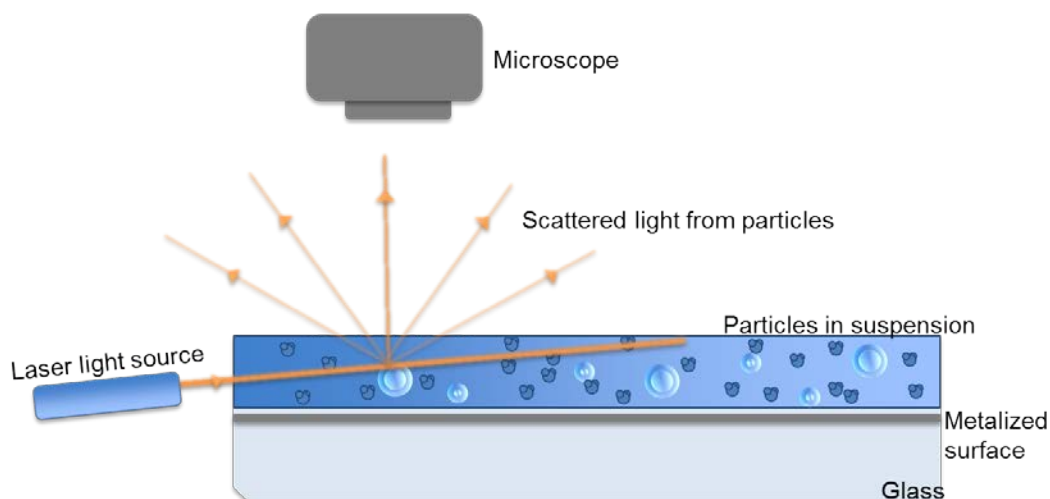


Figure 8: Schematic representation of the optical configuration used in NTA. The laser beam is sent through a sample containing particles in suspension, when this beam hits particles they scatter light. This is observed in a microscope and used to calculate the hydrodynamic diameter using Stokes-Einstein equation. Adapted by [71]

The lower size limit is dependent by the particle's ability to scatter sufficient light to be detectable, with analysis of 10 nm particles only being possible with materials having high refractive index such as gold and silver. This excludes the possibility of determining the presence of impurities during exosome characterization, as it would not be sensitive enough to detect impurities ranging in diameters ≤ 30 nm (e.g. lipoproteins). On the other hand, NTA provides approximate particle concentrations which are useful features in the yield of exosome isolation (i.e. number of particles).

Regardless of the size distribution technique chosen, the values acquired should be combined with microscopy techniques, since DLS/NTA measurements do not distinguish membrane vesicles from co-isolated non-membranous particles of similar size.

1.5.3 Transmission electron microscopy; principle and sample preparation

Lötvall et al. [62] discuss imaging techniques to confirm the presence of membranous vesicles in the samples, to support the results from size distribution (from e.g. DLS or NTA). As there is a need for high resolution images (i.e. the minimum distance of two structural elements, which can be imaged as two individual objects) allowing to image these membrane structures, light microscopy is not suitable for this purpose. Transmission electron microscopy, however, is commonly applied for this purpose. With the use of electrons (the wavelength ranges between 0.004 and 0.00087 nm, depending on the acceleration voltage) instead of light (wavelength ranging between 380-750 nm), this would allow resolution power to reach 10^{-10} m and below, thus being able to image structures on the atomic level.

This can be explained by the correlation between resolution (d_{\min}) and wavelength of incident light (λ) of the source by Abbe's equation (Equation 8),

$$d_{\min} = \frac{0.612\lambda}{NA} \quad \text{Equation 8}$$

where NA is defined as the numerical aperture (i.e an indication on the resolution of the microscope).

A schematic principle of TEM- visualizing is shown in **Figure 9**. The heating of a wolfram filament (which functions as the cathode) induces the filament to emit electrons, which is further focused into an electron beam and accelerated (by the anode) towards the sample. The electromagnetic lens system focuses the electron beam to only allow electrons within a small energy range to pass through, resulting in an electron beam of well-defined energy. Next the electron beam hits the specimen and the transmitted electrons are refocused and the image is enlarged (by the projection lens) in the imaging system, and appears on the screen. This has to be done under vacuum, as the gases in the air would strongly interfere with the electron beam and possible contaminate the specimen.

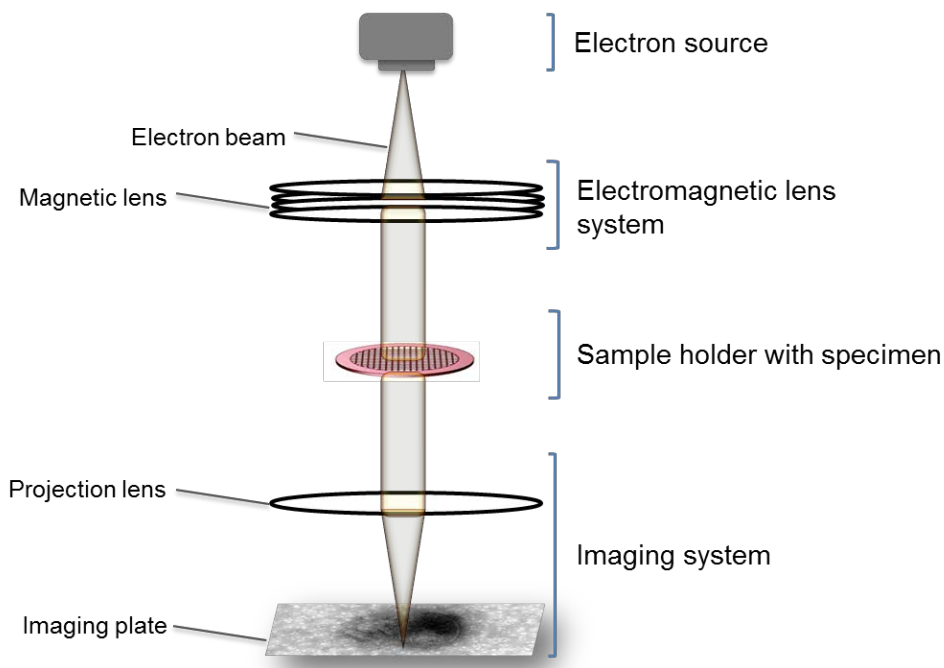


Figure 9: Sketch of a TEM: The electron beam is from the electron source is focused to an electron beam of well-defined energy (by the electromagnetic lens system) and hits the specimen. The transmitted electrons are refocused and the image is enlarged (by the projection lens) in the imaging system, and the image appears on an imaging plate.

As the area observed by TEM is limited, there is only a small part of the specimen that will be visualized and examined. In addition it is commonly known that when working with biological samples, easy shrinkage of e.g. the exosomes often arises due to the removal of liquid prior to visualization.

Sample preparation with immunogold labelling

Most work is done on small square-mesh grids (standard size is around 3 mm diameter) prior to TEM-imaging (See **Figure 10 A**). The grids can either be of copper, gold or nickel, and the choice is often depending on the chemical properties (e.g. chemical oxidation or magnetic properties) and the price [72]. The grids are often coated with a support film (standard is polyvinyl formal, also called formvar) as it is electron-transparent, stable and holds the sample in place throughout the sample preparation and imaging with electron microscopy (EM).

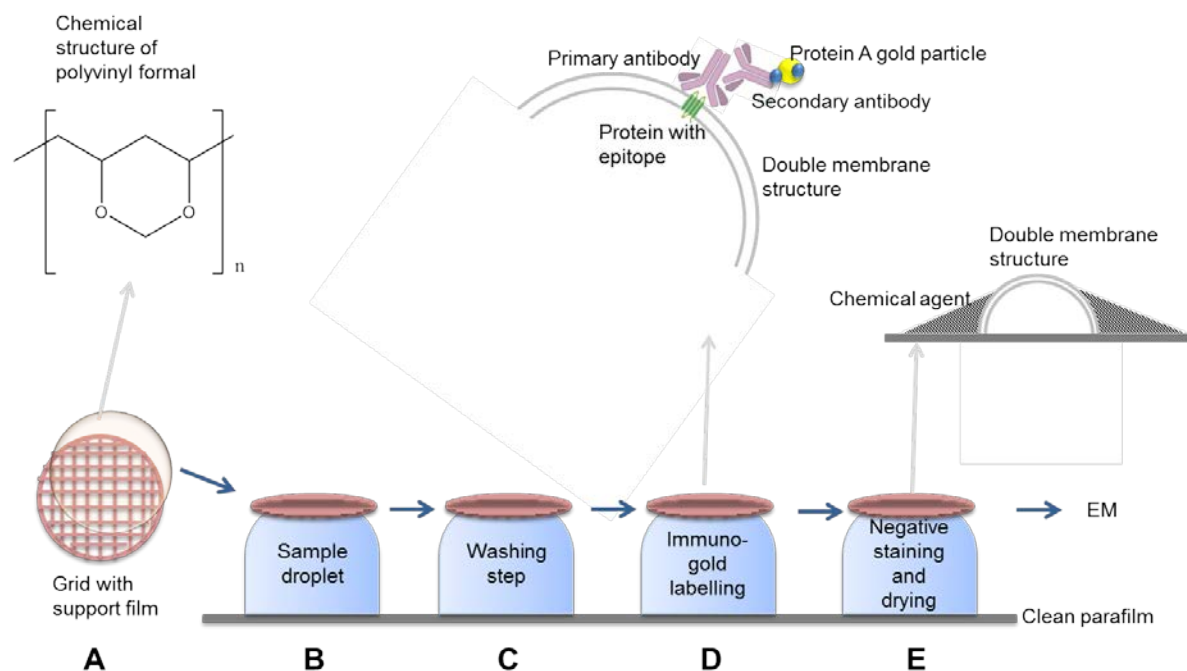


Figure 10: An overview of the sample preparation steps prior to TEM-imaging. **A)** The grid can be of various materials, and often holds a support film made of poly (vinyl formal). **B)** The grid is placed on the sample droplet where to the sample components are adsorbed. **C)** Washing steps with phosphate buffered saline (PBS) are performed between each preparation. **D)** Immunogold labelling with the antibody of interest; the antibody is specific to a given amino acid sequence on the protein and binds to it. Next a secondary antibody bound to a protein A gold particle (PAG) is specific for the amino acid sequence of the primary antibody and binds to this. The process is shown with the example of labelling with CD9 (i.e. transmembrane protein) on an exosome (shown as a double membrane structure). **E)** At last, the sample is negative stained with a chemical agent. Prior to this step, the grid is rinsed with water. When dry, the sample is ready for EM.

All sample preparations are done on a clean surface covered with clean parafilm to avoid contamination. The formvar coated grid is initially placed on a droplet of the sample examined, with the coated side facing the sample (**Figure 10 B**). As the film holds a

hydrophobic surface, hydrophobic interactions occur between the sample components and the film resulting in an embedding to the resin. The concentration of the specimen is usually higher on the surface of the droplet than inside, and this ensures high sample embedding [73]. Consequently TEM is not a quantitative technique. The grids are washed between each incubation step (**Figure 10 C**) with a buffered solution to wash away non-interacting components and to sustain the pH and salt concentration of the sample (and avoid the formation of (protein) aggregates). If the sample is of biological material, phosphate buffered saline (PBS) (water-based salt solution containing sodium phosphate, sodium chloride among others, reflecting the osmolality and ion concentrations of the human body) is commonly used. Immunogold labelling with antibodies is done in order to locate a molecule with a particular function (i.e. antigen), if this is of interest (**Figure 10 D**) (For more information on antibodies, see section **1.6.1, Antibodies**). This enables structural analysis related to functional properties, and in this case the molecule to be recognized would be proteins known to be exposed on exosomal membranes (e.g. CD63, CD9, and CD81). The primary antibody (The host is mouse or rabbit) is specific and chemically binds to the epitope (i.e. the specific amino acid sequence) of this protein, further the secondary antibody (opposite animal host) is specific against the primary antibody and will fix to it. The gold nanoparticle (5-20 nm diameters) can either be fixed to the secondary antibody or to a protein complex (i.e. protein A) which binds to the secondary antibody and is characterized as a circular black spot in TEM. For further information of the synthesis and conjugation of gold particles to protein A (PAG), see **Box 2**.

As the work of this thesis is with biological materials (composed of light elements as C, O, H and N), there is a need for contrasting of the sample as the material most likely is too transparent to the electrons to be viewed directly. This is done by surrounding the sample with a chemical agent that is dense to the electrons; forming a dark background around these bright structures (**Figure 10 E**). This is called negative staining, and the components used are often diluted heavy elements such as uranium (uranyl acetate) or molybdenum (ammonium molybdate), adsorbing to the support film and the sample surface [74]. As some of these negative stains are sensitive to pH above 5 and of phosphate ions, rinsing with water prior to contrasting is essential. In addition this removes the salts from PBS, preventing the formation of salt crystals during the final drying step prior to TEM-imaging.

Box 2: Brief description of synthesis and conjugation of gold particles to protein A.

Synthesis and conjugation of gold particles to protein A

There are many different methods for synthesis of gold nanoparticles, most commonly this is done by chemical reduction of Au^{3+} (l) to form Au^+ (l) and Au (s) using the Turkevich method, where citrate is used both as the reducing and stabilizing agent [75] (for further details about the different method principles and recent improvements, see [76-80]). Further functionalization is essential to obtain a hydrophilic/ hydrophobic surface, to prevent agglomeration and to obtain other characteristics using ligand molecules (e.g. alkanethiolates and or PEG) [81, 82]. Next, the strategy for the conjugation of biomolecules (i.e. in this case protein A, a protein able to interact with antibodies) to the gold nanoparticle generally falls into three possible interactions, shown in **Figure B**.

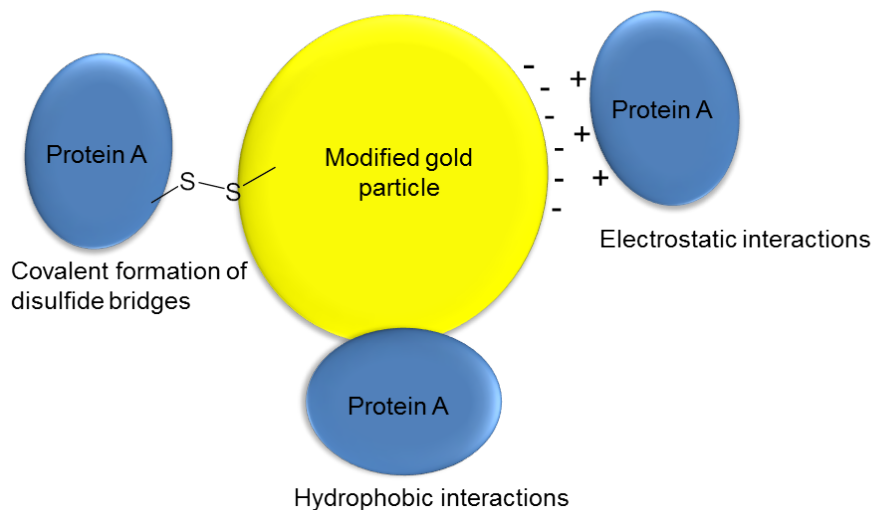


Figure B: Three possible interactions that can occur when modified gold particles are conjugated with the biomolecule protein A; covalently created disulfide bridge with cysteine residues on the protein, hydrophobic interactions and electrostatic interactions. Adapted from [83].

The adsorption of protein A to the modified gold particle seem to be concentration and pH-dependent, with the maximal binding and higher stability occurring at pH higher than the pI of this protein (pI 5.16) [84]. This leads to the reduction of the electrostatic interactions, preventing possible aggregation of the protein. Thus the main interactions would then be through hydrophobic interactions and possibly through the formation of disulfide bridges with cysteine residues on the protein (this would be the case if the gold particle was modified with sulfide as the active group). The adsorption of protein onto gold inhibits other gold particles binding.

1.6 Protein characterization

Next, it is preferred [62] to perform a semi-quantitative study of the protein composition of the preparations, testing for both proteins expected to present (i.e. different transmembrane- and cytosolic proteins with membrane- or receptor-binding capacity) and proteins not expected to be present (i.e. proteins related to intracellular compartments other than plasma membrane- or endosomes), using techniques as western blot (WB) or mass spectrometry (MS) (coupled to a liquid chromatography (LC) system) among others. A semi quantitative study would typically compare the protein composition in the preparations with that of the secreting cells (e.g. by intensity analysis of signals obtained from WB) to determine a possible enrichment of markers which further argues the presence/absence of exosomes in the sample. Proteomics can be comprehensive (also called discovery) searching for the proteins present in a sample, or targeted when only one specific protein is of interest.

1.6.1 Immunoblotting with western blot

Western blotting or immunoblotting, is a widely used technique in targeted proteomics that enables the identification of specific proteins with the use of antibodies selective for the proteins of interest [85]. First, the separation of the proteins is based on charge and/or size (i.e. molar mass) when moving through an electric field (also called gel electrophoresis (GE)). In this thesis they are separated according to size only, using sodium dodecyl sulphate (SDS) – polyacrylamide gel electrophoresis (SDS-PAGE).

The WB workflow

Prior to SDS-PAGE, SDS is added (chemical structure shown in section **1.6.3, Figure 15**) to obtain a uniform negative charge on the proteins (1.4 g SDS/ 1 g protein). This makes the charge of the protein proportional to its molar mass. **Figure 11** shows the workflow of WB, firstly separating the proteins with the use of GE.

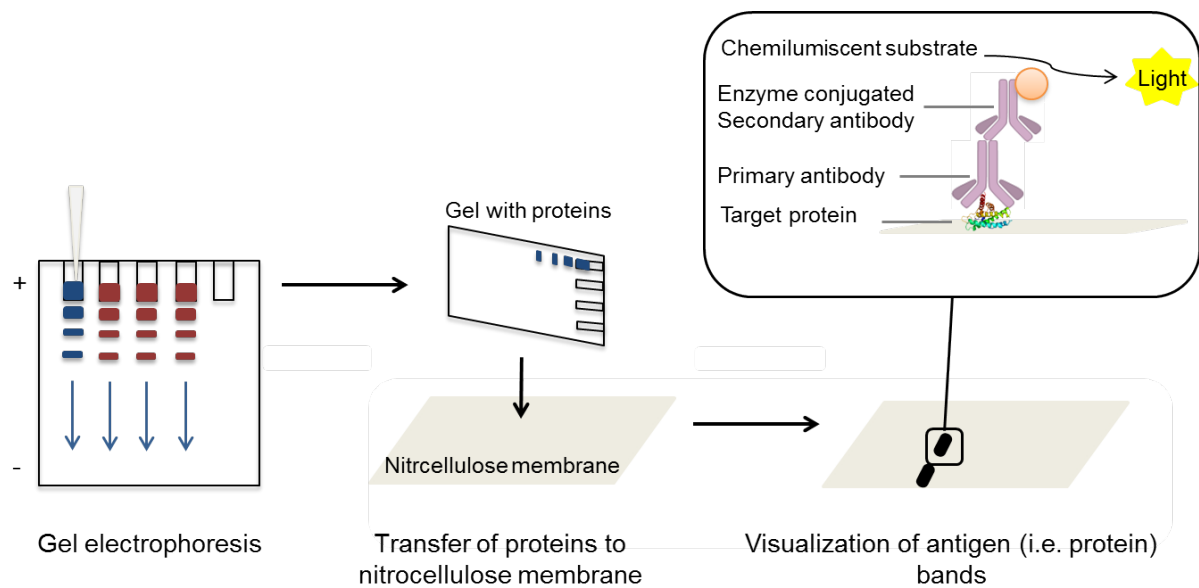


Figure 11: The workflow of western blotting; Firstly the proteins are separated with gel electrophoresis. Next an applied voltage is applied to transfer the proteins from the gel onto a membrane (made of nitrocellulose or polyvinylidene difluoride). Subsequently the membrane is incubated with primary- and secondary antibodies with the primary antibody being specific for the protein of interest. When adding a chemiluminescent substrate, the reaction with the enzyme conjugate produces light detected by a sensitive camera.

The gel with the separated proteins is transferred (by applying voltage) to a membrane made of nitrocellulose or polyvinylidene difluoride. This membrane has high affinity for proteins and by adding a blocking agent after the transfer; this prevents nonspecific binding of the antibodies to the unoccupied membrane surface. Non-fat dry milk is commonly used for this purpose. Next the membrane is incubated with primary- and secondary antibodies with the primary antibody being specific for the protein (i.e. antigen) of interest. The secondary antibody is often conjugated to an enzyme, the enzyme horseradish peroxidase (HRP) was applied in this thesis. When adding a chemiluminescent substrate, the reaction produces light detected by a sensitive camera.

Antibodies

Due to their potentially high specificity and selectivity antibodies are utilised in a broad area of different techniques in research, diagnostics and therapeutics. In research, the use can be to immuno-localize a particular protein in a sample (i.e. immunolabeling) or identification of a protein using WB [85] or enzyme-linked immunosorbent assay (ELISA) [86, 87].

Antibodies or immunoglobulins (Ig) are glycoproteins produced by the immune system as a response to foreign molecules, also called antigens [88-90]. Each antibody binds specifically to this target molecule (at a specific binding site, called epitope), with the goal of either directly inactivating it or marking it for destruction. They are heterodimeric protein

structures, and the most abundant antibody in humans is shaped as a Y (called immunoglobulin G, IgG) (**Figure 12**) and generally consists of two identical polypeptide chains (the heavy or H chains) covalently linked through disulfide bridges to two identical smaller polypeptide chains (the light or L chains).

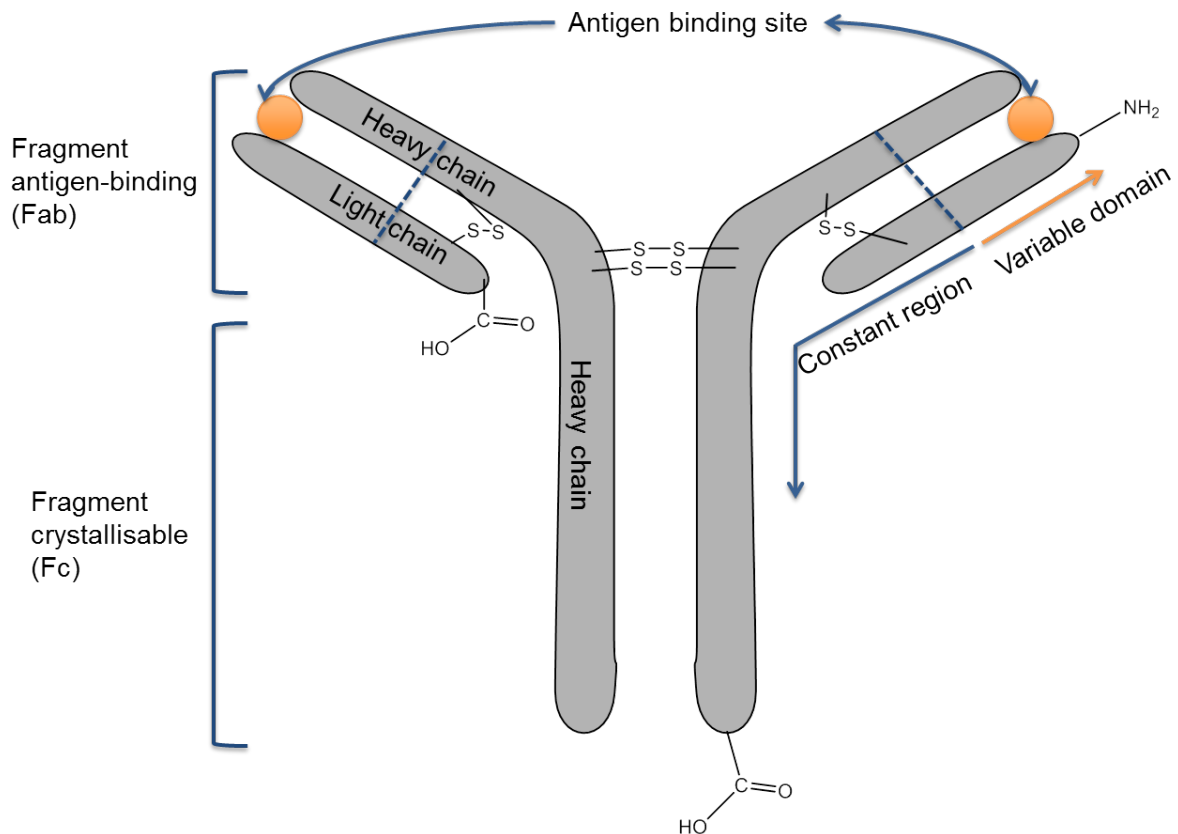


Figure 12: Structure of an antibody with COO- and NH₂-terminal sites. It is made up of two identical polypeptide chains (the heavy) covalently linked through disulfide bridges to two identical smaller polypeptide chains (the light). The constant region holds an amino acid sequence which is constant and will not change from one antibody to another. The variable domain has large variance in the amino acid sequence from one antibody to another. This is sequences where the antigen binds. The Fab- and Fc region are regions created when the antibody is exposed to the cleavage protein pepsin.

Each of the heavy- and light chains has regions where the amino acid sequence is constant and will not change from one antibody to another. However there are variable domains (showed with an orange array in **Figure 12**) attached to the constant regions that do vary in their amino acid sequence from one antibody to another and show the largest difference among the different antibodies. The antigen binding site is between the light- and heavy chains of the variable domain. This region is also called fragment antigen-binding (Fab) (when the antibody is exposed to the cleavage protein pepsin). The heavy chain at the constant region and C-terminal site (called the fragment crystallisable (Fc) region) provides with so-called effector functions, such as complement fixation of other antibodies.

Antibodies are produced by a variety of host animals (e.g. mouse, rabbit, goat and chicken), and can be both mono- and polyclonal meaning they recognizes only one or multiple epitopes on an antigen. Very often there is a need for a secondary antibody to assist in detection, which is generating an immune response to the Fc region of the primary antibody in other species (e.g. chicken anti-mouse is used if the primary antibody has mouse as the host animal). This is done because it is often very costly to both produce an antibody specific towards only one antigen in addition to tagging this with the component used for detection. Having a universal secondary antibody being specific only towards the host animal enables amplification of the signal, as this antibody can possibly bind to several areas in the Fc region.

The interactions occurring when the antigen binds to the antibody is shown in **Figure 13**; hydrogen and ionic bonding in addition to Wan der Vaals and hydrophobic interactions.

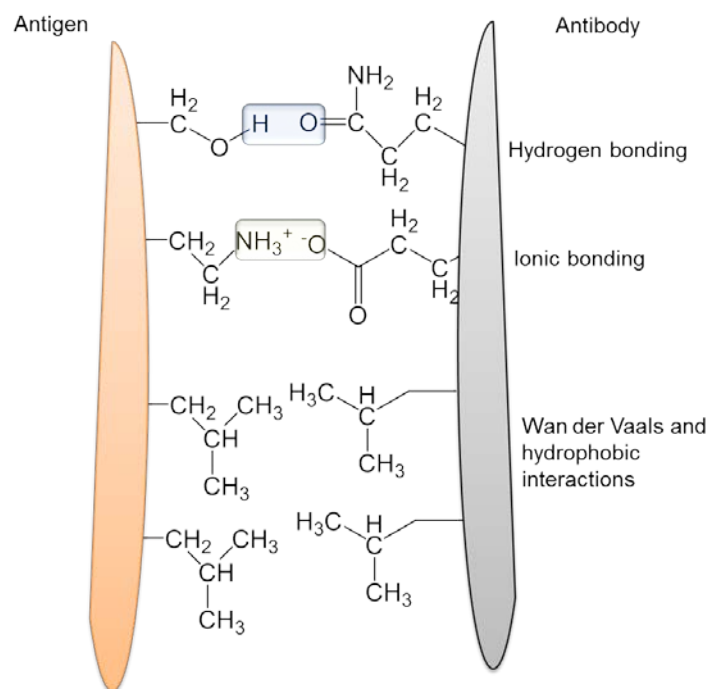


Figure 13: The interactions occurring when the antigen binds to the antibody with suggestions of the amino acids involved. Hydrogen bonding, showed here between serine (antigen side) and glutamine (antibody side). Next ionic bonding occurs between lysine (the full structure not shown) and glutamate. At last Wan der Vaals and hydrophobic interactions occurs with leucine amino acids.

The reproducibility is a potential problem in all scientific disciplines, and there is no exception with the use of antibodies to identify proteins. The sensitivity and specificity of the antibody can vary between batches and differences in protein conformation and target accessibility may cause inadequate performance in different contexts [91-93].

1.6.2 Bottom-up and top-down proteomics

While WB generally depends on the specificity of the antibody used, MS rely on multiple parameters (as retention time, mass to charge ratio of the precursor ion and selected fragment ions of the peptide or protein) leading to the identification and or quantification of the protein of interest, often with a higher quality than with WB. This can be done by analysing intact proteins (called top-down proteomics) and their direct fragmentation to peptides enabling the protein identification by database retrieval. One other technique is analysing the digested (controlled digestion) peptides from the proteins of interest by proteolysis (called bottom-up proteomics, see **Figure 14**). Here, the fragmentation pattern of these peptides is used identify the protein by database retrieval.

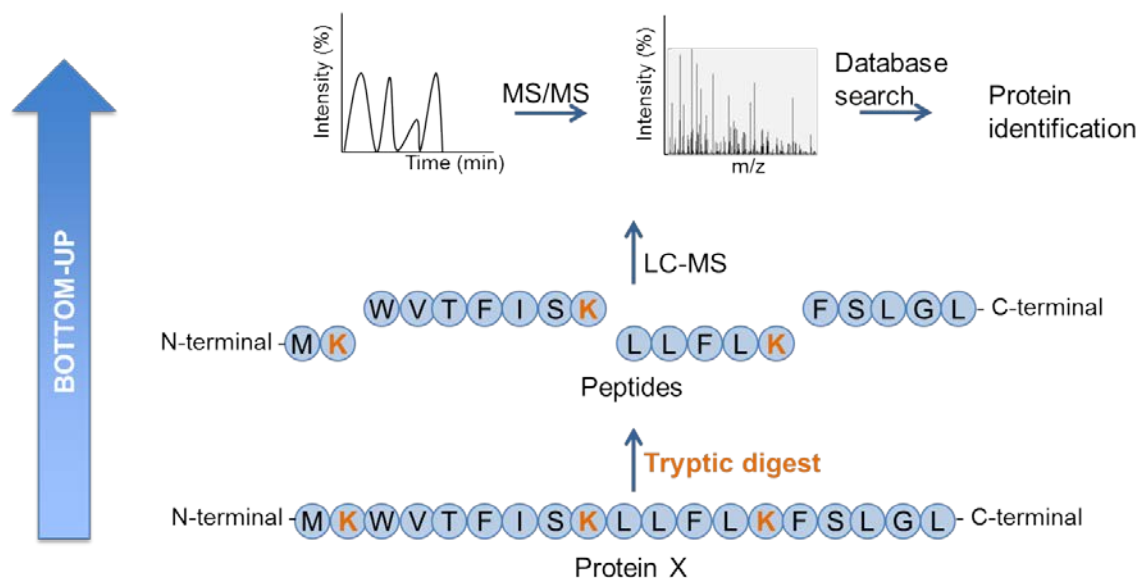


Figure 14: Schematic presentation of bottom-up proteomics. Protein X is digested to peptides by proteolysis (with trypsin). The sample is run through a LC-MS system resulting in a peptide chromatogram with peptide fragmentation pattern (MS/MS). The raw files are searched against a database and protein X is identified with certain coverage.

Even though the mass spectrometers are able to measure the mass of intact proteins, the bottom-up approach is preferred. Partly hydrophobic proteins are not always soluble under the same conditions as other proteins; in addition the sensitivity of the MS is much lower for peptides than for proteins. When handling complex protein mixtures, the top-down approach has large difficulties in the separation of these, and it often requires 1-2 orders of magnitude more material than the current bottom-up analysis [94]. At last, bottom-up MS is the most commonly used method as peptides provides with less complex spectra than intact proteins (peptides have limited charge and possible modifications). However, top-down proteomics

would be of interest when the purpose is to achieve information to distinguish between protein isoforms and on post-translational modifications [95, 96].

1.6.3 Sample preparation prior to analysis

Although MS plays a central role in proteomics, optimized sample preparation is required for obtaining reliable results. The sample preparation for bottom up proteomics typically encompasses the extraction of proteins via cell and exosome lysis, enrichment and digestion steps for intact proteins, with the goal for these steps to be performed efficiently, without sample loss or residual interferences.

Extraction

To extract the proteins present in the cells or exosomes the plasma membrane has to be disrupted, this can either be done by mechanical disruption (e.g. freeze-thaw cycles or sonication) or by non-mechanical methods using enzymes or chemicals. To solubilize the proteins, detergents are required. Detergents are molecules containing both hydrophilic and hydrophobic domains, which allow the formation of micelle structure. By binding to the hydrophobic surfaces of the proteins they extract the partly hydrophobic integral membrane proteins and maintain the solubility of these. The chemical structures of two commonly used detergents are shown in **Figure 15**.

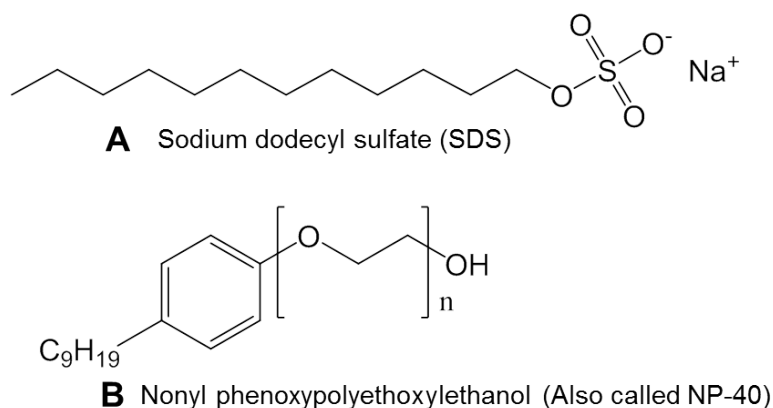


Figure 15: Chemical structure of two commonly used detergents; A) Sodium dodecyl sulfate (SDS) and B) Nonyl phenoxypolyethoxyethanol (also called NP-40).

SDS (**Figure 15 A**) is an anionic detergent which forms hydrophobic interactions (with the hydrophobic tail) with polypeptide chains, thus breaking the existing protein-protein interactions. In addition its head group interacts with positively charged side chains of the proteins, disrupting the ionic protein-protein interaction. The proteins are solubilized and are sterically hindered against enzymatic digestion; however it is challenging to remove SDS

completely. SDS binds to the reversed-phase (RP) column used for separation of the peptides prior to MS-analysis, and serve as an ion exchanger and retard the peptide elution time out from the column (also called retention time). In addition their high concentration compared to the low-abundant proteins result in ion suppression during ionization [97]. NP-40 is an example of a non-ionic detergent (**Figure 15 B**). Contrary to SDS it disrupts lipid-lipid and lipid-protein interactions and is considered a rather mild detergent. Neither this component is fully compatible with the MS-system.

When the protein is extracted, there are two options for further sample preparation; in-gel or in-solution. In-gel proposes an additional step by further separation/purification of the proteins by GE (for principles with this technique see paragraph 1.6.1). This is mostly used if there is a need for additional resolution when investigating complex protein mixtures or proteins of low abundance.

Denaturation, unfoldment, reduction and alkylation

To ensure optimal recovery of the proteolytic digestion of proteins, the contact area of the protein has to be as large as possible. Unfolding of the proteins is firstly done by denaturation either by heat (in-gel) or by adding a chaotrope (in-solution), a strong denaturing agent which stabilizes the unfolded protein states by hydrogen bonding and electrostatic interactions (e.g. urea, thiourea or guanidinium chloride). To further unfold the protein, disulfide bridges between cysteine residues need to be broken; this is most commonly done by reduction with the reducing agent dithiothreitol (DTT) (**Figure 16**).

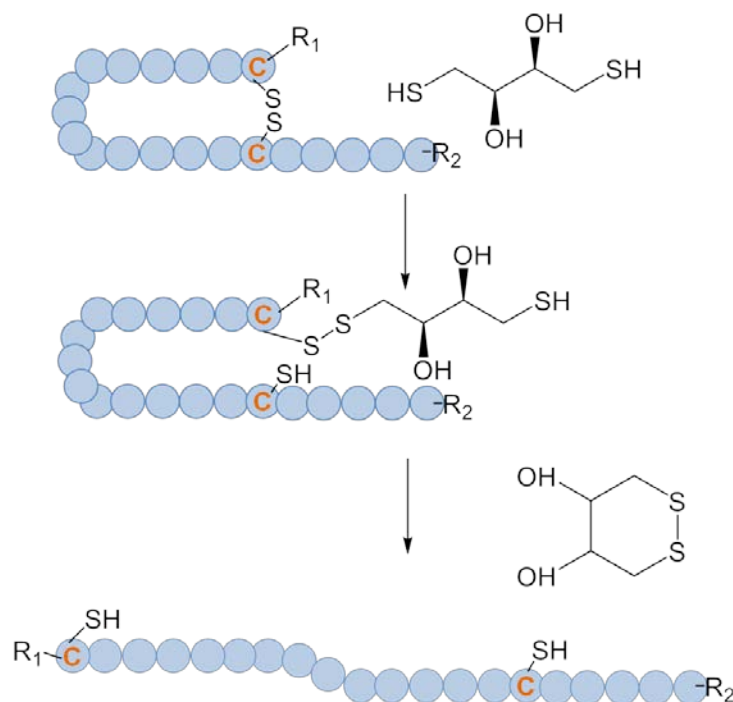


Figure 16: Reduction of disulfide bridges between cysteine (C) residues with DTT by two sequential thiol-disulfide exchange reactions. The blue circles symbolises an amino acid residue whereas the blue circles marked with C are cysteine residues. R1 and R2 are continuous peptide chains. The first reduction occurs when DTT forms a disulfide bridge with the sulfur of one cysteine. This releases one hydrogen ion forming thiol with the sulfur atom of the other cysteine. At last the ring structured DTT is formed, breaking the disulfide bond with cysteine. The second thiol group is formed by the released hydrogen ion.

Further, the free thiol groups are irreversible alkylated (S_N2 reaction) by Iodoacetamide (IAM) (also iodoacetic acid is used) preventing oxidation; hence the formation of new disulfide bridges (**Figure 17**).

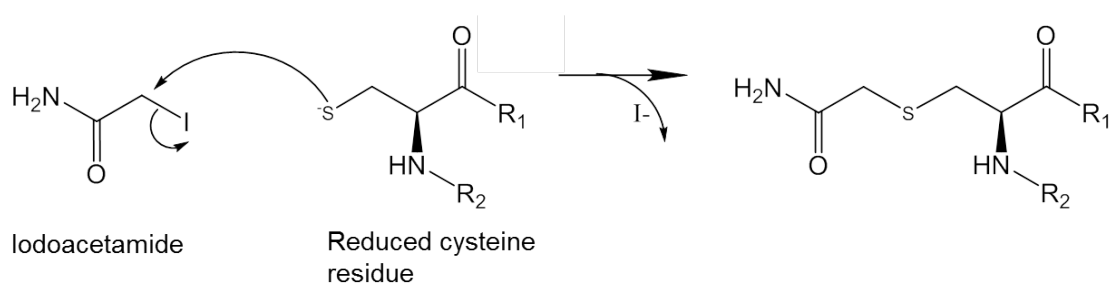


Figure 17: Alkylation of cysteine residues with IAM where R_1 and R_2 are continuous peptide chains. A nucleophilic attraction of sulfur (cysteine) to the carbon-atom of iodoacetamide occurs. This results in the formation of a covalent bond between these two, with the loss of an iodide ion.

A nucleophilic attraction of sulfur (cysteine) to the carbon-atom of iodoacetamide occurs. This results in the formation of a covalent bond between these two, with the loss of an iodide ion.

Proteolytic cleavage

Further the proteins have to be digested to peptides by a protease. The choice of proteases depends on if there is a special need for peptides of long sequences, where the cleavage will be performed or how repeatable the protease cuts. With very few exceptions trypsin is used for this purpose as it is stable, and specifically cleaves the C-terminal site of the amino acid residues arginine and lysine, by hydrolysis (**Figure 18**) [98, 99].

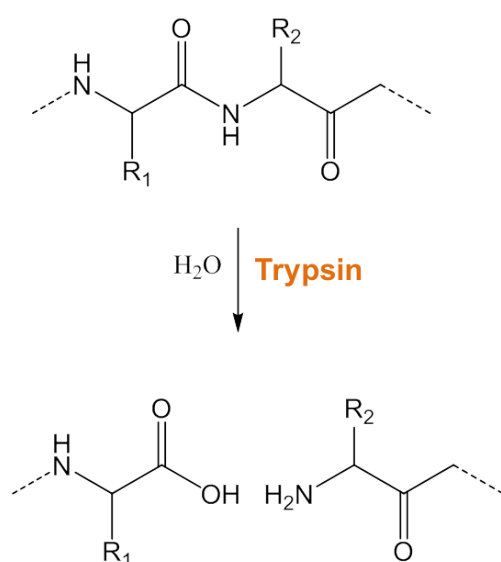


Figure 18: Proteolytic cleavages of C-terminal sites with trypsin, if R_1 is lysine or arginine, by hydrolysis.

However the cleavage specificity is often observed to be not complete if the following amino acid to arginine or lysine is proline, if two or more arginine, lysine or protonated histidine follows each other (cleaved after the most C-terminal positively charged residue). At last this also concerns if the deprotonated residues like aspartate or glutamate are close to lysine or arginine [98]. Often Lys-C is used before or in parallel [100] with trypsin digestion, this under harsh solubilizing conditions.

1.6.4 Liquid chromatography

Subjecting each protein to a tryptic digest generates high complexity sample and requires extensive separation prior to MS analysis. With liquid chromatography (LC) the peptides (i.e. analytes) are separated as a result from their different distribution (hydrophobic interactions) between the mobile phase (MP) (transporting the peptides) and the stationary phase (SP) which is bound to a column [101].

The particles are most commonly totally porous (pore size of 100-300 Å) and can range in size from 2-5 μm . The column length varies from 5-30 cm (longer columns being more suited

for higher peak-capacity while shorter columns would be more suited for faster analysis) and the inner diameter (ID) varying from 2-5 mm (conventional columns) down to 0.01-0.10 (nano-columns).

In proteomics the SP is usually highly hydrophobic C₁₈ coated silica particles (see **Figure 19** for chemical structure of the SP). The peptides are eluted in order of their hydrophobicity by increasing the organic solvent ratio of the MP (acetonitrile (ACN) or methanol: water), also called gradient elution. This is contrary to isocratic elution holding a constant organic solvent ratio of the MP throughout the run. This method is called reversed-phase (RP) high performance (or pressure) liquid chromatography (HPLC).

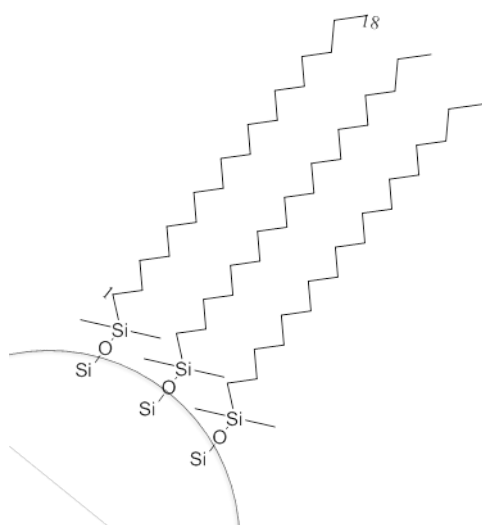


Figure 19: The chemical structure of the silica particle connected with C₁₈ stationary phase.

Another method in peptide chromatography is ion exchange chromatography (IEX), where the particles (often a polymer, due to its wider pH stability compared to silica) are coupled to

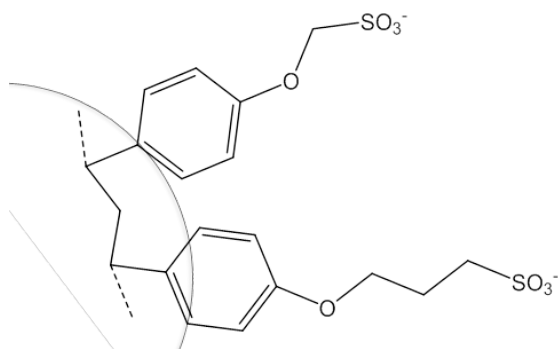


Figure 20: The chemical structure of a polystyrene surface of a polymer particle, connected with the acids sulfonate (top) and sulfopropyl (bottom) as examples of strong cation exchangers.

a cation exchanger (often a strong cation exchanger as sulfopropyl, or sulfonate, structures shown in **Figure 20**). The peptides are separated according to their charge and gradient eluted by increasing the ion strength gradient or pH of the MP. However, having high ion strength (high salt content) in the mobile phase

is not compatible with MS [102]. This is one of the reasons for why IEX chromatography is more commonly used in combination with RP

chromatography (called 2D chromatography) when higher peak capacity (i.e. how many compounds the system can separate) is required [103].

Downscaling

A comprehensive analysis of the low-abundant peptides in complex mixtures requires a system of high sensitivity, resolution and a wider dynamic range. For this reason, nano-columns are commonly applied in proteomics [104-106]. The narrow inner diameter of the nano LC columns (0.01-0.10 mm) reduces the radial dilution of the chromatographic bands (when equal amount of sample is injected), theoretically enhancing the sensitivity for concentration sensitive detectors (i.e. ESI-MS) (The chromatographic dilution of a conventional and narrow column is seen in **Figure 21**). The axial dilution remains equal.

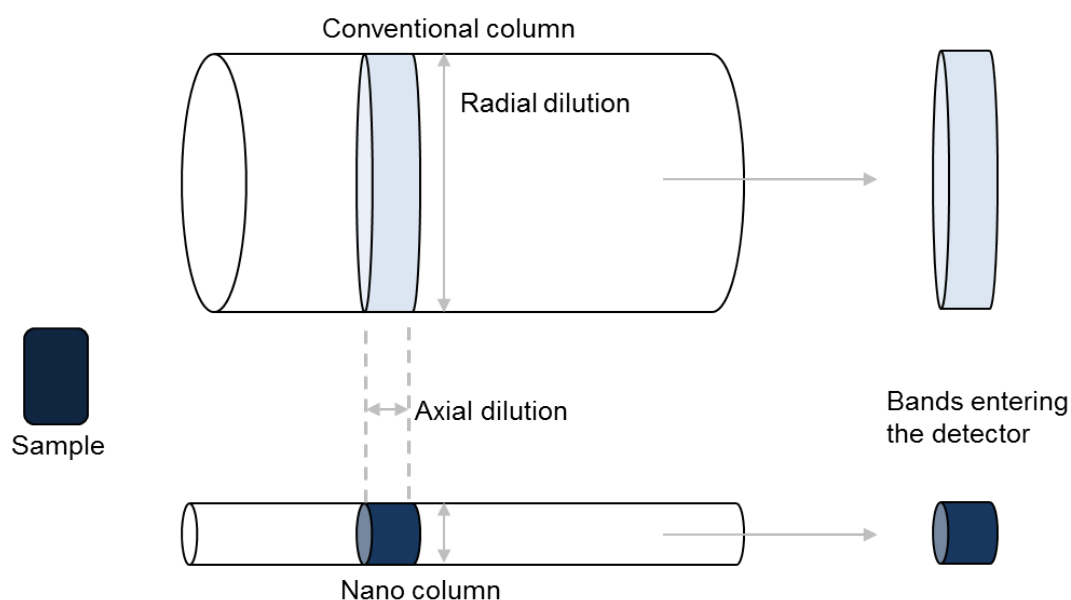


Figure 21: Chromatographic dilution of a conventional and narrow column. The colour intensity reflects the concentrations of the sample throughout the run; darker colour reflects higher concentration. Equal amount of sample is injected to the two columns of different inner diameter. The axial dilution stays the same, while the radial dilution of the sample is larger through the conventional column than the narrow column. When reaching the concentration sensitive detector, the signal from the conventional column is reduced. Contrary, an enhanced signal is achieved when a narrow column is used. Figure adapted from [105].

Operating at the same linear velocity (cm/s) as conventional columns, the separation length and backpressure (pressure drop over the column) still remains the same. The lower flow rate created when the same linear velocity is achieved (20-500 nL/min) compared to conventional systems (500-2500 nL/min), is favourable as the ESI unit generates smaller droplets improving the transfer of ions into the MS [107]. Downscaling from a conventional system is easily proceeded [108, 109]. However, obtaining uniformed packing of the particles inside these columns is one concern (i.e. influences the efficiency of the column hence the peak broadening) [110] and the robustness of the system one other.

1.6.5 Electrospray ionization (ESI)

The peptides are of high masses (kDa), highly polar and non-volatile. This makes them rather difficult to transform into gas phase without decomposing. A way out of this challenge is the use of softer ionization techniques (non-decomposing) as ESI or matrix-assisted laser desorption/ionization (MALDI) [94]. Contrary to MALDI, ESI is easily coupled on-line with the chromatographic system and the process is performed at atmospheric pressure [111]. As ESI was applied in this thesis, the principles of MALDI will not be further described.

The analytical column is coupled to a conducting needle (also called an emitter) which is held at a high electrical potential (up to 5 kV) between the needle and the MS-inlet creating an electric field. When in positive mode, the mobile phase containing the peptides (already protonated and positively charged) is dispersed and creates a spray forming a Taylor cone [112] at the outlet of the emitter (while the negative ions . In addition to the mixing with a nebulizing gas (often N₂); this facilitates the formation of positively charged droplets. The droplets are attracted towards the negatively charged MS inlet, while a stream of dry gas is moving in the opposite direction to further evaporate the solvent (MP content has to be volatile) from the droplets. This decreases the size of the droplets and increases the charge density (of the equally charged ions). When the repulsive forces (Coulomb) inside the drop exceed the surface tension, the droplet explodes into smaller droplets. This is a continuous process. For the last process of transforming the highly charged droplets into gas phase ions, two models are proposed. One model suggests the explosion of droplets continuous until only charged analyte ions (in gas phase) are left, commonly suggested for larger molecules (e.g. proteins or peptides). Regarding smaller molecules, it has been suggested that the ion leaves the highly charged droplet when the solvent evaporates (because of the high surface tension).

Nano-ESI

With the downscaling of a chromatographic system, the electrospray source is also miniaturized down to what is called a nano-ESI (or nanospray) [113] (**Figure 22**). The principles are the same, however without the use of nebulizing and drying gas. The small capillaries allow small flow rate, yielding in the formation of smaller highly charged droplets exploding into smaller droplets at a higher rate. This process is further escalating as the evaporation of the solvents also occurs at a higher rate with smaller droplets. As a result this

releases more ions into gas phase, also the analyte ions with lower mobilities, giving lower detection limit (sensitivity) of the system.

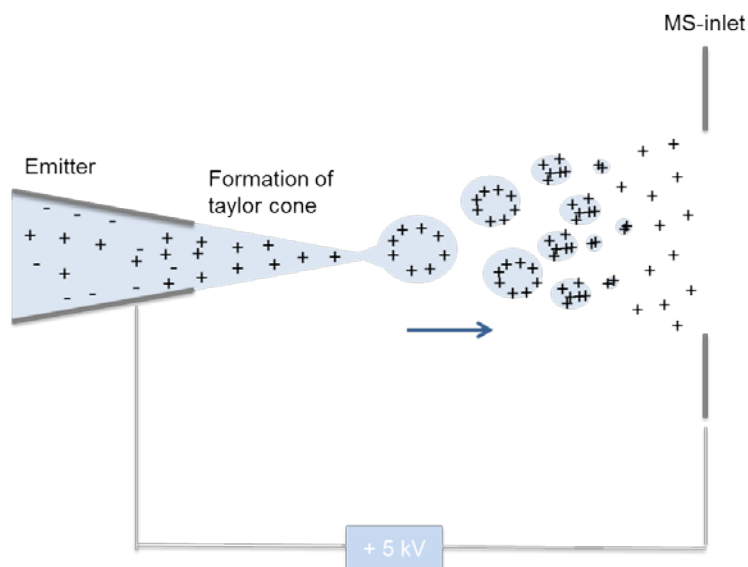


Figure 22: The process of ionization with nano-electrospray before entering the MS. A high electrical potential (up to +5 kV) is held between the needle and the MS-inlet creating an electric field. The mobile phase containing the peptides (already protonated and positively charged) is dispersed and creates a spray forming a Taylor cone from the emitter outlet. The droplets are attracted towards the negatively charged MS inlet, while the high charge density of the droplets leads to an explosion into smaller droplets (when repulsive forces inside the drop exceed the surface tension) This continues until each droplet contains only one analyte ion.

1.6.6 Mass spectrometry

Mass spectrometry is used to separate and identify ions according to their mass to charge ratio (m/z). This is done by controlling the ion trajectories by either applying a dynamic electric field or a magnetic field throughout a mass analyzer. The Q-exactive used in this work holds both a quadrupole and an orbitrap for this purpose (**Figure 23**). The path of the ions through the mass spectrometer starts with entering the MS-inlet from the ion source. The ions are led through the ion guide entering the quadrupole. The quadrupole (also called a mass filter) consist of four rod electrodes where each pair operates with direct current and alternating current. This creates an oscillating electrical field along the axis. The ions with unstable trajectories hit the rods, while stable trajectory ions reach the end of the mass filter. The combination of direct and alternating current can be adjusted depending on the m/z of the molecule ions of interest; the potential increases with the increasing charge and mass of the ions. However in comprehensive proteomics there is not only one target molecule; hence a range of potentials corresponding to the m/z range of interest is applied (which is commonly ranging from 350-2000 m/z).

The ions reach the C-trap, where they are relaxed and accelerated at high velocity towards the Orbitrap. The orbitrap consist of two electrodes; the central and outer electrode. High voltage is applied between these electrodes; the occurring electric field bends the trajectory of the ions towards the central electrode while their tangential velocity (the velocity created when moving in circular path) creates an opposing centrifugal force. The oscillation frequencies (proportional to $(m/z)^{1/2}$) of the ions are detected using image current detection and transformed into a mass spectrum with the use of a Fourier Transform algorithm [114].

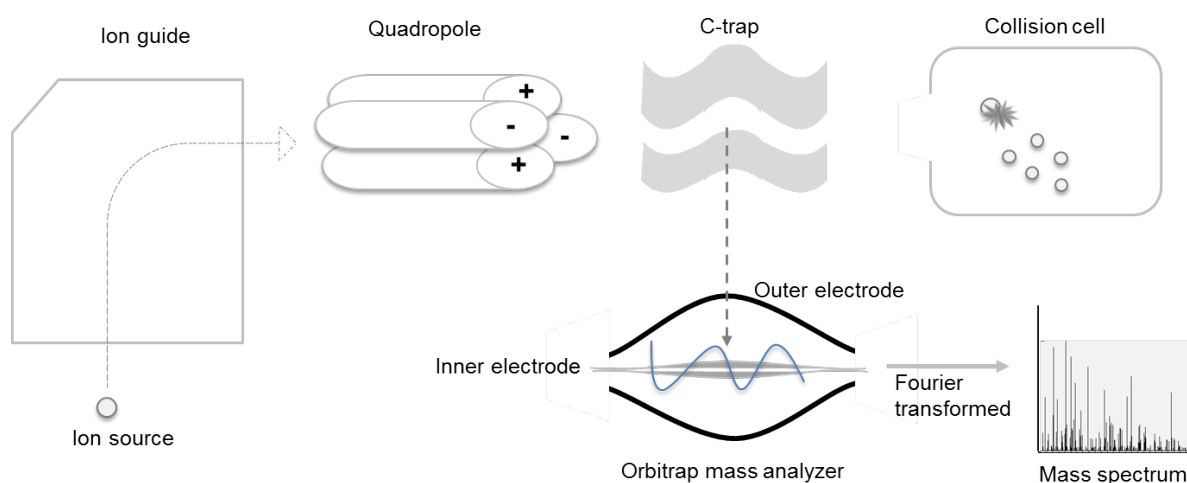


Figure 23: The sketch of sentral parts of a Q-exactive orbitrap. The ions enter the mass analyzer from the ion source and are led through an ion guide to the mass selective quadropole. By optimization of direct- and alternating current, the unwanted ions with get unstable trajectories and hit the rods, while stable trajectory ions reach the end of the mass filter. Reaching the C-trap, the ions are relaxed and accelerated at high velocity towards the Obritrap. Here, the ions oscillate with different frequencies around the inner electrode which is detected using image current detection and transformed into a mass spectrum with the use of a Fourier Transform algorithm. When in MS/MS mode, the ions are transferred from the C-trap to a higher energy collisional dissociation cell (HCD), where fragmentation occurs (with N_2). The drawing is not to scale.

When in MS/MS mode (or tandem-MS) the ions are transferred from the C-trap to a higher energy collisional dissociation cell (HCD), and the precursor ions are fragmented by colliding with an inert gas (such as nitrogen). The precursor ions entering the HCD can be controlled by data dependent acquisition, choosing only the most intense precursor ions (commonly 10) in a full scan MS are isolated to be further fragmented in an HCD.

The fragmentation of peptides in the HCD is caused by cleavage of the amide bonds (lowest energy pathway) forming b-ions and y-ions (**Figure 24**) [94]. Also a, c, z and x-ions might occur, however these fragmentations are not as frequently observed since their cleavage require greater energy.

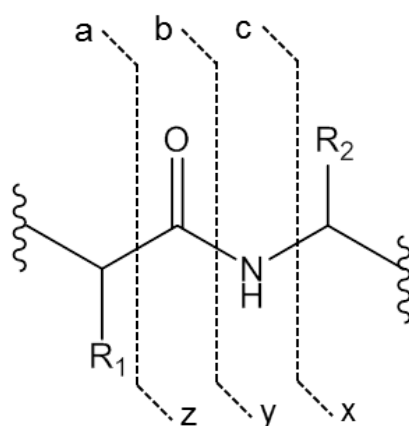


Figure 24: Schematic representation of the fragmentation of a precursor peptide ion in the MS. The fragmentation is performed in the HCD, leading to the cleavage of the amide bonds forming b- and y-ions. a, c, z and x-ions also occur, however this is not frequently observed as their cleavage require greater energy.

After fragmentation, the product ions are transferred back to the orbitrap for measurement via the C-trap, resulting in an MS/MS spectrum.

1.6.7 Protein identification

The peptide raw mass spectrometry data obtained from MS and MS/MS now needs to be transformed to the identification of the protein of origin [115]. There are several database search algorithms for this purpose including MASCOT [116], SEQUEST [117] and OMASSA [118]. First the algorithms use the ion spectrum of a peptide examining the theoretical mass of all possible peptides against a mass interval around the experimental precursor mass of the peptide. Next the matching peptides are in silico fragmented (i.e. the fragmentation pattern is simulated by a software), and matched against the experimental fragmentation spectrum. The best ranked match is identified as the precursor peptide, identified with a search score which is a measure on the grade of similarity between the experimental and theoretical spectrum.

However the best match is not necessarily correct. Peptide identifications are further evaluated by estimating the rate of false-positive peptide identification of the results. This is done by performing a false discovery rate (FDR) analysis, by target-decoy search [119] (This can be done by Empirical Bayes approaches, but will not be described in this thesis) were all spectra are searched against a database of peptide sequences of reversed, randomized or shuffled sequences from the same database. The peptides identified by this search, are considered as false-positive peptides.

2 Aim of study

The aim of this study was to evaluate two different techniques for the isolation of exosomes from the cultured breast cancer cell lines MCF-7 and MDA-B-231; the commercial isolation kit from Thermo Fisher and differential ultracentrifugation. For evaluation, the following characterization techniques were used; BCA assay, DLS, TEM, WB and protein characterization with the use of nanoLC-MS/MS.

3 Materials and methods

Cell culturing, exosome isolation, protein measurements and WB were performed at the unit for Cell Signalling, led by Professor Stefan Krauss, Oslo University Hospital (OUS). Unless otherwise stated, the water used was type 1 water purified by a Direct-Q® water purification system from Millipore (Billerica, MA, USA).

3.1 Cell culturing and exosome isolation

The cell culture handling was performed in a Scanlaf biological safety cabinet class 2-Mars from Labogene (Lyngø, Denmark). All cell culture handling was performed sterile. The liquids were pre-heated to 37.5 °C either by an incubator from Termaks (Bergen, Norway) or in a water bath (Julabo, Seelbach, Germany). All cell lines were incubated in Forma™ Stericycle™ CO₂ incubator (Thermo Fisher, Waltham, MA, USA) holding a temperature of 37 °C in humidified atmosphere (5 % CO₂). Rosewell Park Memorial Institute (RPMI) 1640 growth medium depleted of phenol red (Sigma-Aldrich, St.Louis, MO, USA) was used as cell culture media supplemented with 50 mL fetal bovine serum (FBS, 10 %) (Thermo Fisher) or 50 mL exosome-depleted FBS (10 %) (System Biosciences, SBI, Palo Alto, CA, USA), in addition to 5 mL penicillin/streptomycin (P/S, 1 %) (Sigma- Aldrich). Information about the two different breast cancer cell lines applied in this study is shown in **Table 2**. They were purchased from American Type Culture Collection (ATCC®, Manassas, VA, USA).

Table 2: Information about the two different breast cancer cell lines applied in this study with their abbreviation, catalogue number, type of organism and organ (disease).

Cell line	Abbreviation	Catalogue number	Organism	Organ (disease)
Michigan Cancer Foundation-7	MCF-7	HTB-22™	<i>Homo sapiens</i>	Mammary gland; breast (adenocarcinoma). Estrogen receptor positive.
-	MDA-MB-231	HTB-26™	<i>Homo sapiens</i>	Mammary gland; breast (adenocarcinoma). Estrogen receptor negative.

When a new batch of cell line was to be grown, frozen cells (1 mL) were thawed and immediately added to the flask of interest (T75 or T175, Thermo Fisher) containing cell culture media (10 mL or 25 mL). Vortexing was performed by pipetting up and down with

pipettes from Sarstedt (Nümbrecht, Germany). The cell culture media was exchanged the following day. All cell lines were regularly examined for mycoplasma by Dr. Kaja Lund (unit for Cell Signalling, OUS) using MycoAlert™ detection kit from Lonza (Basel, Switzerland).

An Axiovert 200M microscope from Zeiss (Oberkochen, Germany) equipped with AxioCam was used to visualize the cell morphology of the cell lines grown. These were taken with Ph1 filter using the software AxioVision (version 3.1), adjusting the settings to 5x or 10x magnification.

3.1.1 Cell splitting

When reaching 80-90 % confluency, the cells were split; the cell culture media was removed, the flask was washed by adding phosphate buffered saline (PBS), purchased from the Department of Microbiology (MIK, OUS, Oslo, Norway) (8 mL or 16 mL), followed by carefully swirling of the flask and removal of the PBS. Next, trypsin-ethylenediaminetetraacetic acid (EDTA) (Sigma Aldrich) (2.5 mL) was used to detach cells from the flask surface. The cells were incubated (37 °C and in humidified atmosphere containing 5 % CO₂) until loosened (i.e. small white sheets floating in the cell culture media) and mixed by resuspension with cell culture media (normally 7.5 or 17.5 mL). The cells were split by removal of the desired amount of cell cultured media (e.g. when splitting 1+9, 9 mL or 18 mL of cell cultured media was removed) and refilled with freshly cell culture media. The removed cell cultured media was transferred to 15 mL tubes from Greiner Bio-One (Kremsmünster, Austria) and was further used for cell culturing prior to exosome isolation, discharged or further cryopreserved.

3.1.2 Cryopreserving

When cryopreserving, the amount of cells (cells/ mL cell culture media) was counted by adding 6 µL of the freshly vortexed solution onto a sterile cell counter glass which was inserted into the cell counter, both from Bio Rad (Hercules, CA, USA). Next, the liquid corresponding to 1 x10⁶ cells was added to 15 mL tubes, centrifuged at 684 RCF (g) (3 minutes at 23 °C) with a A-4-62 rotor centrifuge from Eppendorf (Hamburg, Germany), discharging the supernatant and dissolving the pellet in 900 µL FBS and 100 µL dimethyl sulfoxide (DMSO, Sigma Aldrich). The solution was transferred to a CryoTube™ vial, and the tubes were placed in an Mr.Frosty™ freezing container and stored at – 80 °C until frozen

(both purchased from Thermo Fisher). The tubes were then transferred to a nitrogen tank (containing N₂ (l) holding a temperature between - 195.95 °C and -210.15 °C).

3.1.3 Cell culturing prior to exosome isolation

The cells were counted (as in 3.1.2), and the proper amount of liquid (containing 1 x10⁶ or 2.3 x10⁶ cells) was distributed to 15 mL tubes and spun down at 906 RCF (g) (5 minutes at 23 °C). The supernatant was discharged and the pellet was suspended in 6 mL cell culture media (RPMI 1640, holding 10 % exosome depleted FBS and 1 % P/S), transferred to new flasks and refilled with additional cell culture media if required. An overview of the different amount of cells seeded out, duration of the experiment, flask size used and amount of media added- and harvested is shown in **Table 3**. The passage number of the cells grown prior to exosome isolation was from 7-11.

Table 3: Overview of differential experimental conditions; cell number seeded, duration of the experiment, flask size used, and amount of media seeded- and harvested.

Number of cells seeded	Duration, hours (days)	Flask size	Media added mL	Media harvested for isolation mL
1 x10⁶	72 (3)	T75	6	5
1 x10⁶	144 (6)	T75	6	5
1 x10⁶	168 (7)	T75	6	5
1 x10⁶	192 (8)	T75	6	5
2.3 x10⁶	168 (7)	T175	14	12

When harvesting, the cell culture media was transferred to 15 mL tubes and spun down at 906 RCF (g) (30 minutes at 23 °C), the supernatant was transferred to new 15 mL tubes and cryopreserved (-20 °C for three months, then moved to -80 °C) until further use. The remaining cells were washed by adding PBS (8 mL or 16 mL) followed by carefully swirling of the flask and removal of the PBS. Next, trypsin-EDTA (2.5 mL) was used to detach cells from the flask surface. The cells were incubated until loosened and mixed by resuspension with cell culture media (7.5 or 17.5 mL). Next the suspension was transferred to 15 mL tubes and the cell number was counted (as in 3.1.1). The tubes were centrifuged twice at 906 RCF (g) (5 minutes at 23 °C, the supernatant was discharged and the pellet suspended in 2 mL

PBS), and the pellet was dissolved in the preferred lysis buffer (see section **3.1.6**) or cryopreserved until further use (-20 °C).

3.1.4 Exosome isolation by ultracentrifugation

When isolating with the use of ultracentrifugation, volumes of 9 and 12 mL cell culture media was firstly thawed on ice and centrifuged at 1811 RCF (g) (5 minutes 20 °C). The supernatant was transferred to centrifuge tubes with round bottom from Greiner Bio-One (leaving suspension 0.5 cm above the pellet) and centrifuged at 20 000 RCF (g) (20 minutes 20 °C) with the Allegra 25R centrifuge (equipped with TA-14-50 rotor) from Beckman Coulter (Brea, CA, USA). The supernatant was transferred to polycarbonate ultracentrifugation tubes (Beckman Coulter) (leaving suspension 0.5 cm above the pellet), diluted with PBS until the tubes were full (~ 68 mL) and balanced with a TE2101 balance from Sartorius AS (Göttingen, Germany). The tubes were ultracentrifuged at 100 000 RCF (g) (90 minutes at 4 °C) with an L-80 ultracentrifuge (45 Ti rotor) from Beckman Coulter, the supernatant was removed (leaving suspension 1 cm above the pellet) and the pellet was suspended with PBS. The tubes were again balanced to hold equal weight, and run at 100 000 RCF (g) (90 minutes 4 °C). The supernatant was fully removed and the pellet was suspended in either 50 µL PBS (for DLS- and TEM-analyses) or the preferred lysis buffer (see section **3.1.6**).

3.1.5 Exosome isolation by isolation kit

The isolation of exosomes with the use of the Total Exosome Isolation Reagent (from cell culture media) was from Thermo Fisher. The isolation was performed using the protocol prepared by the supplier (See appendix, **Figure 40**). Volumes ranging from 0.5-9 mL cell culture media were isolated. The samples were centrifuged in centrifuge tubes with round bottom with the Allegra 25R centrifuge. The amount of volume isolated was limited by the amount of cell culture media available.

3.1.6 Cell and exosome lysis

RIPA ++ buffer

The RIPA ++ buffer was prepared by adding one tablet of both Phosphatase inhibitor tablets and EDTA-free protease inhibitor tablets (both from Roche, Basel, Switzerland) to 10 mL of radioimmunoprecipitation assay (RIPA) lysis and extraction buffer (Thermo Fisher),

vortexing until fully dissolved and kept on ice until use or stored in 1 mL aliquots (1.5 mL tubes from VWR) at -20 °C. RIPA ++ was reusable when kept on ice and refrozen after use.

NP-40 buffer

2.5 mL 1M 2-amino-2-(hydroxymethyl) propane-1,3-diol (tris) (pH 8, from MIK), 1.5 mL 5 M NaCl (99.995 % trace metals basis, Sigma), 1.5 mL NP-40 (Thermo Fisher) and 200 µL EDTA (Sigma) were mixed in a 50 mL tube and diluted with 43.4 mL water. The solution was frozen at -20 °C in 10 mL aliquots. When needed, one 10 mL aliquot was thawed; one protease inhibitor tablet and phosphatase inhibitor tablet were added and vortexed until dissolved. The solution was further aliquoted into 1 mL tubes, which were stored at -20 °C (stable for a few months). The NP-40 buffer was reusable when kept on ice and refrozen after use.

Lysis

For further analyses with LC-MS, the lysis of cells and exosomes was performed with the use of NP-40 buffer. WB analyses required lysis of cells and exosomes with RIPA ++ buffer. The cell pellet was dissolved in 1 mL RIPA ++ or NP-40 buffer, while the exosome pellet was dissolved in 100 µL RIPA ++ buffer or 50 µL NP-40 buffer. The suspension was transferred to 1.5 mL tubes and rotated on a SB3 rotator from Stuart Equipment (Stone, Staffordshire, UK) at 8 RPM (30 minutes, 4 °C) and snap frozen using liquid nitrogen. The samples were frozen until further use (-20 °C).

3.2 Determination of protein concentrations with BCA assay

The protein concentration was measured with PierceTM BCA Protein Assay Kit from Thermo Fisher. Lysed samples were thawed and centrifuged at 14 800 RPM (30 minutes at 2°C) using Heraeus Fresco 21 centrifuge (Thermo Fisher). The supernatant was transferred to new tubes and the pellet was disposed. Reagent A and B were mixed at a ratio of 50:1, and 100 µL of the mixture were distributed in a 96-microwell plate (VWR). The bovine serum albumin (BSA) calibration-standard following the BCA assay kit was distributed to the wells (triplicates) and diluted with PBS to a total volume of 110µL, yielding in seven wells with increasing amounts of BSA (0-7µg). Next, vortexing was performed by pipetting up and down. 10 µL of the sample were distributed to the wells as a duplicate or triplicate depending on the amount of sample available. The micro well plate was placed in an incubator holding

40

37.5 °C for 30 minutes prior to the protein measurement. Measurement was performed at 562 nm using Wallac Victor2 1420 multilabel counter and Wallac 1420 Workstation software (version 3.00), both from Perkin Elmer (Waltham, MA, USA). For calculation of μg protein, see appendix, section 7.1.2.

3.3 Western Blot

3.3.1 Sample preparation

5x loading buffer was made by mixing 0.6 mL 1M Tris-HCl (pH 6.6), 1mL 1 % bromophenol blue (w/v), 2 mL 10 % SDS, 0.5 mL 2-mercaptoethanol and 5 mL 50 % glycerol (v/v) (all from Sigma Aldrich) and 0.9 mL water. The mixture was vortexed and kept in 15 mL tubes at room temperature (RT) until use.

Prior to gel electrophoresis, lysed samples were thawed on ice if frozen, and the same amount of protein (μg) was distributed to new tubes, diluted giving equal volume with water before adding the correct amount of 5x Loading buffer to yield 1x.

3.3.2 Gel electrophoresis

The samples were placed on a heating block (2-3 minutes at 91 °C) from Grant Instruments (Shepreth, Cambridgeshire, UK). Meanwhile the proper gel (4-12 % 2-bis (2-hydroxyethyl) amino-2-(hydroxymethyl) propane-1,3-diol (Bis-Tris)) was inserted to the midi or mini Cell electrophoresis chamber (both Thermo Fisher). The chamber was filled with the proper running buffer; 10 mL of 2-(N-morpholino) ethanesulfonic acid (MES) or 3-morpholinopropane-1-sulfonic acid (MOPS) SDS Running Buffer (20x) diluted to 200 mL with tap water.

Two wells of the gel were merged using a scalpel if the distribution volume of the samples was above the maximum volume of the wells. The samples were distributed to the wells of the chamber (of volumes from 15-35 μL) by using microcapillary tips pipettes (VWR). One well per gel was loaded with 10 μL PageRuler™ Prestained protein ladder (Thermo Fisher). A voltage of 75 V (150 mA) was applied to the chamber with the power supply (Bio-Rad) for one hour, and increased to 110 V (150 mA) if the blue lane from bromophenol blue was horizontally distributed. The gel was monitored every 30 minutes until the lane had reached the end of the gel, and the voltage was turned off. The gel was opened with a spatula, the blue

lane at the end of the gel was cut and the upper part of the gel was cut at the proper kDa (which could be seen by blue lanes at different kDa by the protein ladder).

3.3.3 Protein transfer

The 10 x transfer buffer was made by mixing 30.3 g Trizma® base ($\geq 99\%$) and 144.0 g glycine ($\geq 99\%$, HPLC) both from Sigma, diluted to 1000 mL with water. Prior to use, 100 mL of the 10x buffer were mixed with 200 mL technical methanol (VWR) and 700 mL water. Both buffers were stored at RT.

The 45 μm nitrocellulose membrane (Thermo Fisher) was cut to fit the size of the gel and both the membrane and the gel were separately incubated in the 1x transfer buffer for 15 minutes.

Two Extra Thick Blot Filter Papers (Bio-Rad) were drenched with the 1x transfer buffer, and all four components were placed in the transfer chamber (Bio-Rad) with the following layering order starting at the bottom; filter paper, membrane, gel, filter paper. At every layer, 1x transfer buffer was added to keep the components moisturized. In addition, the body of a 10 mL pipette was rolled over every layer to remove air bubbles between the layers and excess fluid outside the transfer sandwich was wiped away. 1 W was applied, and the transfer chamber was left over night at 4 °C. The following day, the membrane was cut and the individual protein bands marked using a pencil.

3.3.4 Immunolabeling and visualizing

Tris buffered saline in polyoxyethylene (20) sorbitan monolaurate (TBS-T) was made by adding 10 TBS-Tween tablets from Medicago (Uppsala, Sweden) to a 5 L glass flask, diluted to the 5 L mark with water. The buffer was stored at RT.

A solution of 5 % (w/v) non-fat dry milk in TBS-T (5 % TBS-T) was made by diluting 25 g non-fat dry milk powder from PanReac AppliChem ITW reagents (Darmstadt, Germany) to the 500 mL mark of a 500 mL glass flask with TBS-T. The solution was stored at 4-8 °C and discharged subsequently 7 days.

The membranes were blocked in 5 % TBS-T for 1 hour on a mixing plate. The mixture of 5 % TBS-T was discharged and the membranes were transferred to 50 mL tubes containing 5

mL of the corresponding primary antibody solutions with dilution factor (diluted with 5 % TBS-T), listed in **Table 4**. The tubes were kept on a roller from Stuart (Stone, Staffordshire, UK) over night at 4 °C before the membranes were removed and washed twice with TBS-T for 10 minutes on a mixing plate. The membranes were transferred to new 50 mL tubes containing 5 mL of secondary antibody solutions reflecting the host animal of the primary antibody (e.g. anti-mouse, anti-rabbit, **Table 4**), and the tubes were kept on a roller for 2 hours at RT. Both the tubes with the primary and the secondary antibody solution were cryopreserved and reused once.

Table 4: Overview of the primary and secondary antibodies applied in WB and TEM, with information about dilution factor (diluted with 5 % TBS-T), clone if not polyclonal, host animal, catalogue number and supplier.

Antibody	Dilution factor	Clone, if not polyclonal	Host animal	Catalogue number	Supplier
CD9	1000	TS9	Mouse	10626D	Thermo Fisher
CD9	1000	DRAP-27	Rabbit	PA5-11559	Thermo Fisher
CD63	500	TS63	Mouse	10628D	Thermo Fisher
CD81	500	1.3.3.22	Mouse	MA5-13548	Thermo Fisher
CD81	500	M38	Mouse	10630D	Thermo Fisher
TSG101	500	-	Rabbit	T5701	Sigma
ALIX	500	-	Rabbit	ABC40	Millipore
flotillin-1	500	18/Flotillin-1	Mouse	610821	BD Biosciences, San Jose, CA, USA
calnexin	1000	37/Calnexin	Mouse	610523	BD Biosciences
actin	1000	-	Rabbit	A2066	Sigma
GAPDH	1000	6C5	Mouse	Sc-32233	Santa Cruz
Anti-mouse	10 000	-	Chicken	Sc-2954	Santa Cruz
Anti-rabbit	10 000	-	Chicken	Sc-2955	Santa Cruz
Anti-mouse		-	Rabbit	Z0259	Dako, Glostrup, Denmark

Next the membranes were further washed three times with TBS-T (30 minutes on a mixing plate). The fluid was replaced with equal amount of freshly mixed enhanced chemilumiscense prime (ECL-prime) (0.5 mL per membrane) from GE Healthcare (Buckinghamshire, UK) and pipetted from membrane to membrane for 3-5 minutes. Transparency films from Nobo (integrated part of ACCO Brands Corporation, Lake Zurich, IL, USA) were cut, and the membranes were put in between two sheets of the film with additional ECL-prime poured over the membranes. Bubbles in between the sheets were removed by “ironing” the film surface with thick filter paper. The bands were developed in a Chemidoc™ touch imaging system from Bio-Rad. To visualize the bands, the proper size of the live view was chosen inside the developer, chemilumiscense was chosen as setting and the exposure time was set depending on the antibody. For the proteins actin, GAPDH, TSG-101 and flotillin-1, a short exposure time of 60 seconds was sufficient for visualization. Other proteins were exposed for 3000-5000 seconds. The raw files were processed with the Image Lab™ Software (version 6.0) from Bio-Rad.

3.4 Sample preparation and TEM of exosomes

The copper grid (100 square mesh) from Electron Microscopy Sciences (Hatfield, PA, USA) was coated with formvar from Agar Scientific (Stansted, Essex, UK). This was performed by Professor Norbert Roos, Section for Physiology and Cell Biology, Department of Biosciences, University of Oslo (UiO). The solutions of 4 % uranyl acetate (w/v in water) and 1% gelatin from cold water fish skin (FSG) (v/v, in PBS) were purchased from Sigma and prepared by Professor Norbert Roos.

One drop of 5 to 50 μ L (depending on the amount of sample available) of the exosome samples was placed on clean Parafilm (VWR), and the formvar coated cobber grid was carefully placed to float on the drop with the coated side facing the suspension. The material was adsorbed for 5-20 minutes, before rinsing on two large drops of PBS (approximately 1000 μ L) for 5 minutes followed by incubation on a drop (8 μ L) of the desired primary antibody diluted (anti-CD9, 1+9 with 1 % FSG (v/v)) for 20 minutes.

Next the grids were washed on two large drops of PBS (approximately 1000 μ L) for 5 minutes. If bridging (i.e. secondary antibody) was necessary, the grid was incubated on a

drop (5 μL) of rabbit anti-mouse antibody (diluted 1:200 with 1 % FSG (v/v)) for 25 minutes, before repeating the washing on two drops of PBS (approximately 1000 μL) for 5 minutes.

Common for both bridging- and not bridging suspensions was that they were further incubated on a drop of diluted protein A-gold (1:50 in 1 % FSG (v/v)) (10 nm particles size) for 20 minutes, purchased from Cell Microscopy Core (CMC, University Medical Center Utrecht, Utrecht, The Netherlands). A final wash on 5 drops of PBS (2 minutes) followed by 5 drops of water (3 minutes) was performed before negative staining with 4 % uranyl acetate (w/v) for 2 minutes. The excess fluid was blot by gently pushing the grid sideways on a filter Whatman[®] qualitative filter paper (Sigma), and the grids were stored in a storage box at RT until use.

The grids were placed on a specimen quartet holder (EM-01070 SQH) and visualized with a JEM-1400Plus transmission electron microscope from JEOL (Peabody, MA, USA). Images were recorded at 80 kV by Professor Norbert Roos. Further image processing was done with Power Point software.

3.5 DLS

Filtration, analyses and calculations were done by Dr. Sara Bekhradnia, at the group of polymer chemistry led by Professor Bo Nyström, Department of Chemistry, UiO. The isolated samples were diluted to 3 mL with PBS. Filtration of the samples was done (5 μm pores, Millipore) and transferred to nuclear magnetic resonance (NMR) tubes (10 mm ID, 100 mm) prior to analysis. An ALV/CGS-8F multi-detector compact goniometer system with eight off fibre-optical detection units was applied for DLS-analyses, from ALV-GmbH (Langen, Germany).

3.6 Sample preparation prior to LC-MS analysis

All protein preparations were performed with the use of protein LoBind tubes from Eppendorf. Reduction, alkylation and digestion were commonly performed in a thermoshaker from Grand at 600-1000 RPM (Cambridge, Cambridgeshire, UK). Unless otherwise stated, the dilutions during sample preparations were performed using water (HiPerSolv Chromanorm[®]) from VWR. The proteins were digested either in-solution or in-gel.

3.6.1 Protein digestion in-solution with peptide desalting

Solutions

A 100 mM ammonium bicarbonate (ABC) solution was prepared by diluting 82 mg ABC ($\geq 99.9\%$, Sigma) to the 10 mL mark with water (in a 15 mL tube). While 50 mM ABC was made by diluting 1 mL 100 mM ABC with 1 mL water. Freshly prepared 6 M urea/ 100mM ABC was made by adding 359 mg urea (98 %, Sigma) to 1 mL 100 mM ABC, the solution was discharged after use. The 200 mM DTT/ 0.1 M Tris-HCl (pH 8) solution was made by adding 216 mg DTT ($\geq 99.0\%$, Sigma) to 7 mL of 0.1 M Tris-HCl (pH 8) (1 mL 1 M Tris-HCl (pH 8), MIK diluted to the 10 mL mark with water). Freshly made 200 mM IAM ($\geq 99.0\%$, Sigma) was prepared by adding ~37 mg IAM to 1 mL of water. The solution was kept in the dark until used and discharged after use. The solutions not discharged were stored at 4-8 °C.

Lys-C (5 μg from *Lysobacter enzymogens*, Sigma) was prepared by adding 500 μL water to the Lys-C container, vortexing and freezing aliquots of 100 μL (0.01 $\mu\text{g}/\mu\text{L}$) at - 20 °C. The solution of 0.02 $\mu\text{g}/\mu\text{L}$ trypsin solution was made by mixing sequencing grade modified trypsin (20 μg) with trypsin resuspension buffer (1 mL), both from Promega Biotech AB (Madison, WI, USA), freezing aliquots of 1 μg trypsin (50 μL) at - 20 °C. Human serum albumin (HSA) (99 %) was from Sigma. HSA-standards were prepared by solving 5 mg HSA in 10 mL water (0.5 $\mu\text{g}/\mu\text{L}$). Aliquots of 10 μL (5 μg) and 100 μL (50 μg) were stored at -20 °C. At last, 50 % formic acid (FA) (for mass spectrometry ~ 98 %, Sigma) was prepared by mixing 500 μL FA with 500 μL water.

Reduction and alkylation

The protein samples were concentrated by a Speed-VacTM from Thermo Fisher, and the pellet was dissolved in 25 μL 6 M urea/ 100mM ABC. Prior to protein reduction, 200 mM DTT/ 0.1 M Tris-HCl (pH 8) was added to a final concentration of 9.5 mM DTT (1.25 μL). The samples were mixed and incubated for 30 minutes at 30 °C. Next, protein alkylation was performed by adding 200 mM IAM to a final concentration of 25 mM (3.75 μL), and the samples were mixed and incubated for 60 minutes at RT in the dark. Reduction with DTT was repeated by adding 200 mM DTT/ 0.1 M Tris-HCl (pH 8) to a final concentration of 28 mM (5 μL) vortexing and incubating the samples for 30 minutes at 30 °C.

Digestion

The proteins were initially digested by adding 0.1 µg Lys-C (100 µL), followed by vortexing and incubation for 120 minutes at 37 °C. Next, 50 mM ABC was added to a final concentration of 19 mM (80 µL), followed by 1 µg trypsin (50 µL). After incubating the samples for 16 hours at 37 °C, the protease activity was terminated by adding 5 µL 50 % FA(v/v), giving a final concentration of 0.9 % FA.

Peptide desalting

The equilibration solution (giving 0.1 % TFA) was prepared by diluting 5 µL trifluoroacetic acid (TFA) (≥ 99.0 %, from Sigma) to the 5 mL mark with water (in a 15 mL tube). The wash solution (5 % methanol in 0.1 % TFA) was prepared by mixing 500 µL methanol (HiPerSolv Chromanorm®, VWR) with 10 µL TFA diluted to 10 mL with water. The elution solution (30 % ACN in 0.1 % TFA) was made by mixing 10 µL TFA and 3 mL ACN (HiPerSolv Chromanorm®, VWR), diluted to 10 mL with water. The solutions were stored at 4-8 °C.

Desalting and concentrating the samples were preceded with ZipTip® pipette tips (Silica particles with C₁₈ resin) from Millipore. The ZipTip was wetted by pipetting neat ACN (10 µL three times) and equilibrated by pipetting 10 µL of the equilibration solution three times. Next, the sample was pipetted through the ZipTip. Washing the ZipTip was performed by pipetting 10 µL of the washing solution five times. The peptides were eluted by adding 5 µL elution solution to a new tube and pipetting the ZipTip up and down for about 20 times. The filtrate was concentrated to dryness at 30 °C by the SpeedVac. The samples were frozen at -20 °C until further use (not more than 7 days).

3.6.2 Protein digestion in-gel

Solutions

The fixation buffer was made by adding 400 mL type 1 water and 100 mL acetic acid (99.7 + % from Acros organics, part of Thermo Fisher) to 500 mL technical methanol (VWR), giving 40 % water, 50 % methanol and 10 % acetic acid. A solution of 10 mM DTT/ 100 mM ABC was prepared by adding 190 mg DTT to 2.5 mL 100 mM ABC (395 mg in 50 mL water) giving 500 mM DTT/ 100 mM ABC, 4 µL 500 mM DTT was further diluted to 200 µL with 100 mM ABC giving 10 mM DTT/ 100 mM ABC. For alkylation, 55 mM IAM/ 100 mM ABC was made by adding 102 mg IAM to 1 mL 100 mM ABC giving 550 mM IAM/ 100

mM ABC, whereof 10 μ L was further diluted to 100 μ L with 100 mM ABC to give 55 mM IAM/ 100 mM ABC.

Prior to digestion, 10 % ACN in 10 mM ABC (1 mL 100 mM ABC diluted to 10 mL with water) (v/v) was prepared by adding 1 mL ACN to 9 mL 10 mM ABC. Next, 13 ng/ μ L trypsin was prepared by adding the content of one trypsin tube (20 μ g trypsin) to a 1.5 mL solution of 10 % ACN in 10 mM ABC (v/v). To prepare the extraction buffer of 5 % FA/ ACN 1:2 (v/v), 5 mL 5 % FA (v/v) (250 μ L FA diluted to 5 mL with water) was added to 10 mL neat ACN.

Gel electrophoresis and processing of bands from the gels

Prior to in-gel digestion, the samples were prepared (3 μ g protein) and run using the same procedures as with gel electrophoresis (section 3.3.2). BSA (3 μ g, used in BCA assays) was prepared in parallel. The gel was covered by a fixation buffer overnight (18 hours, 4°C), stained with Coomassie brilliant blue (Bio-Rad) for 4 hours at RT and destained overnight with type 1 water. The gel was cut horizontally to yield four fractions from each lane; approximately 0-25 kDa, 25-70 kDa, 70-250 kDa and 250-up kDa. The lane containing BSA was cut in the mass range of 55-70 kDa. Each fraction was sliced into cubes of 1 mm² and transferred to tubes. 500 μ L neat ACN was added and removed after 10 minutes of incubation and “spun-down” of the gel pieces.

Reduction and alkylation

10 mM DTT/ 100 mM ABC was added to cover the gel pieces (approximately 100 μ L) and the samples were incubated and mixed for 30 minutes at 56 °C. Next, the samples were cooled down to RT, 500 μ L neat ACN was once more added and removed after 10 minutes of incubation and “spun-down” of the gel pieces. 55 mM IAM was prepared and added to cover the gel pieces (approximately 100 μ L), the samples were mixed and incubated in the dark for 20 minutes at RT. The step with neat ACN was repeated, however now with occasional vortexing until the coomassie dye was more or less removed from the gel pieces (about 1 hour, until the gel pieces went from being dark purple to almost white).

Digestion and extraction

The buffered solution of 13 ng/ μ L trypsin (in 10 % ACN in 10 mM ABC (v/v)) was added to cover the gel pieces (approximately 100 μ L) and allowed to rehydrate for 30 minutes on ice. Additionally 50 μ L of 13 ng/ μ L trypsin was added to completely cover the gel pieces. The

gel pieces were again left for saturation (90 minutes on ice) before adding 20 μ L 10 mM ABC to ensure that the gel pieces were held wet during the enzymatic cleavage. The tubes were placed into a GC-17A oven from Shimadzu (Kyoto, Japan) with circulating thermostat holding 37 °C. The digest was incubated overnight (\geq 16 hours). The peptides were extracted from the gel by adding 100 μ L extraction buffer, incubating the samples for 15 minutes in a thermoshaker. As a final step, the supernatant was collected, the samples were concentrated to dryness and kept at -20 °C until further use (not more than 7 days). The remaining gel pieces were also kept at -20 °C.

3.7 LC-MS settings

Proteins digested in-gel were analysed in house and proteins digested in-solution were analysed by the Thiede Group, Department of Biosciences, UiO.

3.7.1 LC-MS settings with analyses in house

Prior to LC-MS analyses, the samples were thawed and dissolved in 15 μ L 0.1 % FA (v/v, water). The solution of 0.1 % FA (v/v) was prepared by adding 1 μ L FA to 990 μ L water. The protein samples were transferred to 0.3 mL microvials and enclosed with snap ring caps (11 mm), both from VWR. An EASY-nLC 1000 pump (with autosampler) from Thermo Fisher was applied throughout the experiments.

Columns and connections

Pre- and analytical columns were of 50 μ m ID 20- and 150 mm fused silica capillaries from Polymicro Technologies (Phoenix, AZ, USA), packed with C₁₈- Accucore particles (2.6 μ m beads, 80 Å pore size) from Thermo Fisher by PhD student Henriette Sjønes Berg. Pre- and analytical columns were additionally coupled by capillaries (i.e. fused silica capillaries of 20 μ m ID from Polymicro Technologies), stainless steel unions (ZU1C), steel nuts (1.4 mm) and ferrules (fused silica adapters, FS1.4), all three from Vici Valco (Houston, TX, USA). The LC-column was connected to a 40mm stainless steel nano-bore emitter (ES542, 20 μ m ID) from Thermo Fisher using “Upchurch PEEK Microtight® Connector Butt” with “MicroFingertight I Fittings” and a 360 μ m ID “Upchurch Microtight® Tubing Sleeve” from Sigma.

Mobile phases and gradients

The mobile phases consisted of water /FA (v/v, 99.9/ 0.1) and ACN/ FA (v/v, 99.9/ 0.1) abbreviated as MP A and MP B, respectively 10 μ L of the sample was picked up by the auto sampler with a flowrate of 20 μ L/ min. Trapping of analytes in the pre-column was performed with 100 % MP A with a maximum flow rate restricted not to reach above 500 bar (12 μ L). Both the pre-column and the analytical column were equilibrated between the runs with 2- and 5 μ L MP A with a maximum flow rate restricted not to reach above 600 bar.

The gradients were set depending on the sample complexity. A 50 minutes gradient elution was set for the peptides of HSA or BSA. Time of gradient elution, duration of the gradient, flow rate and percentage of MP B is shown in **Table 5**.

Table 5: The gradient elution set for the peptides of HSA or BSA, with time (minutes), duration of the gradient (minutes), flow rate (nL/min) and percentage of MP B (%).

Time, minutes	Duration of gradient, minutes	Flow nL/min	% B
0	0	130	3
30	30	130	15
33	3	130	50
35	2	130	95
50	15	130	95

A 150 minutes gradient elution was set for the exosome samples. Time of gradient elution, duration of the gradient, flow rate and percentage of MP B is shown in **Table 6**.

Table 6: The gradient elution set for the peptides in the exosome samples, with time (minutes), duration of the gradient (minutes), flow rate (nL/min) and percentage of MP B (%).

Time, minutes	Duration of gradient, minutes	Flow nL/min	% B
0	0	130	3
3	3	130	3
123	120	130	15
128	5	130	50
130	2	173	80
145	15	173	80

MS detection

The Q-Exactive™ (quadrupole orbitrap) MS was equipped with a nanoFlex nanospray ion source, both from Thermo Fisher. The capillary voltage was set to 1.8 kV (250 °C). The MS was operated in data-dependent (dd) positive mode to automatically switch between MS and MS/MS acquisition. Survey full scan MS spectra (with a mass filter of m/z 350 to 1850) were acquired with a resolution of 70 000, automatic gain control (AGC) of 1×10^6 and maximum injection time of 120 ms.

When in dd/MS/MS the resolving power was set to 17 500, the AGC to 1×10^5 and the maximum injection time to 60 ms. The normalized collision energy was set to 28 eV, charges of 1, 7 or ≥ 8 were excluded and dynamic exclusion was set to 70.0 seconds. The method allowed sequential isolation of up to the ten most intense ions depending on signal intensity (intensity threshold 2.0×10^4), with isolation window of m/z 1.8.

3.7.2 LC-MS settings with analyses by the Thiede group

Prior to LC-MS analyses, the samples were thawed and dissolved in 10 μ L 0.1 % FA (v/v, water). An Ultimate 3000 nano ultra-HPLC system from Dionex (Sunnyvale, CA, USA) was connected to the LC-MS system. The analytical column applied was an Acclaim PepMap 100 column (C18, 3 μ m beads, 100 Å, 75 μ m ID) of 500 mm bed length, also from Dionex.

MP A was set to water /FA (v/v, 99.9/ 0.1) and MP B was set to be ACN/ FA/ water (v/v/v, 90/ 0.1/ 9.9). The gradient elution of the analyses with time, duration of the gradient, flow rate and percentage of MP B is shown in **Table 7**.

Table 7: The gradient elution of the analyses performed by the Thiede group, with time (minutes), duration of the gradient (minutes), flow rate (nL/min) and percentage of MP B (%).

Time, minutes	Duration of gradient, minutes	Flow nL/min	% B
0	0	300	4
207	207	300	35
227	20	300	50
229	2	300	80

MS detection

The Q Exactive mass spectrometer was equipped with nano-ESI source and the MS was operated in data-dependent (dd) positive mode. Survey full scan MS spectra (with a mass filter of m/z 400 to 1700) were acquired with a resolution of 70 000, automatic gain control (AGC) of 3×10^6 and maximum injection time of 100 ms.

When in dd/MS/MS the resolving power was set to 35 000 and the maximum injection time to 120 ms. The dynamic exclusion was set to 60.0 seconds. The method allowed sequential isolation of up to the ten most intense ions depending on signal intensity (intensity threshold 1.7×10^4) isolation window was m/z 2 without offset.

3.8 Data procession and protein identification with gene ontology annotation

XCaliburTM (version 2.1) and Proteome Discoverer (version 1.4.0.228) were softwares used to identify peptides and proteins.

Mass spectra and chromatograms were acquired using the Xcalibur software, while protein identifications were implemented using Proteome Discoverer software. When only single proteins were to be identified (i.e. HSA or BSA), the respective FASTA-file (Fast-All, a DNA and protein sequence alignment) was downloaded (from the websites of UniProt) and searched against the obtained mass spectra with the use of SEQUEST algorithm. When the proteins in exosome samples were to be identified, both SEQUEST and MASCOT algorithms were applied and percolated to yield the protein identification, by searching with SwissProt (*Homo sapiens*, 20 198 reviewed sequences).

All searches were performed setting the digestion enzyme to be trypsin with maximum one missed cleavage, fragment ion mass tolerance of 0.10 Da, and a precursor mass tolerance of 10.0 ppm. Signal to noise (S/N) threshold was set to 1.5 and the minimum ion count to 1. Carbamidomethyl of cysteine was specified as static modification. Oxidation of methionine, acetylation of the N-terminus and deamidation of glutamine and asparagine (abbreviated Q and N) were specified as dynamic modifications. The proteins were identified as protein groups with high peptide confidence filter. All data was exported to Excel sheets and proteins identified as keratin or trypsin was removed from the list.

When the proteins identified were to be search for (with UniProt accession) gene ontology annotations the online search tool DAVID (version 6.8) was applied. The GO category “*Cellular component*” was selected and specific GO terms where manually chosen according to their appropriate relevance towards the identification of non-exosome and exosome related proteins in the samples which is presented in **Table 8**.

Table 8: Manually selected GO term IDs for different cellular components related to non-exosome and exosome related proteins; Extracellular exosome, extracellular matrix, plasma membrane, endosome, cytoskeleton, cytosol, nucleus, endoplasmic reticulum, golgi apparatus and low- and high-density lipoprotein particle.

Selected GO terms	GO term ID
Extracellular exosome	70062
Extracellular matrix	31012
Plasma membrane	5886
Endosome	5768
Cytoskeleton	5856
Cytosol	5829
Nucleus	5634
Endoplasmic reticulum	5783
Golgi apparatus	5794
Low-density lipoprotein particle	34362
High-density lipoprotein particle	34364

4 Results and discussion

In this study, two different techniques for the isolation of MCF-7 and MDA-MB-231 exosomes from cell culture media were evaluated; ultracentrifugation and an isolation kit from a commercial supplier (Thermo Fisher). All steps were evaluated starting with cell culturing considerations, the different aspects related to the isolation techniques (i.e. time, costs and operational simplicity) and the most commonly used characterization techniques; protein concentration with BCA assays, DLS, TEM with immunogold labelling, targeted proteomics by WB and comprehensive proteomic analysis using nanoLC-MS/MS. Central questions when evaluating the characterization techniques were asked; did the isolation methods isolate exosomes, and which isolation method gave the purest extracts (i.e. with little contamination e.g. from cell debris). To avoid false positives, blank samples (cell culture media) were examined in parallel.

The term “exosomes” is used throughout this thesis, however with awareness of that the isolated samples might also contain other EVs [121].

4.1 Cell culturing

The cell lines MDA-MB-231 and MCF-7 were studied in light of our group’s studies of breast cancer. The main difference between the two cell lines is the presence (MCF-7)- and absence (MDA-MB-231) of an estrogen receptor on their surface (which is influenced by the selective estrogen receptor modulator 27-hydroxycholesterol [122]).

4.1.1 Cell morphology

The MCF-7 and MDA-MB-231 cell lines were successfully grown without sign of mycoplasma present. The morphology of the cell lines is shown in **Figure 26**. The MDA-MB-231 morphology presented by the supplier [123] did correspond to the elongated structures of MDA-MB-231 (**Figure 26**). According to MCF-7 images presented by the supplier [124], MCF-7 holds a more rounded morphology than the cells presented in **Figure 26**. However, according to the supplier, it could look like MCF-7 could develop a more angular shape when grown at high density [124].

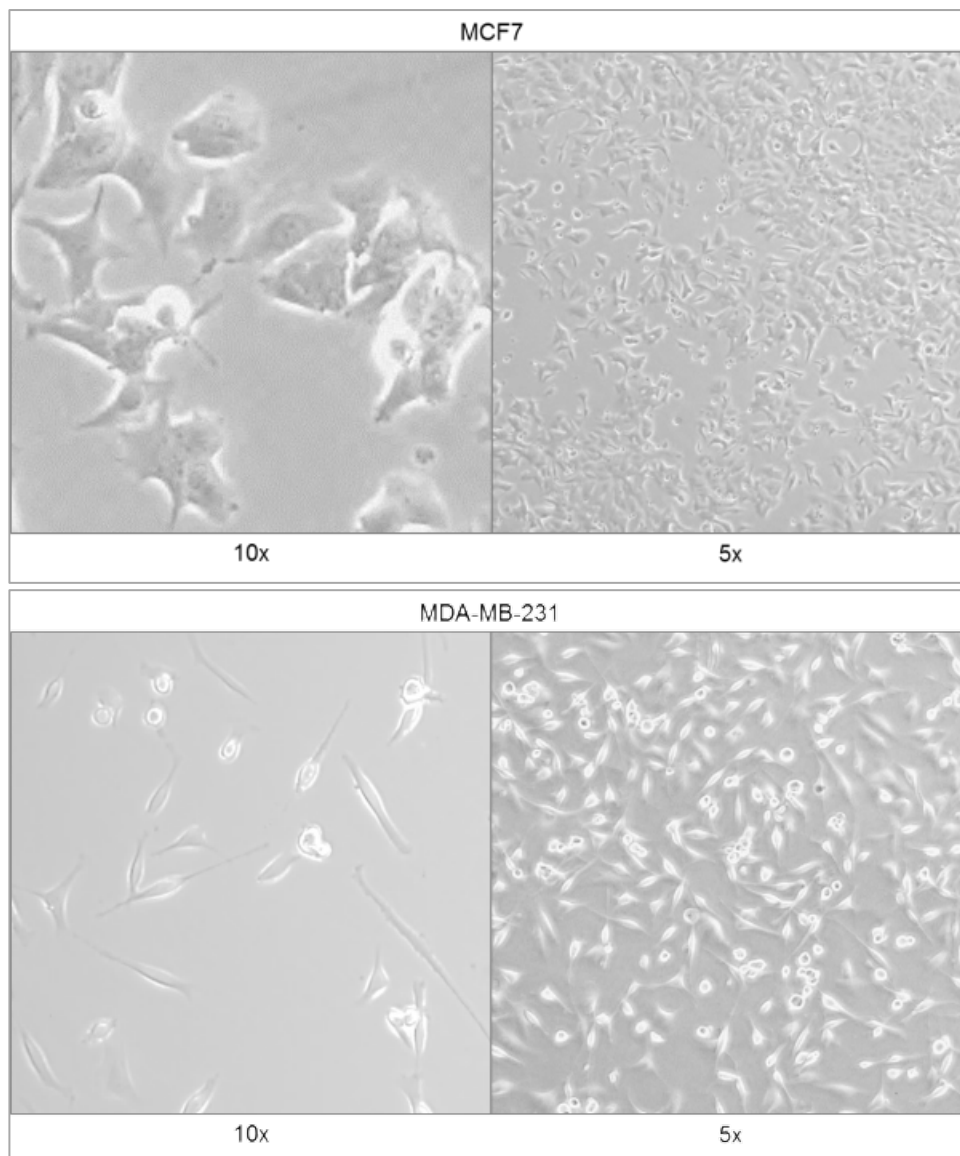


Figure 26: Pictures presenting the morphology of MCF-7 and MDA-MB-231 cell lines in culture, with the magnitude of 10 000 (10x) and 5000 (5x).

4.1.2 Cell confluency

The cells were grown in a T175 flask, and when confluent (i.e. 80-90 %) the counted amount of cells in the flasks was on average $8 \times 10^6 \pm 3 \times 10^6$ for MCF-7 and $20 \times 10^6 \pm 12 \times 10^6$ for MDA-MB-231 (data shown in appendix, section **7.3.1, Table 11**). The large standard deviation displays the uncertainty of this subjective estimation of confluency for the respective cell lines. Cell confluency nevertheless seems to be a widely used starting point for cell culturing prior to exosome isolation [30, 37, 41, 125, 126].

Due to the uncertainty related to the use of confluency as a starting point, seeding out a specific amount of cells was chosen. The cells were seeded out at a number of 1×10^6 cells in T75 flasks to investigate how the duration of incubation (3, 6, 7 and 8 days in 6 mL cell

culture media) affected the amount of cells counted. The amount of cells present at the end of each experiment did not increase linear with the increasing duration of the experiment (**Figure 27**). Plausible reasons could be cell death due to little nutrient available, too high cell confluency or a consequence of the seeding procedure.

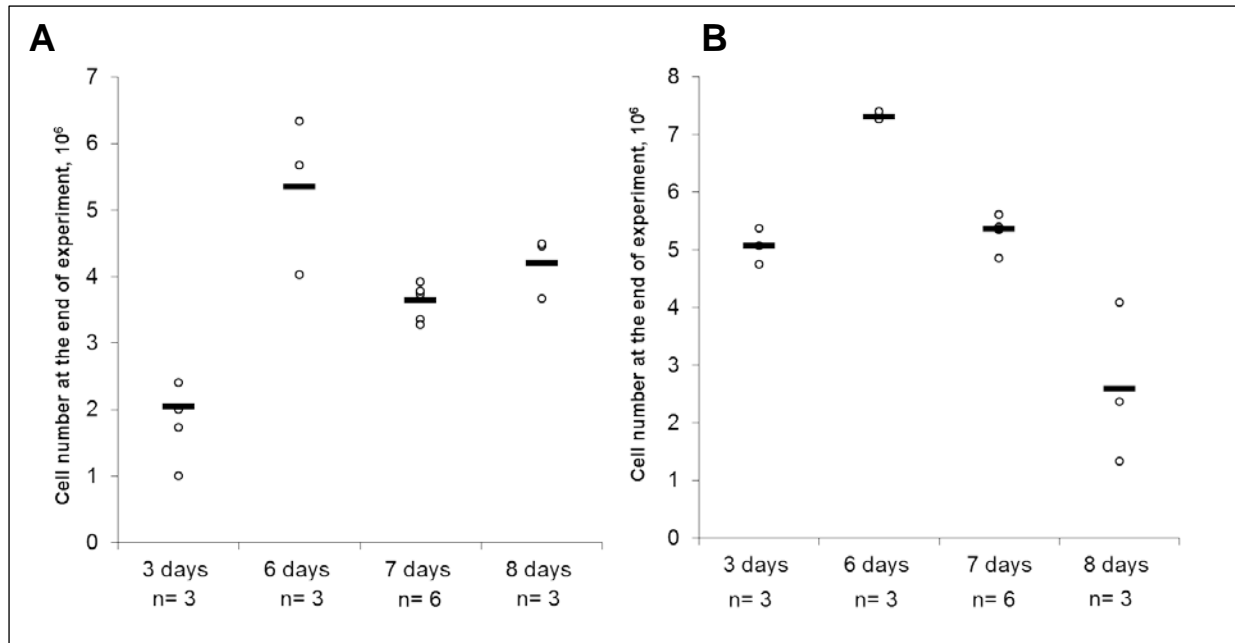


Figure 27: The average amount of cells measured at the end of each experiment, when starting out with a number of 1×10^6 cells grown in T75 flasks for; 3 days, 6 days, 7 days and 8 days for the two cell lines A) MCF-7 and B) MDA-MB-231.

Repeatable experiments were chosen over a high cell yield. Thus, a cell culturing duration of 7 days was chosen, displaying the highest cell yield with low standard deviations for MCF-7 and MDA-MB-231. As the isolation with UC demanded big volumes, the cell culturing duration considerations were upscaled to T175 flasks (by a factor of 2.3, i.e. 2.3×10^6 cells in 14 mL cell culture media).

To sum up, both MCF-7 and MDA-MB-231 cells were successfully cultured. The number of cells did not increase linear with time. Due to repeatability concerns, a cell culturing duration of 7 days was chosen and upscaled prior to UC-isolation experiments.

4.2 Isolation of exosomes

Different volumes of cell cultured media were isolated with isolation kit (0.5-9 mL) and UC (9-12 mL). To have enough material for isolating with UC (6 tubes), this required at least 3 weeks of culturing. A larger volume of cell medium would possibly yield in more exosomes. However, producing enough replicates to be able to implement and evaluate the different characterization techniques was of higher priority.

4.2.1 Time considerations

The isolation of exosomes with UC consisted of four centrifugations with a total duration of 3 hours and 25 minutes (**Table 9**). Additional operational work in between runs consisted of balancing, removal of supernatant and resuspension of the pellet. The isolation kit procedure contained two centrifugations with shorter duration (total of 1 hour and 30 minutes, **Table 9**). Hence the isolation kit was clearly the shortest and easiest method (operationally).

Table 9: Overview of the different centrifugations following the isolation of exosomes with ultracentrifugation and the isolation kit, with duration (minutes).

		Duration, minutes
Ultracentrifugation	Centrifugation 1811 g	5
	Centrifugation 20 000 g	20
	Ultracentrifugation 100 000 g	90
	Second ultracentrifugation 100 000 g	90
Sum		205 (3 hours, 25 minutes)
Isolation kit	Centrifugation 2000 g	30
	Centrifugation 10 000 g	60
Sum		90 (1 hour, 30 minutes)

4.2.2 Technical considerations

The pellet form of the sedimented material was not identical when comparing the different isolation methods (**Figure 28**). The pellet appearing after ultracentrifugation (left image in **Figure 28**) was commonly observed to be hardly visible (diameter of approximately <1 mm). Due to this, the UC-tubes were marked at the place the pellet was expected (**Figure 28**). In addition the pellet was loosely sedimented to the tube wall, hampering the removal of supernatant. One sample was discarded due to this issue. The sedimented material appearing after isolation kit centrifugation (right image in **Figure 28**) was repeatedly shaped as the

outline of a volumetric flask. This was suspected to be due to co-sedimentation of proteins from the FBS applied during cell culturing.

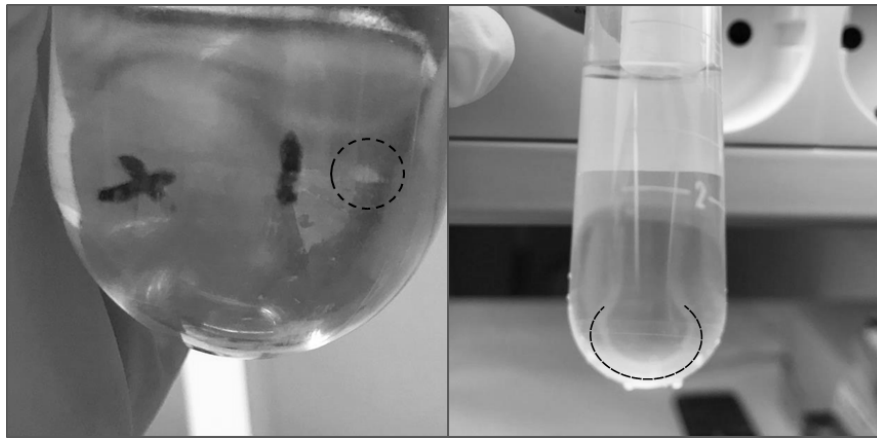


Figure 28: The form of the pellets after ultracentrifugation (left image), appearing inside the black circle. The pellet of the isolation kit (right image), was shaped as the outline of a volumetric flask.

The PBS used for the resuspension of the pellet during ultracentrifugation was sterile. However yellow-coloured precipitations were observed during one of the ultracentrifugations (with MCF-7). This was suspected to be bacterial contamination; hence the differential centrifugation was repeated with the aim to remove the contamination. This could impact the exosome yield and sample content.

Both methods require relatively equally expensive equipment when the centrifuges are omitted. The ultracentrifugation requires solid tubes. These tubes are reusable, but can easily undergo imploding. On the other hand the isolation kit itself was costly (unit size of 50 mL available for 2485 kr).

To sum up, isolation of exosomes with ultracentrifugation was more time consuming than with the isolation kit, in addition it demanded high operational skills. Isolation kit was estimated to be the most costly method.

4.3 Measurement of the protein amount of the isolated exosomes by BCA assay

In the literature the protein levels are presented as μg exosomes per 10^6 cells [37, 127], particle count (by NTA measurements) per μg protein [42, 64] or μg protein/ mL isolated substance [65]. NTA instrumentation was not accessible for this study, thus the protein measurements are presented as μg exosomes per 10^6 .

Isolation with the isolation kit generated approximately 6 orders of magnitude higher protein levels (μg protein/ 10^6 cells) than with UC (**Figure 29**). If directly related to exosome proteins, isolation kit would without doubt display the highest exosome yield. However co-isolation of non-exosome contaminants is a commonly known possible disadvantage with the use of commercial kits.

The low protein levels found with UC (**Figure 29**) could also reflect large sample loss, or purely isolated exosomes with little co-isolated contaminants. As seen in [128], samples isolated with commercial isolation kits provided recovery of noticeably more particles per mL isolated cell cultured media than ultracentrifugation ($2- 3.5 \times 10^{11}$ particles/ mL and $1-1.5 \times 10^9$ particles/ mL, with exosomes derived from the BT474 cell line), also observed by [129] (exosomes isolated from human serum). This could support the higher protein levels in the present study if the particles observed can be directly related to protein content. Additionally, use of the same commercial isolation kit as in this study gave 8 times more protein per 10^8 particles than UC [130] (with exosomes isolated from MCF-7 cell line).

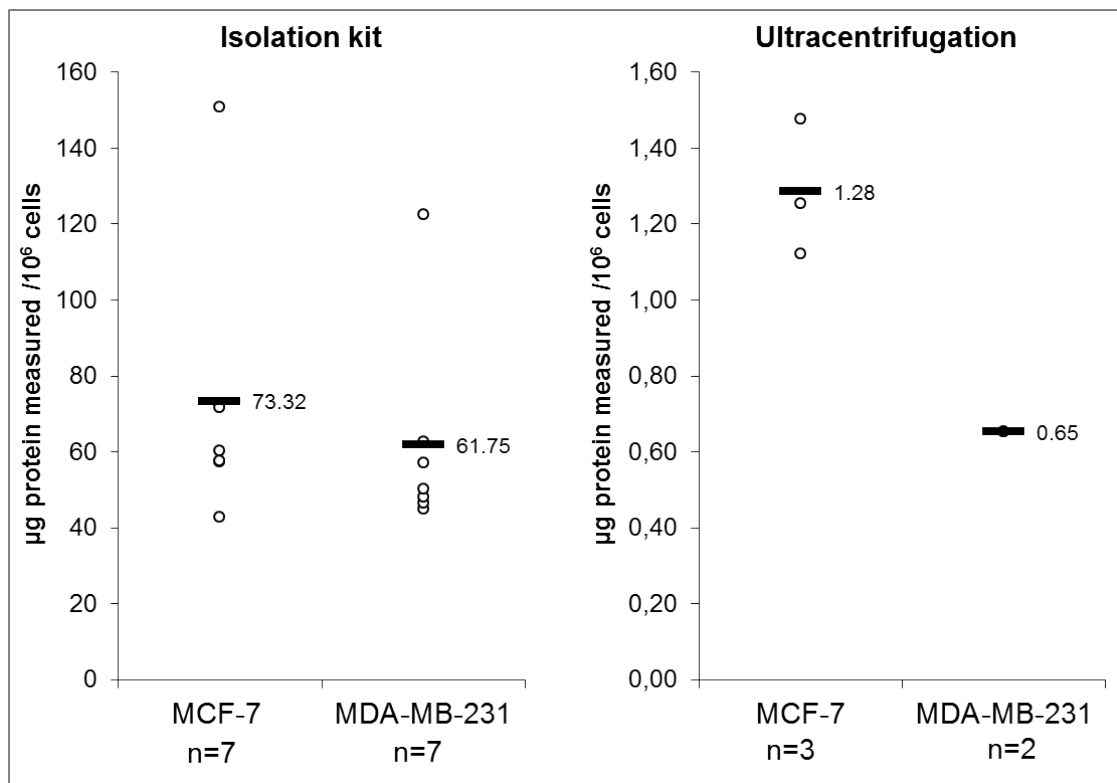


Figure 29: Scatter plot of the average μg protein measured/ 10^6 cells from samples isolated from MCF-7 and MDA-MB-231, by isolation kit (left scatter plot) and ultracentrifugation (right scatter plot). The different number of replicates measured is due to different amounts of material available.

However, as the content of the isolation kit is not stated, the high protein measurement could also possibly be caused by residues from the kit. If presence of reducing agents or Cu^{1+} ions, this would probably interfere with the BCA reagents, thus giving a false indication of the protein level.

To sum up, notable higher protein levels (μg protein/ 10^6 cells) were measured in samples isolated by isolation kit compared to samples isolated with UC. What does this mean? Isolating with the isolation kit potentially generates notably higher exosome yield than UC.

4.4 Size distribution with DLS

To determine the heterogeneity of the sample, the hydrodynamic size distribution of the particles present in the isolated samples was measured with DLS. DLS measurements can also be further used to determine co-isolation of other spherical particles with similar properties (size, density, surface charge), e.g. protein aggregates or lipoproteins (HDL, LDL and other triglyceride rich particles) [131-133]. However, it should be noted that these measurements do not discriminate vesicles from non-vesicular particulate material.

As the MCF-7 exosomes isolated with UC was possibly contaminated, these values were rejected and not further compared (values found in appendix, section 7.3.3). The scatter plot (**Figure 30**) indicated (n=2) that MCF-7 and MDA-MB-231 samples isolated with the isolation kit contained two populations of different hydrodynamic diameters, with sizes of approximately minimum 27 nm and maximum 103 nm (see appendix, section 7.3.3 for DLS raw files). Only one population was present of MDA-MB-231 derived exosomes with ultracentrifugation, and with larger hydrodynamic particle diameter (138 ± 25 nm).

The small populations measured (i.e. 33 and 27 nm, **Figure 30**) with samples isolated with the isolation kit could possibly be co-isolation with the lipoprotein LDL (25 nm diameter). However, populations in the lower size range (lower than 60 nm) were not observed when isolating with other commercial isolation kits (NTA measurements) [41]. However, one common drawback of NTA measurements is its limitations on the measurements of smaller particles. Hence not fully stating the purity of the different isolation methods, as proposed by [64]. On the other hand, DLS does not display if the samples are further polydisperse. In addition DLS is known for its sensitivity towards the presence of larger particles; hence this could also impact the accurate determination [70].

The hydrodynamic diameter of particles present in blank samples was measured to be about 67 nm (n=1). This could indicate the presence of possible contaminating particles of 67 nm. However this measurement needs to be repeated for confirmation.

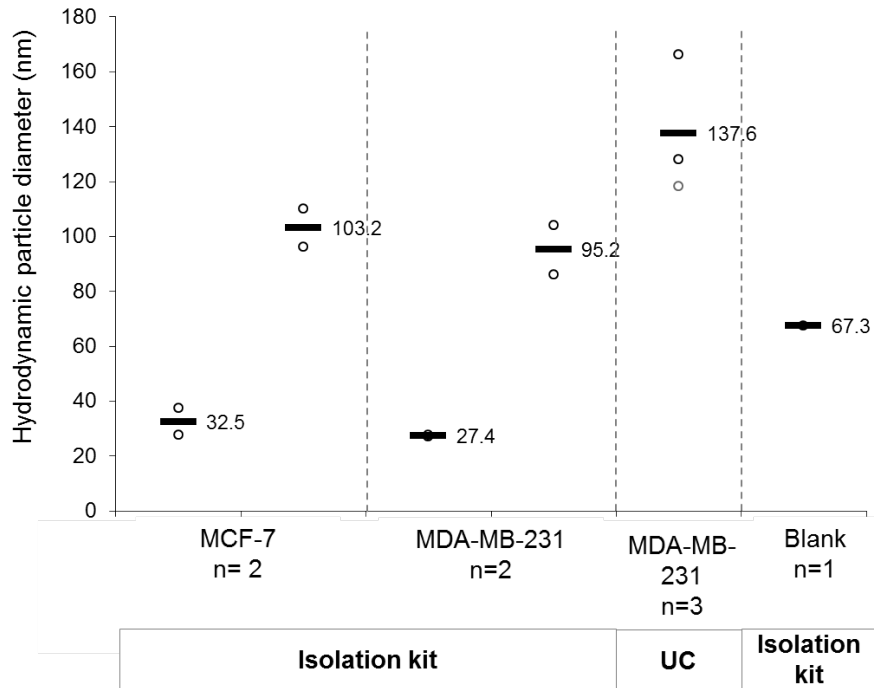


Figure 30: Hydrodynamic particle size distribution (measured by DLS) presented by a scatter plot of the average hydrodynamic particle diameter (in nm) of the isolated exosomes isolated by isolation kit and UC, using MCF-7 and MDA-MB-231 cell lines (in addition to blank sample isolated with the isolation kit). MCF-7 isolated with UC was rejected due to contamination during ultracentrifugation.

To sum up, two particle populations of different hydrodynamic diameters were measured in samples isolated with the isolation kit from both cell lines (approximately 27 nm to 103 nm). One particle population was measured in samples isolated with UC from MDA-MB-231 (138 nm). This shows a clear difference in particles isolated with the two procedures, originally with the shared aim of isolating exosomes.

4.5 Targeted proteomics; Western Blot

An established technique to confirm the presence of exosomes is the determination of protein exosome markers with WB [37, 62]. Consequently, protein exosome markers were determined with WB to investigate the presence of exosome related proteins in the isolated samples. To confirm that the observed data were not due to gel loading- or protein transfer errors, actin (42 kDa) or GAPDH (36 kDa) was used as loading controls. Choosing which one of them to use, was depending on the kDa of the protein to be determined. However, actin and GAPDH was not certain to be present in exosome samples.

A selection of the most commonly used exosome protein markers were used, namely CD9, CD81 and CD63, as they represent the transmembrane proteins and should confirm the presence of a membrane in the isolated samples. Flotillin-1, ALIX and TSG101 are proteins involved in the endocytic pathway and the biogenesis of the exosomes; hence their presence should confirm the presence of biogenesis related compounds which distinguish the exosomes from vesicles of different biogenesis [134, 135]. Calnexin, a protein linked to be present in other organelles of the cell other than exosomes (i.e. endoplasmic reticulum, ER), would not be expected to be seen in the isolated samples, as this would indicate the presence of cell contamination, i.e. impure extracts [37, 62].

None of these exosome protein markers are specific for exosomes only. Nevertheless an enrichment of exosome protein markers in the isolated samples compared to cell lysates was expected, presuming that the exosome protein markers would be present at higher concentrations in the exosome samples [39, 62, 136, 137]. Conversely it was not certain if all of these exosome protein markers would be present in the isolated samples from the two cell lines applied, as this often depends on the biological function of the cell of origin.

4.5.1 WB of protein exosome markers with cell lysates

Initially, cell lysates from MCF-7 and MDA-MB-231 were western blotted to investigate whether these proteins were present in the possible exosome-secreting cells. Bands occurring at the kDa corresponding to CD9, TSG101, flotillin-1 and calnexin were observed. Therefore these proteins were most likely present in cell lysates from both cell lines (**Figure 31**).

Even though CD63 is a well-used marker for exosomes, its antibody should in these experiments be used with caution (see appendix, section **7.2.1**). In addition, the antibodies for

CD81 were found not to be repeatable. The absence of band with anti-ALIX (**Figure 31**) could be due to the repetitive thawing and incubating of the diluted antibody (this was performed up to four times) as limited amounts of this antibody was available. This may have reduced the antibody quality by inactivating its native structure, and hence lead to absence of bands. Thus, incubation with anti-ALIX should be repeated.

In general the performance of the antibodies had poor repeatability, as the performance could vary in between days and batches. The intensity of the bands could also depend on the other performance of antibodies detected at the same time (during imaging). Antibodies of high specificity and intensity could suppress the intensity of the bands from other antibodies of less specificity and intensity. Hence this could cause false negative results. For this reason, semi-quantitative measurements were not performed.

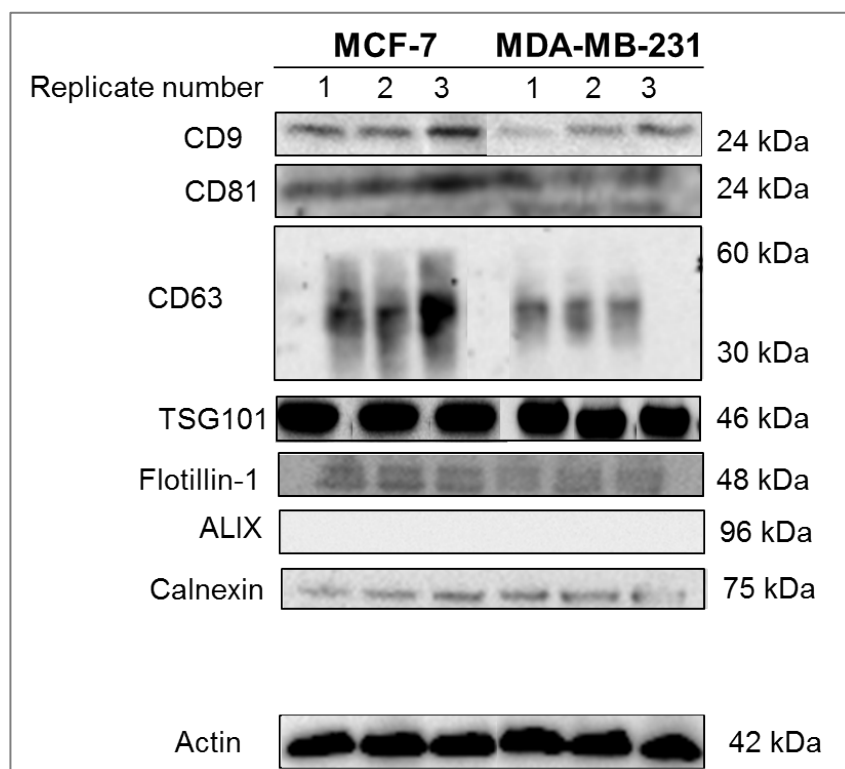


Figure 31: WB of three cell lysate replicates from the two breast cancer cell lines MCF-7 and MDA-MB-231 with antibody and expected kDa. Antibodies applied from the top; anti-CD9, anti-CD81, anti-CD63, anti-TSG101, anti-flotillin-1, anti-ALIX and anti-calnexin. Actin was used as loading control and 10.6-15.0 µg proteins were loaded to each well.

To sum up, most of the antibodies to be used for exosome identification were functioning.

4.5.2 WB of protein exosome markers with isolated lysates

The isolated lysates were analysed for the same exosome markers. As the samples isolated with UC were of low protein concentration, only 3 µg was loaded to the wells compared to 15 µg proteins with the samples isolated with isolation kit.

Bands occurring at the kDa corresponding to TSG101 and flotillin-1 were observed (**Figure 32**). In addition flotillin-1 did seem to be enriched in isolated lysates compared to cell lysates (observing bands at higher intensity). Thus TSG101 and flotillin-1 were most likely present in the isolated lysates from both cell lines (**Figure 32**).

Bands occurring at the kDa corresponding to CD9 and CD63 were observed in the samples isolated by isolation kit, and in the samples (two of three replicates) from MCF-7 cells isolated with UC (**Figure 32**). No bands occurred at the kDa corresponding to CD81, and only at some extent to ALIX. No bands occurred at the kDa corresponding to calnexin, representing isolated samples free from cell contamination (i.e. from ER).

The findings of MCF-7 derived exosomes are supported by that of other studies showing CD9, CD63, TSG101, flotillin-1 and ALIX in exosomes [26, 34, 136]. On the other hand, CD81 was found to be present in these studies, thus questioning the reproducibility of this characterization method.

MDA-MB-231 derived exosomes in previous studies were determined to contain CD81, flotillin-1 [30] and CD9 [138], in addition to the absence of ALIX and TSG101 [26]. Commonly observed for these studies, was the use of non-reducing conditions when determining the proteins CD9, CD81 and CD63.

The analyses in this study were performed under reducing conditions (i.e. presence of the reducing agent 2-mercaptoethanol). One possible explanation for the non-repeatable response of CD9, CD81 and CD63 antibodies could be that certain antibodies are not able to detect proteins in their reduced form. As tetraspanins (i.e. CD9, CD81 and CD63) are highly conserved of cysteine residues on the second extracellular loop [139], antibodies with epitope specificity or affinity to this domain would most likely be affected by the reduction of the

cysteine residues. It should be further investigated whether this is the case for the antibodies applied in this study.

The loading controls GAPDH and actin were not repeatedly observed in the isolated lysates. An option could be to choose TSG101 as a loading control, due to its more repeatable observation of presence.

Limitation such as detection limits and the reliability of the antibody compromise the results in this study. One possible explanation could be that the WB method consists of several extensive operational steps, increasing the possible error sources. This could be solved by automatization with the use of Simple Western™ [140]. Higher sensitivity could also be achieved using MS analyses.

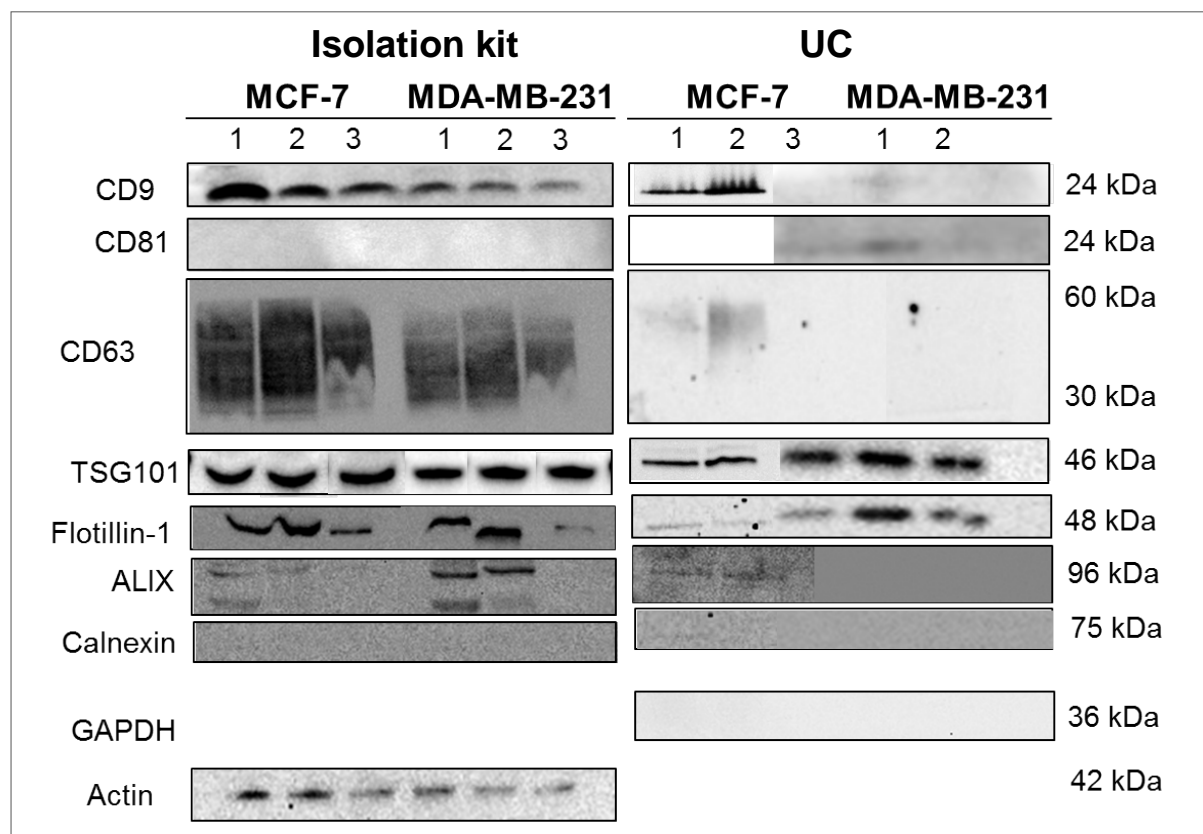


Figure 32: WB of three isolate lysate replicates from the two breast cancer cell lines MCF-7 and MDA-MB-231 performed with either isolation kit (left side 15 µg proteins were loaded to each well) or UC (right side 3 µg proteins were loaded to each well), with antibody and expected kDa. Antibodies applied from the top; anti-CD9, anti-CD81, anti-CD63, anti-TSG101, anti-flotillin-1, anti-ALIX and calnexin. Actin or GAPDH was used as loading control.

To sum up, the isolated lysates have hallmarks of the presence of exosomes, excluding calnexin. What does this mean? We have most likely isolated exosomes.

4.6 TEM with immunogold labelling

TEM was used to confirm the presence of double membranous circular structures [37, 62]. As TEM displays dehydrated samples, the native state of the structures is not reflected. Thus the exact size of the structures was not measured. However indications on the approximate size are given.

Double membrane structures were successfully observed (See appendix, section 7.2.2). To determine the presence of double membrane structures related to exosomes, immunogold labelling with a membrane specific protein exosome marker was essential. As bands occurred at the kDa corresponding to CD9 with almost all isolated lysates with WB (**Figure 35**), the membrane protein CD9 was chosen for immunogold labelling. This protein marker has also been used for the same purpose, from one of the respective cell lines (MDA-MB-231) in articles written by Melo et al. [30, 141]. However, immunogold labelling of exosomes turned out to be a rather extensive process demanding optimization (described in appendix, 7.2.3). This can explain why several published articles do not practice this technique [26, 61, 134, 142]. After optimization, immunogold labelling with mouse anti-CD9 antibody with a secondary antibody displayed specificity and repeatability.

It is to be noted that isolation with the isolation kit and UC were performed with different starting volumes of cell culture media (1-2 mL with the isolation kit and 9-13 mL with UC). The number of observed double membrane structures and PAGs cannot be compared between the different isolation methods, as these observations are not representative to the whole sample.

4.6.1 Immunogold labelling with MCF-7 exosomes

Immunogold labelling of MCF-7 isolated samples with UC were rejected, as the sample was suspected to be contaminated from PBS (section 4.2.2). Nonetheless, circular double membrane structures were observed (appendix, section 7.2.4).

Double membrane structures were observed with the MCF-7 isolated samples with the isolation kit (presented with increasing numbers in **Figure 33 A, B**). In **Figure 33 A-1**, one PAG was observed close to a circular shaped double membrane structure, thus indicating the

presence of a CD9-positive membrane. The cluster of membrane structures in **Figure 33 A-2** did not exhibit a visible circular shape. One reason could be the collapsing of the original membrane structure during sample preparation, or the membrane structures were lying on top of each other resulting in non-visible parts. Fixation (by crosslinking with glutaraldehyde or formaldehyde) as an additional step during sample preparation can be used to better preserve the morphology, however this can again influence the binding capacity of the antibody to the epitope [143]. Nevertheless the presence of PAG indicated that the double membrane structures were positive for the protein CD-9 (**Figure 33 A-2**). In **Figure 33 B-1** the cluster of double membrane structures did exhibit visible circular shapes of ± 50 nm, however with no sign of PAGs nearby these. Two possible reasons for the absence of PAGs could be that the clustering displays a smaller area for the antibodies and PAG to bind, or the double membrane cluster does not display CD9-positive membranes. PAG nearby double membrane structures of non-circular shape were observed in **Figure 33 B-2**.

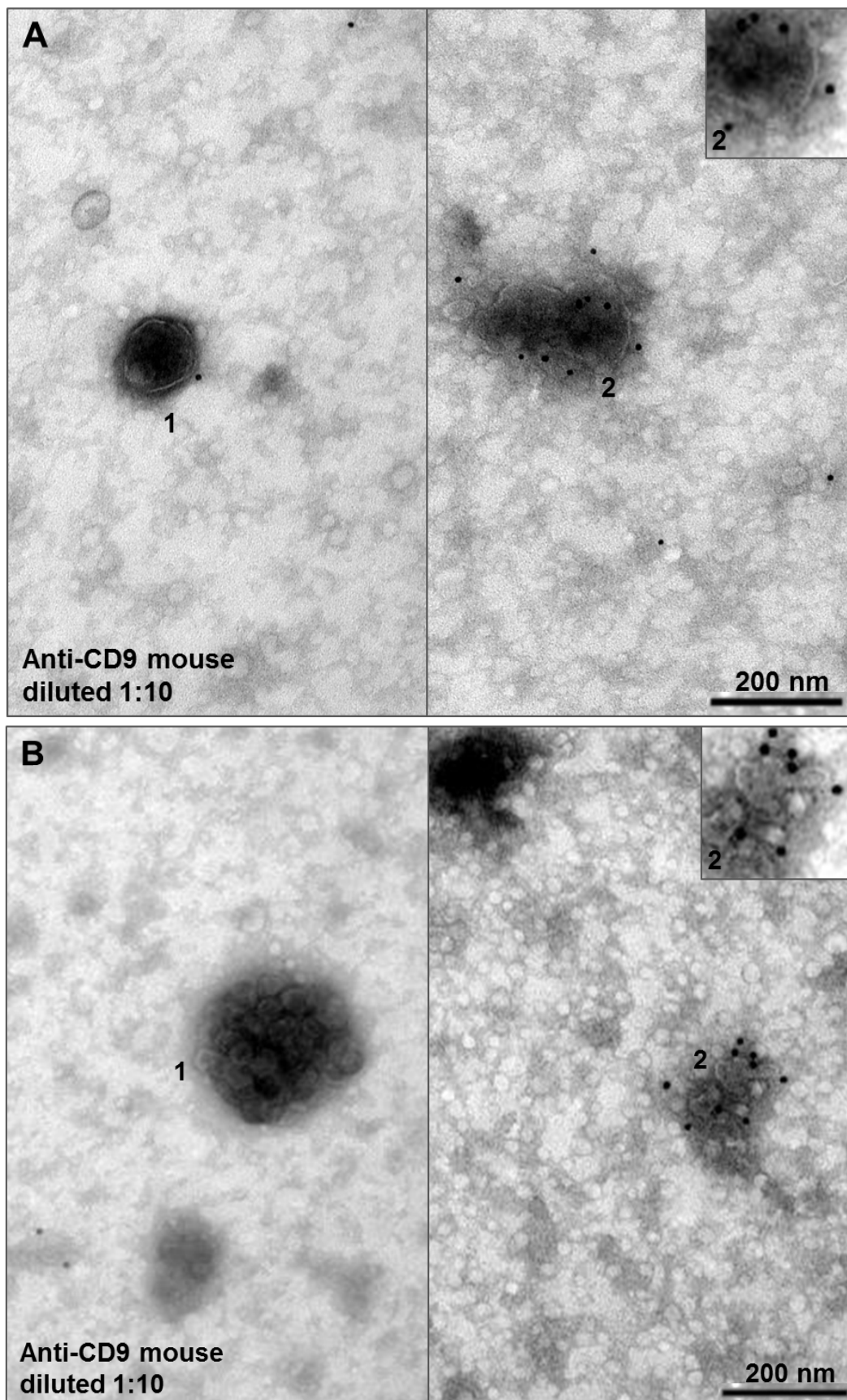


Figure 33: Images of immunogold labelled (mouse anti-CD9 with secondary antibody) MCF-7 isolated samples with the isolation kit, with numbers indicating the presence of structures that appear as double membrane structures. Gold particles were depicted as 10 nm diameter black dots. Images were taken with a magnification of 40 000. The images are cropped, and the photo at upper right corner was digitally zoomed approximately 50%.

4.6.2 Immunogold labelling with MDA-MB-231 exosomes

Clusters of double membrane structures were observed with MDA-MB-231 isolated samples with the isolation kit (**Figure 34 A, B**). PAGs were observed close to the double membrane structures (**Figure 34 A-2**), indicating the presence of a CD9 positive double membrane. However, it was difficult to state whether the immunogold labelling occurring in **Figure 34 B-1** was specifically bound or not, as the morphology of the structure (possible fraction) close to the PAG was blurry. The double membrane structures seemed to exhibit diameters of 100 nm and above (**Figure 34 A-1, A-2, B-1**), but also smaller structures were observed (**Figure 34 A-2**).

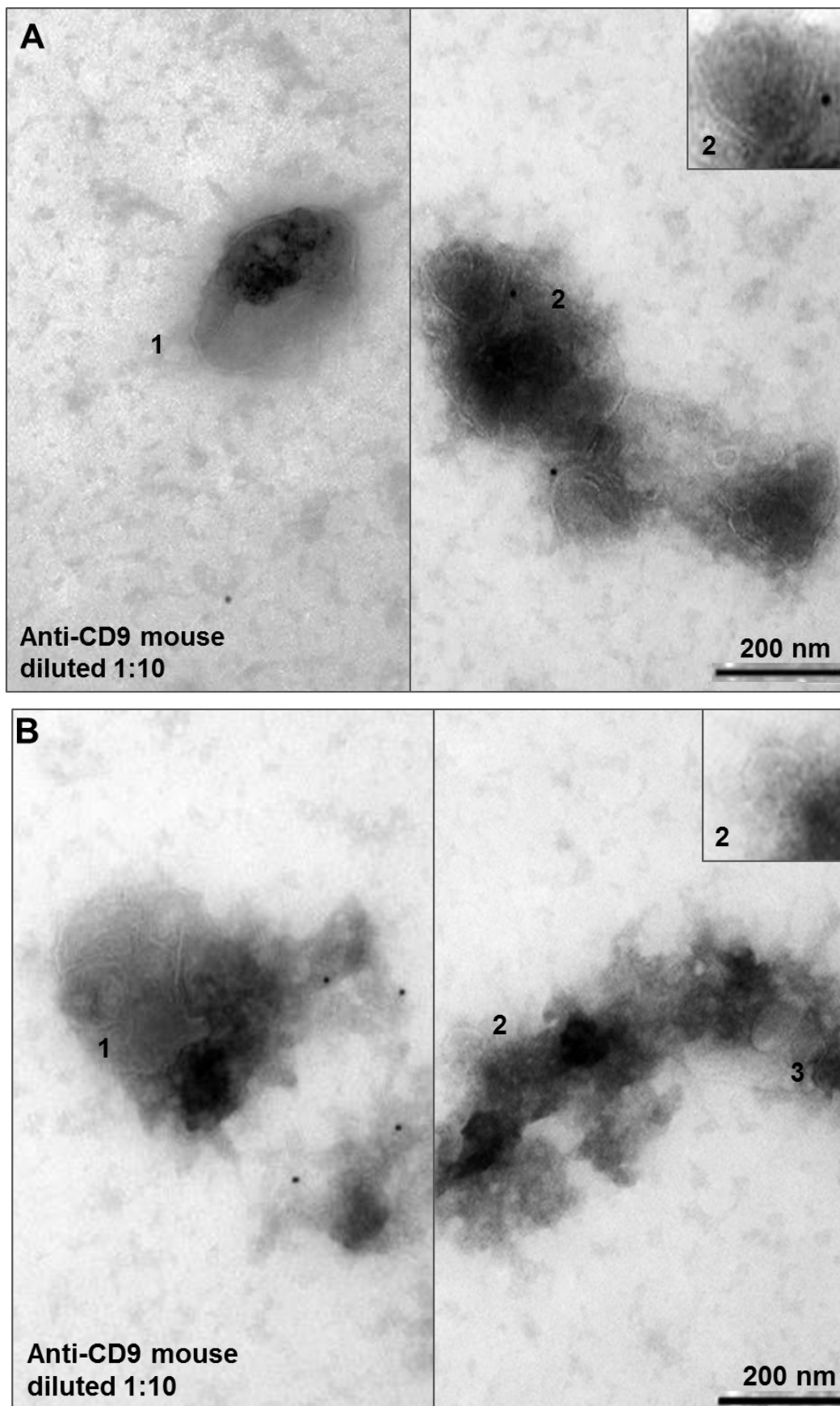


Figure 34: Images of immunogold labelled (mouse anti-CD9 with secondary antibody) MDA-MB-231 isolated exosome samples with the isolation kit, with numbers indicating the presence of double membrane structures. Gold particles were depicted as 10 nm diameter black dots. Images were taken with a magnification of 40 000. The images were cropped, and the photo at upper right corner was digitally zoomed approximately 50%.

Clustering of the membrane structures was observed with the MDA-MB-231 samples isolated with UC (**Figure 35** A-1). PAGs were observed distributed close to the double membrane structures (**Figure 35** A, B), hence indicating the presence of CD9-positive membrane structures. The size of the majority of the membrane structures was observed to be bigger than 100 nm diameter, approximately, and could support the hydrodynamic diameters measured with DLS (of 138 nm). However, also smaller structures were observed (**Figure 35** A-1, A-3 and B-1, B-2)

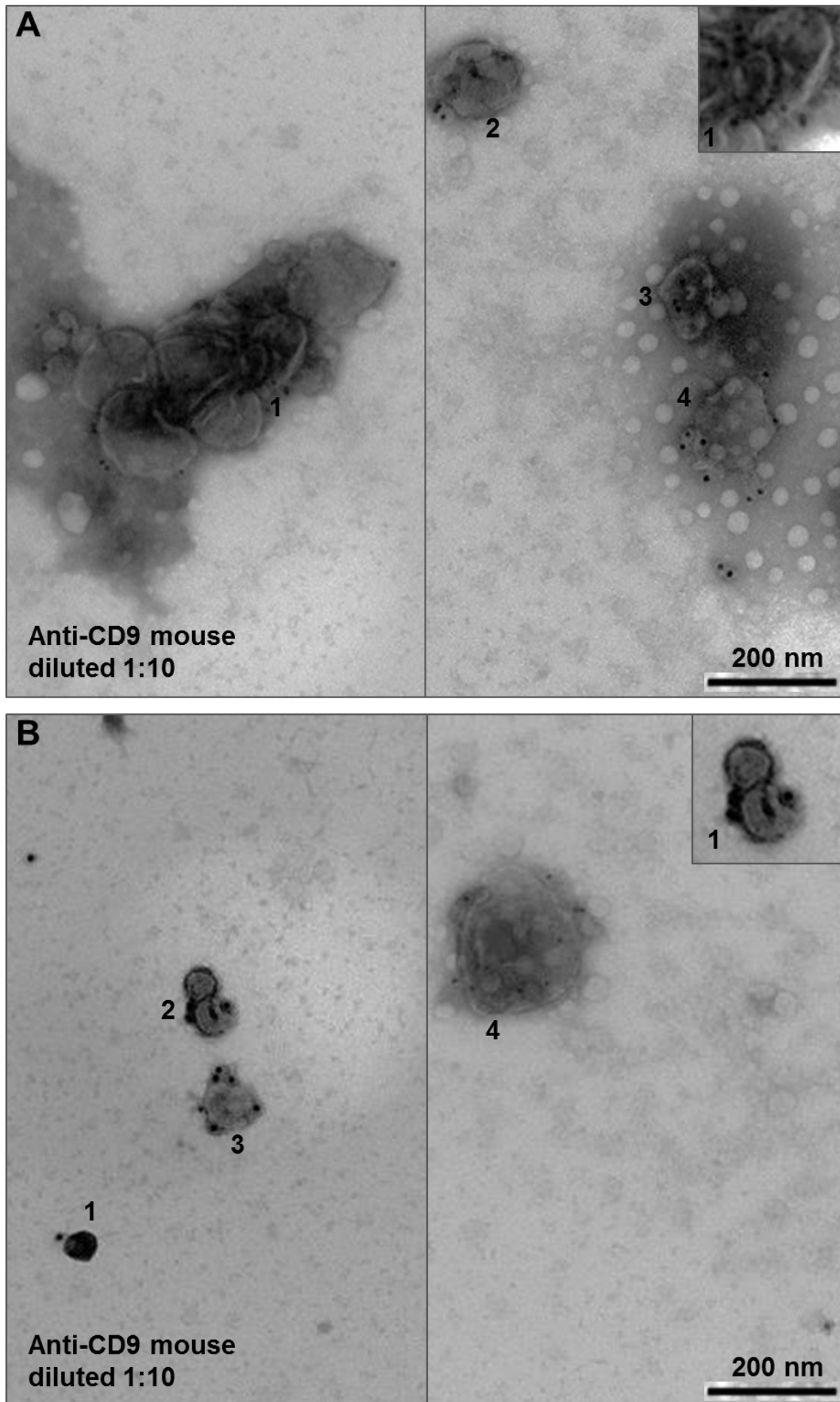


Figure 35: Images of immunogold labelled (mouse anti-CD9 with secondary antibody) MDA-MB-231 isolated exosome samples with UC, with numbers indicating the presence of double membrane structures. Gold particles were depicted as 10 nm diameter black dots. Images were taken with a magnification of 40 000. The images were cropped, and the photo at upper right corner was digitally zoomed approximately 50%.

4.6.3 Immunogold labelling with blank

No circular shaped double membrane structures were observed in the blank (i.e. cell culture media) isolated with the isolation kit (**Figure 36**), however circular shaped membrane structures were observed in the blank isolated with UC (**Figure 36**). The membrane structures observed with UC was suspected to be contaminants from FBS, although FBS was exosome depleted. The protocols for the depletion of exosomes in FBS only seemed to eliminate approximately 95% of the exosomal genetic material (i.e. RNA) in a previous study [144]. Supplementing with FBS is commonly used during cell culturing prior to exosome isolation. As a consequence, research groups pursuing exosome experiments could mistake the exosomes from FBS to be cell derived exosomes. To be certain of that the exosomes investigated are cell derived exosomes the cells should be grown without FBS present; however this could possibly impact on cell viability and growth.

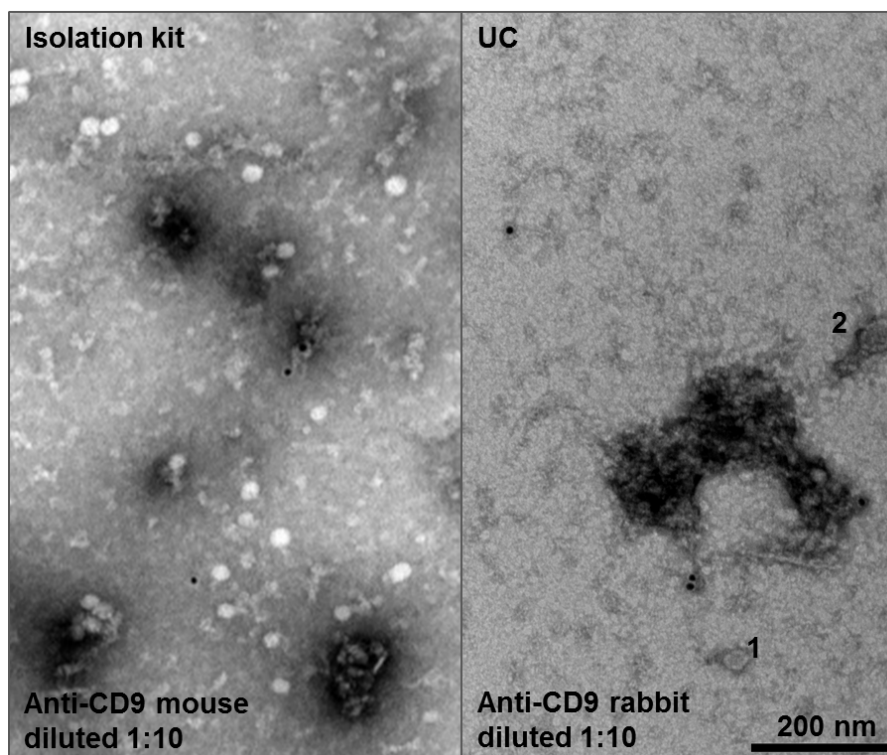


Figure 36: Images of blank isolated samples. The isolated samples with the isolation kit were immunogold labelled with mouse anti-CD9 with secondary antibody. The sample isolated with UC was from a previous point, and was immunogold labelled with rabbit anti-CD9. Gold particles were depicted as 10 nm diameter black dots. Images were taken with a magnification of 40 000.

To conclude, circular shaped membrane structures were observed in the isolated samples with both isolation techniques. Several membrane structures were positive for the protein exosome marker CD9. What does this mean? The isolation techniques did give structures similar to those of exosomes.

4.7 Protein characterization with the use of nanoLC-MS/MS

To support the WB assays, comprehensive analysis of proteins using nanoLC-MS/MS was performed as a complementary technique. The samples were digested in solution and analysed externally by a commercial proteomic lab. In addition, the analyses were reproduced in house. However, high level of noise in the MS spectra was frequently observed when analysing in house, possibly originating from polymers (i.e. PEGs). Thus the detergent NP-40 was suspected to be a source of contamination. This was solved by separating the proteins samples by gel electrophoresis as contaminants with low molar mass (e.g. NP-40) would not be retained by the gel pores (see appendix, section **7.2.5** for more experimental considerations).

4.7.1 Protein identification with external analyses further reproduced in house

The peptides eluted with different retention times and displayed different chromatography depending on the analyses were performed in house or externally (presented in **Figure 37**, MCF-7 and MDA-MB-231 isolated with the isolation kit). Differences in the number of proteins identified were observed between the two experiments, indicating bad reproducibility. The reproducibility of the proteins identified with the two experiments is further discussed in appendix, section **7.2.6** and **7.2.7**.

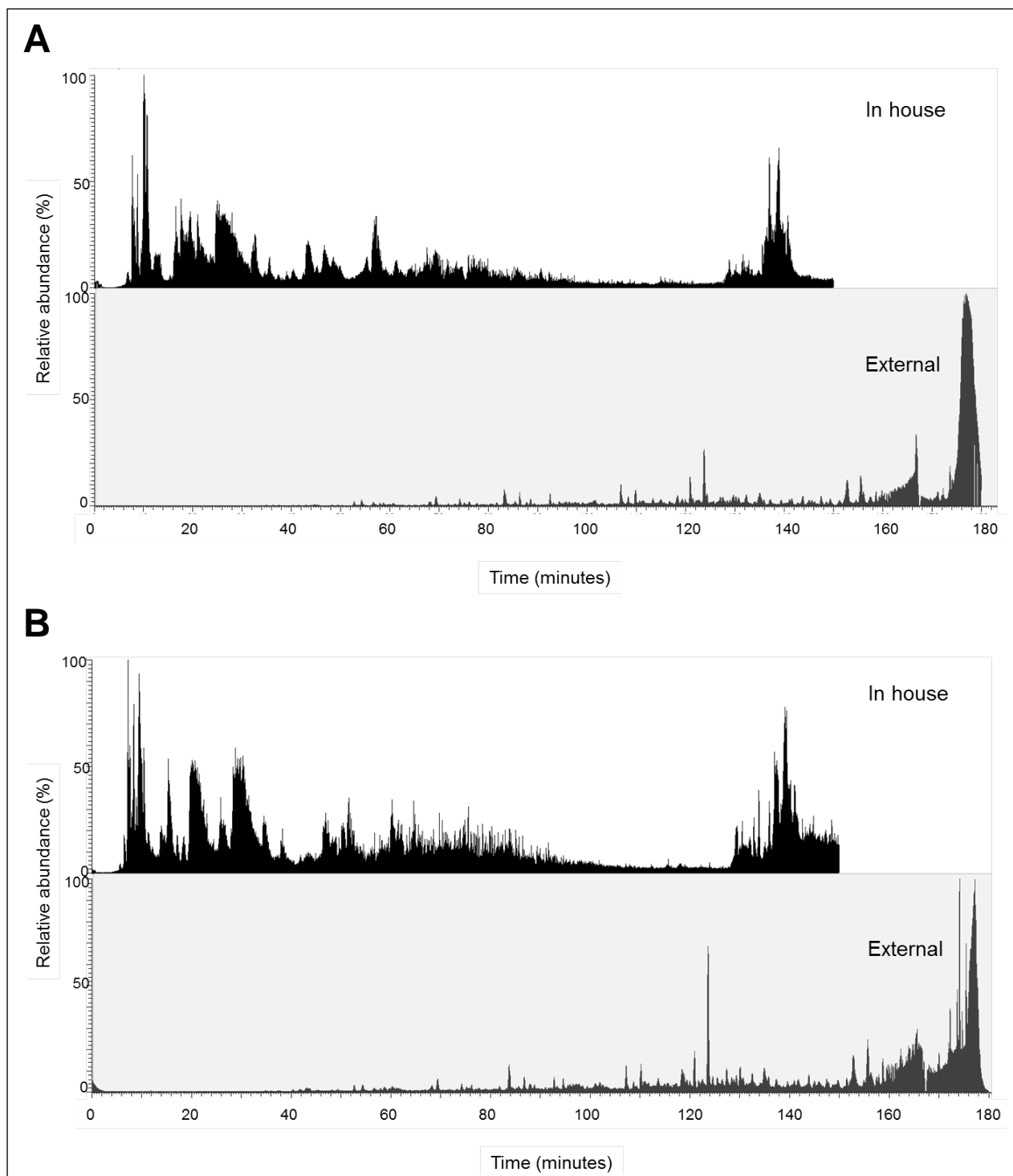


Figure 37: Total ion chromatogram of the isolated exosome samples from the cell lines with the isolation kit. A) MCF-7, showing the first fraction (0-25 kDa) from in house analysis (black, ion intensity of 1.38×10^{10}) and the external analysis (dark grey, ion intensity of 6.82×10^9). B) MDA-MB-231, showing the first fraction (0-25 kDa) from in house analysis (black, ion intensity of 1.50×10^{10}) and the external analysis (dark grey, ion intensity of 5.31×10^9). The gradient elution for the analyses performed in house and external is shown in **Table 6** and **Table 7**.

4.7.2 Protein identification with protein exosome markers and annotation to cellular location

The MS approach is not quantitative, but it can give a rough idea of protein abundance based on the protein coverage together with the number of peptides identified, peptide spectral matches (PSM) and/or the total score. High protein abundance gives a greater amount of peptides entering the MS. As the ion peak generated would be of increased intensity, the ion is most likely further isolated for fragmentation and generation of peptide fragmentation spectra (MS/MS). As there are several peptides generated from one protein, several different peptide fragmentation spectra are generated, thus leading to a greater amount of peptides identified. As a consequence, greater amounts of peptides identified results in higher protein coverage. In addition, the MS is operating with dynamic exclusion leading to a more rapid scanning, potentially enabling the isolation of more ions for fragmentation.

To provide a wider view on the protein content when evaluating the different isolation methods, proteins identified both in-solution and in-gel were pooled and categorized into cell lines and isolation methods (for more information of the proteins identified, see appendix, section **7.5.1**).

A selection of proteins was matched with the different isolation methods; both negative- (from different locations in the cell not related to exosomes) and positive protein exosome markers were chosen from commonly identified exosome proteins in the literature [37, 62, 145-147]. Positive protein exosome markers were chosen to be CD9, CD81, CD63, lactadherin, thrombospondin 1, annexin A2, TSG101, syntenin-1 ALIX and flotillin-1.

As the proteins were identified with both MASCOT and SEQUEST algorithms, several scores were generated for each protein identified with the experiments and fraction analysis. The individual scores were not directly comparable, as it was the highest score that was chosen to give the protein coverage of the identified protein. Thus the protein coverage (%) was chosen.

The positive protein exosome markers were expected to be identified with high protein coverage, as the high coverage should confirm the presence of exosomes in the isolated samples. Negative protein exosome markers were chosen to be calnexin, serine/threonine-

protein kinase 26 and cytochrome c 1. The negative protein exosome markers were expected not to be identified or identified with low protein coverage. The abundance or low coverage should confirm the absence of contaminations as cell debris in the isolated exosomes, hence indicating pure exosome samples.

To get an overview of all proteins identified and their relevance to exosomes, the proteins were additionally annotated to their cellular location with the use of GO annotations [148]. It should be noted that one protein can be annotated to several cellular locations (thus the sum of all cellular locations is higher than 100%). The cellular locations were chosen according to the relevance towards exosome isolation; extracellular exosome, extracellular matrix, plasma membrane, endosome, cytoskeleton and cytosol are annotations positively related to exosomes. Nucleus, ER, golgi apparatus, LDL and HDL are negatively related to exosomes as they are cellular locations not associated with exosome biogenesis.

Protein identification, protein exosome markers and annotation to cellular location with MCF-7 isolated exosomes

Greater amounts of proteins were identified in MCF-7 isolated samples with the isolation kit compared to UC (**Figure 38 A**). However the majority of the proteins identified with UC were also identified with the isolation kit (220 proteins), indicating the presence of common proteins in both samples.

The samples isolated with the isolation kit identified 7 of 10 positive protein exosome markers and no negative protein exosome markers (**Figure 38 B**) (accession number, number of peptides identified and exact protein coverage is found in appendix, section **7.5, Table 17**). Membrane- and surface related proteins were identified (i.e. CD9, CD81 and thrombospondin) indicating the presence of a membrane in the sample. In addition, exosome biogenesis related proteins (annexin A2, syntenin-1 and ALIX) were identified, indicating the presence of exosomes. With no identification of negative protein exosomes markers, this indicates the presence of exosome with little contamination from cell debris (i.e. from the proteins calnexin, serine/threonine-protein kinase 26 and cytochrome c 1) when isolating with the isolation kit.

The samples isolated with UC identified 8 of 10 positive protein exosome markers and one negative protein exosome marker (calnexin, valued with negative protein coverage, %) (**Figure 38 B**). This reduced the probability of the identification of the positive protein

exosome markers being trustworthy, as their identification could possibly originate from cell debris. However, the protein coverage was low (4.05 %, see appendix, section 7.5, **Table 17**). This indicates that the samples isolated with UC were not pure exosomes.

It is to be noted that TSG101 was not identified with MS in samples isolated with the isolation kit (**Figure 38 B**), consequently contradicting with what was observed with WB (**Figure 32**). One reason could be too low concentration of TSG101 peptides for MS detection, perhaps due to co-elution with peptides of higher abundance resulting in ion suppression. Other reasons can be poor specificity of the antibody used with WB, giving false positive. On the other hand, TSG101 was identified in the UC isolated samples with MS (**Figure 38 B**), supporting the reliability of WB antibodies as the outcome could simply be dependent on the isolation method. Other identifications contradicting the observations with WB were identification of CD81 (isolation kit) and CD63 (UC) with MS (**Figure 38 B**) but observed absent with WB, presence of flotillin-1 with WB (**Figure 32**), but not identified with neither isolation kit nor UC with MS (**Figure 38 B**).

Identified proteins from MCF-7 isolated exosomes with the isolation kit and UC displayed similar exosome related cellular locations (**Figure 38 C**). In addition, the identified proteins displayed non-exosome related annotations with a high percentage of the proteins identified located to the nucleus. High percentage of proteins located to nucleus is equally observed by others [58, 149], and can reflect the high genetic content of exosomes [150].

Proteins were also annotated to the cellular location HDL and LDL with the isolation kit. However the respective proteins were also annotated to the cellular location extracellular exosome. Thus the proteins annotated were not exclusively present in HDL/LDL.

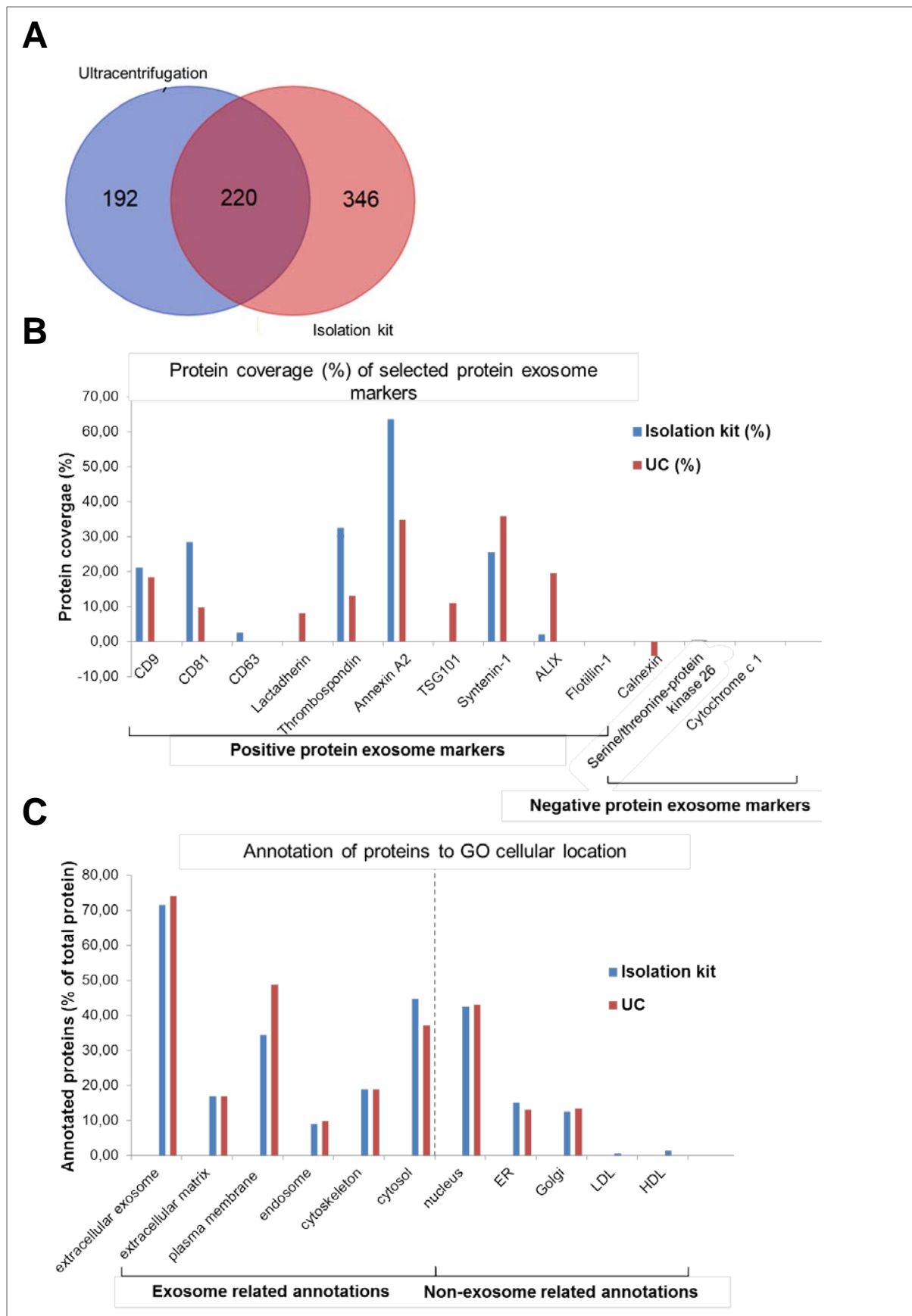


Figure 38: Proteins identified and compared, from isolated samples of MCF-7 cell culture media. A) Venn diagram of proteins identified with UC and isolation kit. B) Selected protein exosome markers with protein coverage (%), with proteins obtained from isolation kit is shown in blue, while proteins obtained by UC are shown in red. C) The annotated proteins (% of total proteins) and their cellular location, with proteins annotated from isolation kit are shown in blue, while proteins annotated by UC are shown in red.

To sum up, proteins related to exosomes were identified in MCF-7 samples isolated with the isolation kit and with UC. However non-exosome related proteins were also identified with both isolation techniques. What does this mean? The exosomes isolated are not completely pure.

Protein identification, protein exosome markers and annotation to cellular location with MDA-MB-231 isolated exosomes

Greater amounts of proteins were identified in MCF-7 isolated samples with the isolation kit compared to UC (**Figure 39 A**). However the majority of the proteins identified with UC were also identified with the isolation kit (442 proteins), indicating the presence of common proteins in both samples.

Negative protein exosome markers were not identified with the isolation kit and UC; hence the positive protein exosome markers identified had higher probability of not originating from contaminating cell debris (**Figure 39 B**) (appendix, section 7.5, **Table 18**). MDA-MB-231 isolated with the isolation kit did identify 6 of 10 positive protein exosome markers, while the samples isolated by UC identified all 10 positive protein exosome markers. The identification of a wider range of exosomal proteins with UC compared to isolation kit can indicate the presence of exosomes at higher certainty in the samples isolated with UC.

The abundance/absence of these proteins did however also question the reliability of WB antibodies for determination; CD9 and CD63 (UC) was identified with MS (**Figure 39 B**), but not present according to observations with WB (**Figure 32**). Additionally CD63, TSG101 and flotillin-1 (isolation kit) were not identified by MS but determined to be present with WB. Thus, it is likely that WB is highly dependent on the specificity of the antibodies applied.

The annotated proteins from isolated MDA-MB-231 samples with the isolation kit and UC displayed annotation to similar exosome related cellular locations (**Figure 39 C**). A higher percentage of the proteins identified with UC were located to the cytoskeleton (reflecting the transport of endosomes and fusion with the plasma membrane to release the exosomes). This could question the biogenesis of the exosome-related proteins identified with the isolation kit. In addition proteins were annotated to HDL for both isolation methods (annotation of proteins to LDL was also detected with the isolation kit). However, apolipoprotein A-1

(protein marker for HDL) has previously been identified in exosomes derived from MDA-MB-231 [151].

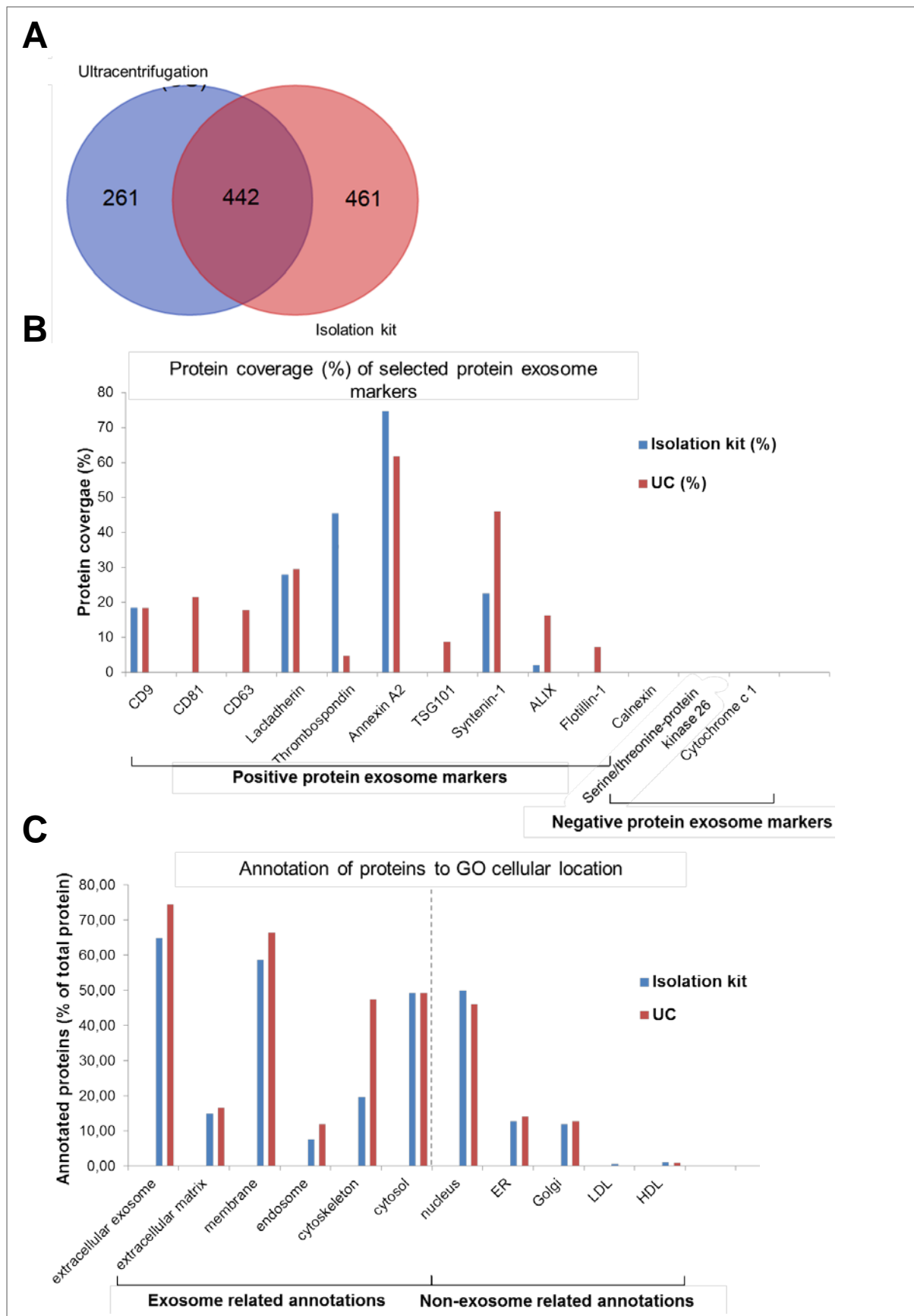


Figure 39: Proteins identified and compared, from isolated samples of MDA-MB-231 cell culture media. A) Venn diagram of proteins identified with UC and isolation kit. B) Selected protein exosome markers with protein coverage (%), with proteins obtained from isolation kit is shown in blue, while proteins obtained by UC are shown in red. C) The annotated proteins (% of total proteins) and their cellular location, with proteins annotated from isolation kit are shown in blue, while proteins annotated by UC are shown in red.

To sum up, isolation with UC identified all 10 positive protein exosome markers compared to 6 positive protein exosome markers identified with the isolation kit. Isolation with both isolation methods did provide with proteins annotated to be localized in lipoproteins. This indicates that the exosomes isolated are not completely pure.

4.7.3 Proteins identified in blank

The lipoproteins related to HDL and LDL (i.e. Apolipoprotein A-1, B, C-3, E and M) were identified in blank samples, thus it is rather difficult to conclude whether the isolated samples contain lipoproteins as contamination from HDL and LDL particles. Additionally CD9 was identified in the blank, questioning its reliability of being a positive protein exosome marker with non-visual techniques such as WB and MS.

5 Conclusion

In this thesis, two different techniques for the isolation of MCF-7 and MDA-B-231 exosomes have been evaluated; commercial isolation kit from Thermo Fisher and differential ultracentrifugation. The characterization techniques confirmed the isolation of exosomes with both isolation kit and UC. However, the isolated samples did contain contaminations, and there was a clear difference in the protein amount, particle size and populations identified with the two isolation methods. In addition, the majority of the characterization techniques provided poor repeatability, reproducibility and/or demanded extensive optimization.

None of the characterization techniques could confirm the presence of exosomes alone, as the different techniques did support and/ or validate each other. DLS provided size and TEM confirmed the presence of a membrane structure. BCA assays did only display the amount of protein present, while WB determined the exosome protein markers present, further validated and complemented by nanoLC-MS/MS. As none of the characterization techniques provided sufficient quantitative data (disregarding BCA assays), it could not be concluded that any of the two isolation techniques did provide a more “pure” exosome sample than the other.

All together, not only did the exosome isolation procedures appear to be far from mature, also the majority of the characterization techniques used in this study provided challenges. This implies that exosome based analyses are not completely suited for the clinic. Isolation techniques of higher specificity and certainty are thus required to fully realize the diagnostic potential of exosomes.

5.1 Future outlook

The isolation methods evaluated here should be examined with cells grown depleted of FBS, to further investigate if the lipoproteins identified in this study are directly related to the isolation methods applied. In addition, other isolation techniques such as immunoaffinity capture and flow field-flow fractionation should be evaluated as they seem to be of higher specificity. Exosome isolation with other breast cancer cell lines (e.g. SKBR3) would provide additional insight into the diverse characteristics of exosomes derived from breast cancer cells.

6 References

1. Trams, E.G., C.J. Lauter, J.N. Salem, and U. Heine, *Exfoliation of membrane ecto-enzymes in the form of micro-vesicles*. Biochimica et Biophysica Acta (BBA)-Biomembranes. Vol. 645 (1981) 63-70.
2. Pan, B.-T., K. Teng, C. Wu, M. Adam, and R.M. Johnstone, *Electron microscopic evidence for externalization of the transferrin receptor in vesicular form in sheep reticulocytes*. The Journal of Cell Biology. Vol. 101 (1985) 942-948.
3. Harding, C., J. Heuser, and P. Stahl, *Receptor-mediated endocytosis of transferrin and recycling of the transferrin receptor in rat reticulocytes*. The Journal of Cell Biology. Vol. 97 (1983) 329-339.
4. Pan, B.-T. and R.M. Johnstone, *Fate of the transferrin receptor during maturation of sheep reticulocytes in vitro: selective externalization of the receptor*. Cell. Vol. 33 (1983) 967-978.
5. Gruenberg, J., *The endocytic pathway: a mosaic of domains*. Nature reviews Molecular cell biology. Vol. 2 (2001) 721-730.
6. Raposo, G., H.W. Nijman, W. Stoorvogel, R. Liejendekker, C.V. Harding, C. Melief, and H.J. Geuze, *B lymphocytes secrete antigen-presenting vesicles*. The Journal of Experimental Medicine. Vol. 183 (1996) 1161-1172.
7. Zitvogel, L., A. Regnault, A. Lozier, J. Wolfers, C. Flament, D. Tenza, P. Ricciardi-Castagnoli, G. Raposo, and S. Amigorena, *Eradication of established murine tumors using a novel cell-free vaccine: dendritic cell derived exosomes*. Nature medicine. Vol. 4 (1998) 594-600.
8. Vincent - Schneider, H., P. Stumptner - Cuvelette, D. Lankar, S. Pain, G. Raposo, P. Benaroch, and C. Bonnerot, *Exosomes bearing HLA - DR1 molecules need dendritic cells to efficiently stimulate specific T cells*. International Immunology. Vol. 14 (2002) 713-722.
9. Roma-Rodrigues, C., A.R. Fernandes, and P.V. Baptista, *Exosome in Tumour Microenvironment: Overview of the Crosstalk between Normal and Cancer Cells*. BioMed Research International. Vol. 2014 (2014) 10.
10. Boukouris, S. and S. Mathivanan, *Exosomes in bodily fluids are a highly stable resource of disease biomarkers*. PROTEOMICS – Clinical Applications. Vol. 9 (2015) 358-367.
11. Cicero, A.L. and G. Raposo, *The Cell Biology of Exosomes: Historical and Perspectives*, in *Emerging Concepts of Tumor Exosome-Mediated Cell-Cell Communication*, H.-G. Zhang, Editor. 2013, Springer New York. p. 1-32.
12. Milane, L., A. Singh, G. Mattheolabakis, M. Suresh, and M.M. Amiji, *Exosome mediated communication within the tumor microenvironment*. Journal of Controlled Release.
13. Raposo, G. and W. Stoorvogel, *Extracellular vesicles: exosomes, microvesicles, and friends*. The Journal of Cell Biology. Vol. 200 (2013) 373-383.
14. Friel, A., C. Corcoran, J. Crown, and L. O'Driscoll, *Relevance of circulating tumor cells, extracellular nucleic acids, and exosomes in breast cancer*. Breast Cancer Research and Treatment. Vol. 123 (2010) 613-625.
15. Fang, Y., N. Wu, X. Gan, W. Yan, J.C. Morrell, and S.J. Gould, *Higher-order oligomerization targets plasma membrane proteins and HIV gag to exosomes*. PLoS biology. Vol. 5 (2007) e158.
16. Dragovic, R.A., C. Gardiner, A.S. Brooks, D.S. Tannetta, D.J. Ferguson, P. Hole, B. Carr, C.W. Redman, A.L. Harris, and P.J. Dobson, *Sizing and phenotyping of cellular*

- vesicles using Nanoparticle Tracking Analysis*. *Nanomedicine: Nanotechnology, Biology and Medicine*. Vol. 7 (2011) 780-788.
17. Llorente, A., T. Skotland, T. Sylvänne, D. Kauhanen, T. Róg, A. Orłowski, I. Vattulainen, K. Ekroos, and K. Sandvig, *Molecular lipidomics of exosomes released by PC-3 prostate cancer cells*. *Biochimica et Biophysica Acta (BBA) - Molecular and Cell Biology of Lipids*. Vol. 1831 (2013) 1302-1309.
 18. Pant, S., H. Hilton, and M.E. Burczynski, *The multifaceted exosome: Biogenesis, role in normal and aberrant cellular function, and frontiers for pharmacological and biomarker opportunities*. *Biochemical Pharmacology*. Vol. 83 (2012) 1484-1494.
 19. Milane, L., A. Singh, G. Mattheolabakis, M. Suresh, and M.M. Amiji, *Exosome mediated communication within the tumor microenvironment*. *Journal of Controlled Release*. Vol. 219 (2015) 278-294.
 20. Record, M., K. Carayon, M. Poirot, and S. Silvente-Poirot, *Exosomes as new vesicular lipid transporters involved in cell–cell communication and various pathophysiologicals*. *Biochimica et Biophysica Acta (BBA) - Molecular and Cell Biology of Lipids*. Vol. 1841 (2014) 108-120.
 21. Simons, M. and G. Raposo, *Exosomes – vesicular carriers for intercellular communication*. *Current Opinion in Cell Biology*. Vol. 21 (2009) 575-581.
 22. Zhang, H.-G. and W.E. Grizzle, *Exosomes: A Novel Pathway of Local and Distant Intercellular Communication that Facilitates the Growth and Metastasis of Neoplastic Lesions*. *The American Journal of Pathology*. Vol. 184 (2014) 28-41.
 23. Théry, C., L. Zitvogel, and S. Amigorena, *Exosomes: composition, biogenesis and function*. *Nature Reviews Immunology*. Vol. 2 (2002) 569-579.
 24. Farahani, M., C. Rubbi, L. Liu, J.R. Slupsky, and N. Kalakonda, *CLL exosomes modulate the transcriptome and behaviour of recipient stromal cells and are selectively enriched in miR-202-3p*. *PloS one*. Vol. 10 (2015) e0141429.
 25. Peinado, H., M. Alečković, S. Lavotshkin, I. Matei, B. Costa-Silva, G. Moreno-Bueno, M. Hergueta-Redondo, C. Williams, G. García-Santos, and C.M. Ghajar, *Melanoma exosomes educate bone marrow progenitor cells toward a pro-metastatic phenotype through MET*. *Nature medicine*. Vol. 18 (2012) 883-891.
 26. Harris, D.A., S.H. Patel, M. Gucek, A. Hendrix, W. Westbroek, and J.W. Taraska, *Exosomes released from breast cancer carcinomas stimulate cell movement*. *PloS one*. Vol. 10 (2015) e0117495.
 27. Lee, T., E. D’Asti, N. Magnus, K. Al-Nedawi, B. Meehan, and J. Rak, *Microvesicles as mediators of intercellular communication in cancer—the emerging science of cellular ‘debris’*. *Seminars in Immunopathology*. Vol. 33 (2011) 455-467.
 28. Logozzi, M., A. De Milito, L. Lugini, M. Borghi, L. Calabro, M. Spada, M. Perdicchio, M.L. Marino, C. Federici, and E. Iessi, *High levels of exosomes expressing CD63 and caveolin-1 in plasma of melanoma patients*. *PloS one*. Vol. 4 (2009) e5219.
 29. Parolini, I., C. Federici, C. Raggi, L. Lugini, S. Palleschi, A. De Milito, C. Coscia, E. Iessi, M. Logozzi, and A. Molinari, *Microenvironmental pH is a key factor for exosome traffic in tumor cells*. *The Journal of Biological Chemistry*. Vol. 284 (2009) 34211-34222.
 30. Melo, S.A., L.B. Luecke, C. Kahlert, A.F. Fernandez, S.T. Gammon, J. Kaye, V.S. LeBleu, E.A. Mittendorf, J. Weitz, and N. Rahbari, *Glypican-1 identifies cancer exosomes and detects early pancreatic cancer*. *Nature*. Vol. 523 (2015) 177-182.
 31. Taylor, D.D. and C. Gercel-Taylor, *MicroRNA signatures of tumor-derived exosomes as diagnostic biomarkers of ovarian cancer*. *Gynecologic Oncology*. Vol. 110 (2008) 13-21.
 32. Skog, J., T. Würdinger, S. Van Rijn, D.H. Meijer, L. Gainche, W.T. Curry, B.S. Carter, A.M. Krichevsky, and X.O. Breakefield, *Glioblastoma microvesicles*

- transport RNA and proteins that promote tumour growth and provide diagnostic biomarkers.* Nature cell biology. Vol. 10 (2008) 1470-1476.
33. Roberg-Larsen, H., K. Lund, K.E. Seterdal, S. Solheim, T. Vehus, N. Solberg, S. Krauss, E. Lundanes, and S.R. Wilson, *Mass spectrometric detection of 27-hydroxycholesterol in breast cancer exosomes.* The Journal of steroid biochemistry and molecular biology. Vol. 169 (2017) 22-28.
 34. King, H.W., M.Z. Michael, and J.M. Gleadle, *Hypoxic enhancement of exosome release by breast cancer cells.* BMC cancer. Vol. 12 (2012) 1.
 35. Ban, J.-J., M. Lee, W. Im, and M. Kim, *Low pH increases the yield of exosome isolation.* Biochemical and Biophysical Research Communications. Vol. 461 (2015) 76-79.
 36. Mitchell, J.P., J. Court, M.D. Mason, Z. Tabi, and A. Clayton, *Increased exosome production from tumour cell cultures using the Integra CELLine Culture System.* Journal of Immunological Methods. Vol. 335 (2008) 98-105.
 37. Théry, C., S. Amigorena, G. Raposo, and A. Clayton, *Isolation and characterization of exosomes from cell culture supernatants and biological fluids.* Current Protocols in Cell Biology. (2006) 3.22. 21-23.22. 29.
 38. Pigati, L., S.C. Yaddanapudi, R. Iyengar, D.-J. Kim, S.A. Hearn, D. Danforth, M.L. Hastings, and D.M. Duelli, *Selective release of microRNA species from normal and malignant mammary epithelial cells.* PloS one. Vol. 5 (2010) e13515.
 39. Mathivanan, S., H. Ji, and R.J. Simpson, *Exosomes: Extracellular organelles important in intercellular communication.* Journal of Proteomics. Vol. 73 (2010) 1907-1920.
 40. Greening, D.W., R. Xu, H. Ji, B.J. Tauro, and R.J. Simpson, *A protocol for exosome isolation and characterization: evaluation of ultracentrifugation, density-gradient separation, and immunoaffinity capture methods.* Proteomic Profiling: Methods and Protocols. (2015) 179-209.
 41. Lobb, R.J., M. Becker, S.W. Wen, C.S. Wong, A.P. Wiegman, A. Leimgruber, and A. Möller, *Optimized exosome isolation protocol for cell culture supernatant and human plasma.* Journal of Extracellular Vesicles. Vol. 4 (2015) 1-11.
 42. Rider, M.A., S.N. Hurwitz, and D.G. Meckes Jr, *ExtraPEG: a polyethylene glycol-based method for enrichment of extracellular vesicles.* Scientific reports. Vol. 6 (2016) 23978.
 43. Svedberg, T. and K.O. Pedersen, *The Ultracentrifuge.* The Ultracentrifuge. (1940).
 44. Becker, E.L., *An introduction to the physical techniques of electrophoresis and ultracentrifugation.* Journal of Allergy. Vol. 24 (1953) 78-89.
 45. Cvjetkovic, A., J. Lötvall, and C. Lässer, *The influence of rotor type and centrifugation time on the yield and purity of extracellular vesicles.* Journal of Extracellular Vesicles. Vol. 3 (2014) DOI: 10.3402/jev.v3i4.23111.
 46. Livshits, M.A., E. Khomyakova, E.G. Evtushenko, V.N. Lazarev, N.A. Kulemin, S.E. Semina, E.V. Generozov, and V.M. Govorun, *Isolation of exosomes by differential centrifugation: Theoretical analysis of a commonly used protocol.* Scientific reports. Vol. 5 (2015) 17319.
 47. Sokolova, V., A.-K. Ludwig, S. Hornung, O. Rotan, P.A. Horn, M. Epple, and B. Giebel, *Characterisation of exosomes derived from human cells by nanoparticle tracking analysis and scanning electron microscopy.* Colloids and Surfaces B: Biointerfaces. Vol. 87 (2011) 146-150.
 48. Momen-Heravi, F., L. Balaj, S. Alian, A.J. Trachtenberg, F.H. Hochberg, J. Skog, and W.P. Kuo, *Impact of biofluid viscosity on size and sedimentation efficiency of the isolated microvesicles.* Frontiers in Physiology. Vol. 3 (2012) DOI: 10.3389/fphys.2012.00162.

49. Palma, J., S.C. Yaddanapudi, L. Pigati, M.A. Havens, S. Jeong, G.A. Weiner, K.M.E. Weimer, B. Stern, M.L. Hastings, and D.M. Duelli, *MicroRNAs are exported from malignant cells in customized particles*. Nucleic acids research. Vol. 40 (2012) 9125-9138.
50. Cantin, R., J. Diou, D. Bélanger, A.M. Tremblay, and C. Gilbert, *Discrimination between exosomes and HIV-1: purification of both vesicles from cell-free supernatants*. Journal of Immunological Methods. Vol. 338 (2008) 21-30.
51. Böing, A.N., E. Van Der Pol, A.E. Grootemaat, F.A. Coumans, A. Sturk, and R. Nieuwland, *Single-step isolation of extracellular vesicles by size-exclusion chromatography*. Journal of Extracellular Vesicles. Vol. 3 (2014) DOI: 10.3402/jev.v3403.23430.
52. Gámez-Valero, A., M. Monguió-Tortajada, and L. Carreras-Planella, *Size-Exclusion Chromatography-based isolation minimally alters Extracellular Vesicles' characteristics compared to precipitating agents*. Scientific Reports. Vol. 6 (2016) DOI: 10.1038/srep33641.
53. Nordin, J.Z., Y. Lee, P. Vader, I. Mäger, H.J. Johansson, W. Heusermann, O.P. Wiklander, M. Hällbrink, Y. Seow, and J.J. Bultema, *Ultrafiltration with size-exclusion liquid chromatography for high yield isolation of extracellular vesicles preserving intact biophysical and functional properties*. Nanomedicine: Nanotechnology, Biology and Medicine. Vol. 11 (2015) 879-883.
54. Grant, R., E. Ansa-Addo, D. Stratton, S. Antwi-Baffour, S. Jorfi, S. Kholia, L. Krige, S. Lange, and J. Inal, *A filtration-based protocol to isolate human plasma membrane-derived vesicles and exosomes from blood plasma*. Journal of Immunological Methods. Vol. 371 (2011) 143-151.
55. Merchant, M.L., D.W. Powell, D.W. Wilkey, T.D. Cummins, J.K. Deegens, I.M. Rood, K.J. McAfee, C. Fleischer, E. Klein, and J.B. Klein, *Microfiltration isolation of human urinary exosomes for characterization by MS*. Proteomics-Clinical Applications. Vol. 4 (2010) 84-96.
56. Umezu, T., K. Ohyashiki, M. Kuroda, and J. Ohyashiki, *Leukemia cell to endothelial cell communication via exosomal miRNAs*. Oncogene. Vol. 32 (2013) 2747-2755.
57. Clayton, A., J. Court, H. Navabi, M. Adams, M.D. Mason, J.A. Hobot, G.R. Newman, and B. Jasani, *Analysis of antigen presenting cell derived exosomes, based on immuno-magnetic isolation and flow cytometry*. Journal of Immunological Methods. Vol. 247 (2001) 163-174.
58. Mathivanan, S., J.W. Lim, B.J. Tauro, H. Ji, R.L. Moritz, and R.J. Simpson, *Proteomics analysis of A33 immunoaffinity-purified exosomes released from the human colon tumor cell line LIM1215 reveals a tissue-specific protein signature*. Molecular & Cellular Proteomics. Vol. 9 (2010) 197-208.
59. Yang, J.S., J.C. Lee, S.K. Byeon, K.H. Rha, and M.H. Moon, *Size dependent lipidomic analysis of urinary exosomes from patients with prostate cancer by flow field-flow fractionation and nanoflow liquid chromatography-tandem mass spectrometry*. Analytical Chemistry. Vol. 89 (2017) 2488-2496.
60. Baranyai, T., K. Herczeg, Z. Onódi, I. Voszka, K. Módos, N. Marton, G. Nagy, I. Mäger, M.J. Wood, and S. El Andaloussi, *Isolation of exosomes from blood plasma: qualitative and quantitative comparison of ultracentrifugation and size exclusion chromatography methods*. PloS one. Vol. 10 (2015) e0145686.
61. Tauro, B.J., D.W. Greening, R.A. Mathias, H. Ji, S. Mathivanan, A.M. Scott, and R.J. Simpson, *Comparison of ultracentrifugation, density gradient separation, and immunoaffinity capture methods for isolating human colon cancer cell line LIM1863-derived exosomes*. Methods. Vol. 56 (2012) 293-304.
62. Lötval, J., A.F. Hill, F. Hochberg, E.I. Buzás, D. Di Vizio, C. Gardiner, Y.S. Gho, I.V. Kurochkin, S. Mathivanan, and P. Quesenberry, *Minimal experimental*

- requirements for definition of extracellular vesicles and their functions: a position statement from the International Society for Extracellular Vesicles.* Journal of Extracellular Vesicles. Vol. 3 (2014) 26913-23078.
63. Smith, P.K., R.I. Krohn, G.T. Hermanson, A.K. Mallia, F.H. Gartner, M.D. Provenzano, E.K. Fujimoto, N.M. Goeke, B.J. Olson, and D.C. Klenk, *Measurement of protein using bicinchoninic acid.* Analytical Biochemistry. Vol. 150 (1985) 76-85.
 64. Webber, J. and A. Clayton, *How pure are your vesicles?* Journal of Extracellular Vesicles. Vol. 2 (2013) 1-6.
 65. Muller, L., C.-S. Hong, D.B. Stolz, S.C. Watkins, and T.L. Whiteside, *Isolation of biologically-active exosomes from human plasma.* Journal of Immunological Methods. Vol. 411 (2014) 55-65.
 66. Gornall, A.G., C.J. Bardawill, and M.M. David, *Determination of serum proteins by means of the biuret reaction.* The Journal of Biological Chemistry. Vol. 177 (1949) 751-766.
 67. Kim, H.-A., J.-K. Seo, T. Kim, and B.-T. Lee, *Nanometrology and its perspectives in environmental research.* Environmental Health and Toxicology. Vol. 29 (2014).
 68. Bryant, G. and J.C. Thomas, *Improved particle size distribution measurements using multiangle dynamic light scattering.* Langmuir. Vol. 11 (1995) 2480-2485.
 69. Elizalde, O., G.P. Leal, and J.R. Leiza, *Particle size distribution measurements of polymeric dispersions: a comparative study.* Particle & Particle Systems Characterization. Vol. 17 (2000) 236-243.
 70. Filipe, V., A. Hawe, and W. Jiskoot, *Critical Evaluation of Nanoparticle Tracking Analysis (NTA) by NanoSight for the Measurement of Nanoparticles and Protein Aggregates.* Pharmaceutical Research. Vol. 27 (2010) 796-810.
 71. *The webpage of Malvern, the supplier of NTA instrumentation.* 22.05.2017]; Available from: <http://www.malvern.com/en/products/technology/nanoparticle-tracking-analysis/>.
 72. Murtey, M.D., *Modern Electron Microscopy in Physical and Life Sciences*, R.K. Milos Janecek, Editor. 2016, InTech.
 73. Cyrklaff, M., N. Roos, H. Gross, and J. Dubochet, *Particle - surface interaction in thin vitrified films for cryo - electron microscopy.* Journal of Microscopy. Vol. 175 (1994) 135-142.
 74. Ayache, J., L. Beaunier, J. Boumendil, G. Ehret, and D. Laub, *Contrast Enhancement and Labeling Techniques*, in *Sample Preparation Handbook for Transmission Electron Microscopy.* 2010, Springer. p. 277-316.
 75. Turkevich, J., P.C. Stevenson, and J. Hillier, *A study of the nucleation and growth processes in the synthesis of colloidal gold.* Discussions of the Faraday Society. Vol. 11 (1951) 55-75.
 76. Zhao, P., N. Li, and D. Astruc, *State of the art in gold nanoparticle synthesis.* Coordination Chemistry Reviews. Vol. 257 (2013) 638-665.
 77. Daniel, M.-C. and D. Astruc, *Gold nanoparticles: assembly, supramolecular chemistry, quantum-size-related properties, and applications toward biology, catalysis, and nanotechnology.* Chemical Reviews. Vol. 104 (2004) 293-346.
 78. Brust, M., M. Walker, D. Bethell, D.J. Schiffrin, and R. Whyman, *Synthesis of thiol-derivatised gold nanoparticles in a two-phase liquid-liquid system.* Journal of the Chemical Society, Chemical Communications. (1994) 801-802.
 79. Zhou, J., J. Ralston, R. Sedev, and D.A. Beattie, *Functionalized gold nanoparticles: synthesis, structure and colloid stability.* Journal of Colloid and Interface Science. Vol. 331 (2009) 251-262.
 80. Frens, G., *Controlled nucleation for the regulation of the particle size in monodisperse gold suspensions.* Nature. Vol. 241 (1973) 20-22.

81. Sperling, R.A. and W. Parak, *Surface modification, functionalization and bioconjugation of colloidal inorganic nanoparticles*. Philosophical Transactions of the Royal Society of London A: Mathematical, Physical and Engineering Sciences. Vol. 368 (2010) 1333-1383.
82. Oh, E., K. Susumu, R. Goswami, and H. Mattoussi, *One-phase synthesis of water-soluble gold nanoparticles with control over size and surface functionalities*. Langmuir : the ACS journal of surfaces and colloids. Vol. 26 (2010) 7604.
83. Jazayeri, M.H., H. Amani, A.A. Pourfatollah, H. Pazoki-Toroudi, and B. Sedighimoghaddam, *Various methods of gold nanoparticles (GNPs) conjugation to antibodies*. Sensing and Bio-Sensing Research. Vol. 9 (2016) 17-22.
84. Geoghegan, W.D. and G.A. Ackerman, *Adsorption of horseradish peroxidase, ovomucoid and anti-immunoglobulin to colloidal gold for the indirect detection of concanavalin A, wheat germ agglutinin and goat anti-human immunoglobulin G on cell surfaces at the electron microscopic level: a new method, theory and application*. Journal of Histochemistry & Cytochemistry. Vol. 25 (1977) 1187-1200.
85. Burnette, W.N., "Western Blotting": *Electrophoretic transfer of proteins from sodium dodecyl sulfate-polyacrylamide gels to unmodified nitrocellulose and radiographic detection with antibody and radioiodinated protein A*. Analytical Biochemistry. Vol. 112 (1981) 195-203.
86. Engvall, E. and P. Perlmann, *Enzyme-linked immunosorbent assay (ELISA) quantitative assay of immunoglobulin G*. Immunochemistry. Vol. 8 (1971) 871-874.
87. Engvall, E. and P. Perlmann, *Enzyme-linked immunosorbent assay, ELISA III. Quantitation of specific antibodies by enzyme-labeled anti-immunoglobulin in antigen-coated tubes*. The Journal of Immunology. Vol. 109 (1972) 129-135.
88. Schroeder, H.W. and L. Cavacini, *Structure and Function of Immunoglobulins*. Journal of Allergy and Clinical Immunology. Vol. 125 (2010) 41-52.
89. Alberts, B., *Essential cell biology*. 3rd ed. ed. 2010, New York: Garland Science.
90. Amzel, L.M. and R.J. Poljak, *Three-dimensional structure of immunoglobulins*. Annual Review of Biochemistry. Vol. 48 (1979) 961-997.
91. Baker, M., *Blame it on the antibodies*. Nature. Vol. 521 (2015) 274-276.
92. Berglund, L., E. Björling, P. Oksvold, L. Fagerberg, A. Asplund, C.A.-K. Szgyarto, A. Persson, J. Ottosson, H. Wernérus, and P. Nilsson, *A genecentric Human Protein Atlas for expression profiles based on antibodies*. Molecular & cellular proteomics. Vol. 7 (2008) 2019-2027.
93. Marx, V., *Finding the right antibody for the job*. nature methods. Vol. 10 (2013) 703.
94. Steen, H. and M. Mann, *The ABC's (and XYZ's) of peptide sequencing*. Nature reviews Molecular cell biology. Vol. 5 (2004) 699-711.
95. Siuti, N. and N.L. Kelleher, *Decoding protein modifications using top-down mass spectrometry*. Nature methods. Vol. 4 (2007) 817-821.
96. Kelleher, N.L., H.Y. Lin, G.A. Valaskovic, D.J. Aaserud, E.K. Fridriksson, and F.W. McLafferty, *Top down versus bottom up protein characterization by tandem high-resolution mass spectrometry*. Journal of the American Chemical Society. Vol. 121 (1999) 806.
97. Bosserhoff, A., J. Wallach, and R.W. Frank, *Micropreparative separation of peptides derived from sodium dodecyl sulphate-solubilized proteins*. Journal of Chromatography A. Vol. 473 (1989) 71-77.
98. Vandermarliere, E., M. Mueller, and L. Martens, *Getting intimate with trypsin, the leading protease in proteomics*. Mass spectrometry reviews. Vol. 32 (2013) 453-465.
99. Olsen, J.V., S.-E. Ong, and M. Mann, *Trypsin cleaves exclusively C-terminal to arginine and lysine residues*. Molecular & Cellular Proteomics. Vol. 3 (2004) 608-614.

100. Glatter, T., C. Ludwig, E. Ahrné, R. Aebersold, A.J. Heck, and A. Schmidt, *Large-scale quantitative assessment of different in-solution protein digestion protocols reveals superior cleavage efficiency of tandem Lys-C/trypsin proteolysis over trypsin digestion*. Journal of proteome research. Vol. 11 (2012) 5145-5156.
101. Lundanes, E., L.o. Reubsaet, and T. Greibrokk, *Chromatography : Basic Principles, Sample Preparations and Related Methods*. Chromatography. 2013, Hoboken: Wiley.
102. Constantopoulos, T.L., G.S. Jackson, and C.G. Enke, *Effects of salt concentration on analyte response using electrospray ionization mass spectrometry*. Journal of the American Society for Mass Spectrometry. Vol. 10 (1999) 625-634.
103. Peng, J., J.E. Elias, C.C. Thoreen, L.J. Licklider, and S.P. Gygi, *Evaluation of multidimensional chromatography coupled with tandem mass spectrometry (LC/LC–MS/MS) for large-scale protein analysis: the yeast proteome*. Journal of proteome research. Vol. 2 (2003) 43-50.
104. Delporte, C., C. Noyon, P. Raynal, D. Dufour, J. Nève, F. Abts, M. Haex, K.Z. Boudjeltia, and P. Van Antwerpen, *Advancement in stationary phase for peptide separation helps in protein identification: application to atheroma plaque proteomics using nano-chip liquid chromatography and mass spectrometry*. Journal of Chromatography A. Vol. 1385 (2015) 116-123.
105. Wilson, S.R., T. Vehus, H.S. Berg, and E. Lundanes, *Nano-LC in proteomics: recent advances and approaches*. Bioanalysis. Vol. 7 (2015) 1799-1815.
106. Ishihama, Y., *Proteomic LC–MS systems using nanoscale liquid chromatography with tandem mass spectrometry*. Journal of Chromatography A. Vol. 1067 (2005) 73-83.
107. Schmidt, A., M. Karas, and T. Dülcks, *Effect of different solution flow rates on analyte ion signals in nano-ESI MS, or: when does ESI turn into nano-ESI?* Journal of the American Society for Mass Spectrometry. Vol. 14 (2003) 492-500.
108. Chervet, J., M. Ursem, and J. Salzmann, *Instrumental requirements for nanoscale liquid chromatography*. Analytical Chemistry. Vol. 68 (1996) 1507-1512.
109. Kennedy, R.T. and J.W. Jorgenson, *Preparation and evaluation of packed capillary liquid chromatography columns with inner diameters from 20 to 50 μm* . Analytical Chemistry. Vol. 61 (1989) 1128-1135.
110. Hsieh, S. and J.W. Jorgenson, *Preparation and evaluation of slurry-packed liquid chromatography microcolumns with inner diameters from 12 to 33 μm* . Analytical Chemistry. Vol. 68 (1996) 1212-1217.
111. Fenn, J.B., M. Mann, C.K. Meng, S.F. Wong, and C.M. Whitehouse, *Electrospray Ionization for Mass Spectrometry of Large Biomolecules*. Science. Vol. 246 (1989) 64-71.
112. Taylor, G., *Disintegration of water drops in an electric field*. Proceedings of the Royal Society of London A: Mathematical, Physical and Engineering Sciences. Vol. 280 (1964) 383-397.
113. Emmett, M.R. and R.M. Caprioli, *Micro-electrospray mass spectrometry: ultra-high-sensitivity analysis of peptides and proteins*. Journal of the American Society for Mass Spectrometry. Vol. 5 (1994) 605-613.
114. Makarov, A., *Electrostatic axially harmonic orbital trapping: a high-performance technique of mass analysis*. Analytical Chemistry. Vol. 72 (2000) 1156-1162.
115. Nesvizhskii, A.I., O. Vitek, and R. Aebersold, *Analysis and validation of proteomic data generated by tandem mass spectrometry*. Nature methods. Vol. 4 (2007) 787.
116. Cottrell, J.S. and U. London, *Probability-based protein identification by searching sequence databases using mass spectrometry data*. Electrophoresis. Vol. 20 (1999) 3551-3567.

117. Eng, J.K., A.L. McCormack, and J.R. Yates, *An approach to correlate tandem mass spectral data of peptides with amino acid sequences in a protein database*. Journal of the American Society for Mass Spectrometry. Vol. 5 (1994) 976-989.
118. Geer, L.Y., S.P. Markey, J.A. Kowalak, L. Wagner, M. Xu, D.M. Maynard, X. Yang, W. Shi, and S.H. Bryant, *Open mass spectrometry search algorithm*. Journal of Proteome Research. (2004) 958-964.
119. Elias, J.E. and S.P. Gygi, *Target-decoy search strategy for increased confidence in large-scale protein identifications by mass spectrometry*. Nature methods. Vol. 4 (2007) 207-214.
120. Brown, J.L. and W. Roberts, *Evidence that approximately eighty per cent of the soluble proteins from Ehrlich ascites cells are Nalpha-acetylated*. The Journal of Biological Chemistry. Vol. 251 (1976) 1009-1014.
121. Gould, S.J. and G. Raposo, *As we wait: coping with an imperfect nomenclature for extracellular vesicles*. Journal of Extracellular Vesicles. Vol. 2 (2013) 20389.
122. DuSell, C.D., M. Umetani, P.W. Shaul, D.J. Mangelsdorf, and D.P. McDonnell, *27-hydroxycholesterol is an endogenous selective estrogen receptor modulator*. Molecular Endocrinology. Vol. 22 (2008) 65-77.
123. *Image of MDA-MB-231 cell line characteristics in culture (ATCC)* 11.05.2017]; Available from: <https://www.lgcstandards-atcc.org/~media/Attachments/5/C/3/0/25935.ashx>.
124. *Image of MCF-7 cell line characteristics in culture (ATCC)* 11.05.2017]; Available from: <https://www.lgcstandards-atcc.org/~media/Attachments/0/E/E/2/1980.ashx>.
125. Hood, J.L., R.S. San, and S.A. Wickline, *Exosomes released by melanoma cells prepare sentinel lymph nodes for tumor metastasis*. Cancer Research. Vol. 71 (2011) 3792-3801.
126. Clark, D.J., W.E. Fondrie, Z. Liao, P.I. Hanson, A. Fulton, L. Mao, and A.J. Yang, *Redefining the breast cancer exosome proteome by tandem mass tag quantitative proteomics and multivariate cluster analysis*. Analytical Chemistry. Vol. 87 (2015) 10462-10469.
127. Van Deun, J., P. Mestdagh, R. Sormunen, V. Cocquyt, K. Vermaelen, J. Vandesompele, M. Bracke, O. De Wever, and A. Hendrix, *The impact of disparate isolation methods for extracellular vesicles on downstream RNA profiling*. Journal of Extracellular Vesicles. Vol. 3 (2014) DOI: 10.3402/jev.v3403.24858.
128. Lane, R.E., D. Korbie, W. Anderson, R. Vaidyanathan, and M. Trau, *Analysis of exosome purification methods using a model liposome system and tunable-resistive pulse sensing*. Scientific reports. Vol. 5 (2015) 7639.
129. Helwa, I., J. Cai, M.D. Drewry, A. Zimmerman, M.B. Dinkins, M.L. Khaled, M. Seremwe, W.M. Dismuke, E. Bieberich, and W.D. Stamer, *A comparative study of serum exosome isolation using differential ultracentrifugation and three commercial reagents*. PloS one. Vol. 12 (2017) e0170628.
130. Van Deun, J., P. Mestdagh, R. Sormunen, V. Cocquyt, K. Vermaelen, J. Vandesompele, M. Bracke, O. De Wever, and A. Hendrix, *The impact of disparate isolation methods for extracellular vesicles on downstream RNA profiling*. Journal of extracellular vesicles. Vol. 3 (2014).
131. Paolini, L., A. Zandrini, G. Di Noto, S. Busatto, E. Lottini, A. Radeghieri, A. Dossi, A. Caneschi, D. Ricotta, and P. Bergese, *Residual matrix from different separation techniques impacts exosome biological activity*. Scientific reports. Vol. 6 (2016).
132. Yuana, Y., J. Levels, A. Grootemaat, A. Sturk, and R. Nieuwland, *Co-isolation of extracellular vesicles and high-density lipoproteins using density gradient ultracentrifugation*. Journal of Extracellular Vesicles. Vol. 3 (2014) DOI: 10.3402/jev.v3403.23262.

133. Sódar, B.W., Á. Kittel, K. Pálóczi, K.V. Vukman, X. Osteikoetxea, K. Szabó-Taylor, A. Németh, B. Sperlág, T. Baranyai, and Z. Giricz, *Low-density lipoprotein mimics blood plasma-derived exosomes and microvesicles during isolation and detection*. Scientific reports. Vol. 6 (2016).
134. Théry, C., M. Boussac, P. Véron, P. Ricciardi-Castagnoli, G. Raposo, J. Garin, and S. Amigorena, *Proteomic analysis of dendritic cell-derived exosomes: a secreted subcellular compartment distinct from apoptotic vesicles*. The Journal of Immunology. Vol. 166 (2001) 7309-7318.
135. Kleijmeer, M.J., W. Stoorvogel, J.M. Griffith, O. Yoshie, and H.J. Geuze, *Selective enrichment of tetraspan proteins on the internal vesicles of multivesicular endosomes and on exosomes secreted by human B-lymphocytes*. The Journal of Biological Chemistry. Vol. 273 (1998) 20121-20127.
136. Yoshioka, Y., Y. Konishi, N. Kosaka, T. Katsuda, T. Kato, and T. Ochiya, *Comparative marker analysis of extracellular vesicles in different human cancer types*. Journal of Extracellular Vesicles. Vol. 2 (2013) DOI: 10.3402/jev.v3402i3400.20424.
137. Théry, C., A. Regnault, J. Garin, J. Wolfers, L. Zitvogel, P. Ricciardi-Castagnoli, G. Raposo, and S. Amigorena, *Molecular characterization of dendritic cell-derived exosomes*. The Journal of Cell Biology. Vol. 147 (1999) 599-610.
138. Higginbotham, J.N., M.D. Beckler, J.D. Gephart, J.L. Franklin, G. Bogatcheva, G.-J. Kremers, D.W. Piston, G.D. Ayers, R.E. McConnell, and M.J. Tyska, *Amphiregulin exosomes increase cancer cell invasion*. Current Biology. Vol. 21 (2011) 779-786.
139. Hemler, M.E., *Tetraspanin functions and associated microdomains*. Nature reviews Molecular cell biology. Vol. 6 (2005) 801-811.
140. Harris, V.M., *Protein detection by Simple Western™ analysis*. Western Blotting: Methods and Protocols. (2015) 465-468.
141. Melo, S.A., H. Sugimoto, J.T. O'Connell, N. Kato, A. Villanueva, A. Vidal, L. Qiu, E. Vitkin, L.T. Perelman, and C.A. Melo, *Cancer exosomes perform cell-independent microRNA biogenesis and promote tumorigenesis*. Cancer Cell. Vol. 26 (2014) 707-721.
142. Kalra, H., C.G. Adda, M. Liem, C.S. Ang, A. Mechler, R.J. Simpson, M.D. Hulett, and S. Mathivanan, *Comparative proteomics evaluation of plasma exosome isolation techniques and assessment of the stability of exosomes in normal human blood plasma*. Proteomics. Vol. 13 (2013) 3354-3364.
143. Mleczko, J., L. Litke, H. Larsen, and W. Chaffin, *Effect of glutaraldehyde fixation on cell surface binding capacity of Candida albicans*. Infection and Immunity. Vol. 57 (1989) 3247-3249.
144. Shelke, G.V., C. Lässer, Y.S. Gho, and J. Lötvall, *Importance of exosome depletion protocols to eliminate functional and RNA-containing extracellular vesicles from fetal bovine serum*. Journal of Extracellular Vesicles. Vol. 3 (2014) DOI: 10.3402/jev.v3403.24783.
145. Simpson, R.J., S.S. Jensen, and J.W. Lim, *Proteomic profiling of exosomes: current perspectives*. Proteomics. Vol. 8 (2008) 4083-4099.
146. Kruger, S., Z.Y.A. Elmageed, D.H. Hawke, P.M. Wörner, D.A. Jansen, A.B. Abdel-Mageed, E.U. Alt, and R. Izadpanah, *Molecular characterization of exosome-like vesicles from breast cancer cells*. BMC cancer. Vol. 14 (2014) 44.
147. Staubach, S., H. Razawi, and F.G. Hanisch, *Proteomics of MUC1 - containing lipid rafts from plasma membranes and exosomes of human breast carcinoma cells MCF - 7*. Proteomics. Vol. 9 (2009) 2820-2835.


148. Ashburner, M., C.A. Ball, J.A. Blake, D. Botstein, H. Butler, J.M. Cherry, A.P. Davis, K. Dolinski, S.S. Dwight, and J.T. Eppig, *Gene Ontology: tool for the unification of biology*. Nature genetics. Vol. 25 (2000) 25-29.
149. Sandvig, K. and A. Llorente, *Proteomic analysis of microvesicles released by the human prostate cancer cell line PC-3*. Molecular & Cellular Proteomics. Vol. 11 (2012) M111. 012914.
150. Valadi, H., K. Ekström, A. Bossios, M. Sjöstrand, J.J. Lee, and J.O. Lötvall, *Exosome-mediated transfer of mRNAs and microRNAs is a novel mechanism of genetic exchange between cells*. Nature cell biology. Vol. 9 (2007) 654-659.
151. Palazzolo, G., N.N. Albanese, G. Di Cara, D. Gyga, M.L. Vittorelli, and I. Pucci-Minafra, *Proteomic analysis of exosome-like vesicles derived from breast cancer cells*. Anticancer Research. Vol. 32 (2012) 847-860.
152. Chiba, M., M. Kimura, and S. Asari, *Exosomes secreted from human colorectal cancer cell lines contain mRNAs, microRNAs and natural antisense RNAs, that can transfer into the human hepatoma HepG2 and lung cancer A549 cell lines*. Oncology reports. Vol. 28 (2012) 1551-1558.
153. Linares, R., S. Tan, C. Gounou, N. Arraud, and A.R. Brisson, *High-speed centrifugation induces aggregation of extracellular vesicles*. Journal of extracellular vesicles. Vol. 4 (2015).
154. Heijnen, H.F., A.E. Schiel, R. Fijnheer, H.J. Geuze, and J.J. Sixma, *Activated Platelets Release Two Types of Membrane Vesicles: Microvesicles by Surface Shedding and Exosomes Derived From Exocytosis of Multivesicular Bodies and Granules*. Blood. Vol. 94 (1999) 3791-3799.
155. Smith, Z.J., C. Lee, T. Rojalin, R.P. Carney, S. Hazari, A. Knudson, K. Lam, H. Saari, E.L. Ibañez, and T. Viitala, *Single exosome study reveals subpopulations distributed among cell lines with variability related to membrane content*. Journal of Extracellular Vesicles. Vol. 4 (2015) 28533.

7 Appendix

7.1 Experimental supplementary

7.1.1 Isolation with the isolation kit

The isolation with the isolation kit from Thermo Fisher was performed using the protocol from the supplier, presented in **Figure 40**.



invitrogen
by *Life* technologies

Rev. Date: 28 June 2012

Store at 2°C to 8°C

Total Exosome Isolation (from cell culture media)

Publication No. MAN0006949 Catalog Number: 4478359

Product Description

Exosomes are small vesicles (30–120 nm) containing RNA and protein that are secreted by various types of cells in culture, and found in abundance in body fluids including blood, saliva, urine, and breast milk. Exosomes are thought to function as intercellular messengers, delivering their cargo of effector or signaling macromolecules between specific cells, however, their formation, the makeup of the cargo, and biological pathways in which they are involved remain incompletely understood.

The biological study of exosome function and trafficking requires the isolation of intact exosomes, but the current methods used are tedious, non-specific, and difficult. The Total Exosome Isolation (from cell culture media) reagent provides a simple and reliable method of concentrating intact exosomes from cell culture media samples. By tying up water molecules, the Total Exosome Isolation (from cell culture media) reagent forces less-soluble components (i.e. exosomes) out of solution, allowing them to be collected after brief, low-speed centrifugation.

Product Contents

Total Exosome Isolation (from cell culture media) reagent contains reagents sufficient for processing 100 mL of cell culture media.

Components	Amount	Storage
Total Exosome Isolation (from cell culture media)	50 mL	2°C to 8°C

General Guidelines

- To ensure that isolated exosomes originate from your cells of interest, culture the cells with exosome depleted fetal bovine serum (FBS), because normal FBS contains extremely high levels of exosomes that will contaminate the cell derived exosomes.
If you cannot obtain exosome depleted FBS, certain cell lines can be grown for up to 12 hours in media without FBS.
- If you are isolating intact exosomes from serum, use the Total Exosome Isolation (from serum) reagent.
- After exosomes are isolated, total RNA and protein can be purified using the Total Exosome RNA and Protein Isolation Kit.
- To isolate exosomal proteins for immunoprecipitation, use Exosome Immunoprecipitation (Protein A) or Exosome Immunoprecipitation (Protein G).

Prepare Sample

- Harvest cell culture media.
- Centrifuge the cell media at 2000 × g for 30 minutes to remove cells and debris.
- Transfer the supernatant containing the cell-free culture media to a new tube without disturbing the pellet.

Isolate Exosomes

- Transfer the required volume of cell-free culture media to a new tube and add 0.5 volumes of the Total Exosome Isolation (from cell culture media) reagent.

Culture Media	Reagent
1 mL	500 µL
10 mL	5 mL

- Mix the culture media/reagent mixture well by vortexing, or pipetting up and down until there is a homogenous solution.
- Incubate samples at 2°C to 8°C overnight.
- After incubation, centrifuge the samples at 10,000 × g for 1 hour at 2°C to 8°C.
- Aspirate and discard the supernatant. Exosomes are contained in the pellet at the bottom of the tube (not visible in most cases).
- Resuspend the pellet in a convenient volume of 1X PBS or similar buffer.

Starting Cell Culture Media Volume	Resuspension Volume
1 mL	25–100 µL
10 mL	100 µL–1 mL

- Once the pellet is resuspended, the exosomes are ready for downstream analysis or further purification through affinity methods.
Keep isolated exosomes at 2°C to 8°C for up to 1 week, or at ≤20°C for long-term storage.

Figure 40: Protocol for the total exosome isolation (from cell culture media), from Thermo Fisher.

7.1.2 Example on measurements and calculations of protein concentration

The protein concentration (or amount, μg) of a lysed sample was calculated from a calibration curve. BSA was used as standard protein, with the measurements of absorbance (562 nm) using 8 standard concentrations (**Table 10**).

Table 10: Standard BSA protein (μg) at increasing amounts (0-7 μg) showing the absorbance at 562 nm (triplicate)

μg protein (BSA)	Replicate number		
	1	2	3
0	0.118	0.116	0.119
1	0.304	0.246	0.227
2	0.454	0.394	0.381
3	0.533	0.548	0.536
4	0.687	0.653	0.637
5	0.784	0.715	0.722
6	0.937	1.033	0.874
7	1.046	0.956	1.046

These values (μg protein (BSA) and the corresponding absorbance) were plotted to yield a calibration curve (**Figure 41**), by adding a linear trendline. The trendline equation was used to calculate the amount of protein in the amount of sample added by the unknown (i.e.

$$x = \frac{y - 0.1158}{0.1291}.$$

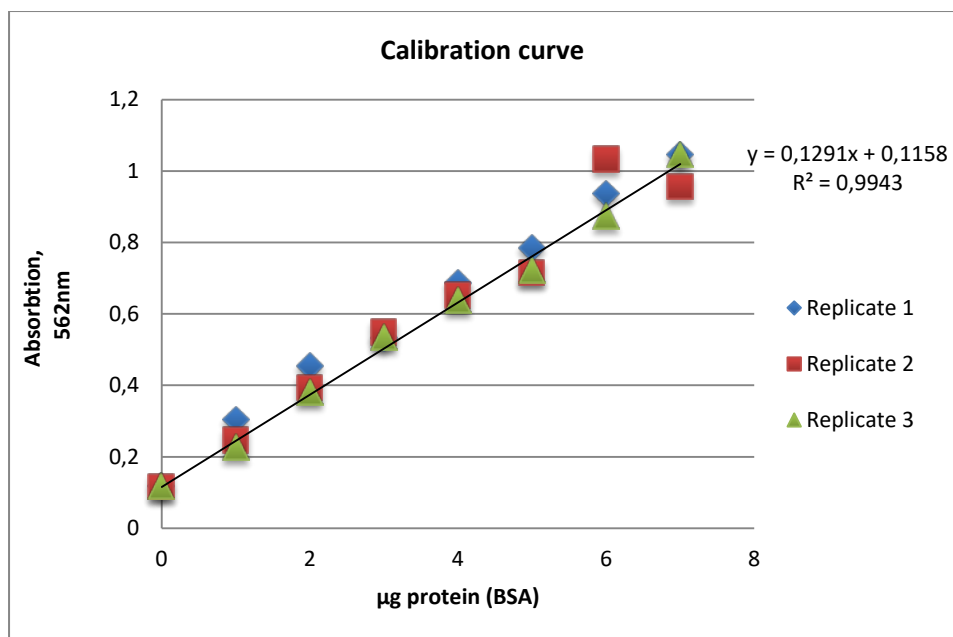


Figure 41: Calibration curve of standard BSA protein amounts (µg) in the x-axis, and the measured absorbance (562 nm) at the y-axis. A linear trendline is added, with equation and R-squared value.

7.2 Experimental considerations and discussions

7.2.1 Experiences with CD63 antibodies

The first batch of anti-CD63 did not display bands of reproducible quality (**Figure 42**); the characteristic band form of CD63 did both occur of high- and low intensity, or it did not occur at all. When analysing the cells with WB after ordering a new batch of this antibody, the characteristic band form of CD63 did however occur (**Figure 31**).

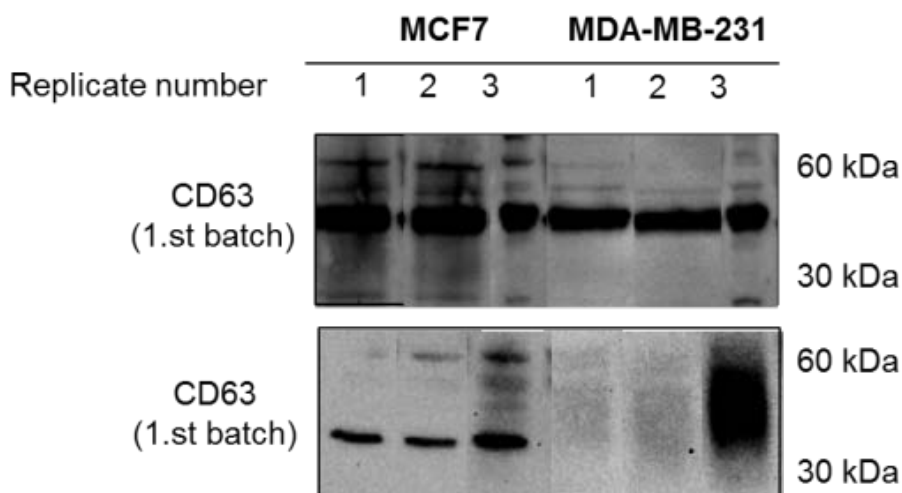


Figure 42: WB of three cell lysate replicates from the two breast cancer cell lines MCF-7 and MDA-MB-231 (from F3, F4 and F5), with antibody and expected kD of anti-CD63 from the first batch. The bands of high intensity at approximately 42 kDa are due to incubation with anti-actin. 10.6-15.0 µg proteins were loaded to each well.

7.2.2 Experimental considerations and observations of membrane structures with TEM

At first, the samples were prepared without immunolabeling, to examine if the concentration of particles was high enough for the double membrane structures to successfully adsorb to the grid. Exosomes from MCF-7 were set as a standard as the respective cells and exosomes (from isolation kit) seemed to express commonly positive protein exosome markers with WB (with the presence of bands at higher intensity at kDa corresponding to CD9, **Figure 31**, **Figure 32**). Particles from 2 mL medium suspended in 20 μ L PBS and a grid incubation time of 5 minutes was sufficient to observe a darker structure (**Figure 43 2**) encircled by two parallel electron-dense lines separated by an electron-lucent central line. The electron-dense lines most likely represent the phospholipid leaflets of the double membrane and the electron-lucent line most likely represents the fatty acids of the phospholipids creating the intersection of the membrane. Thus this observation indicated the presence of lipid double membranous compartments (marked as 1. 2). However the membrane structure marked as 1 was considerable larger than the theoretical size of exosomes (30-100 nm), and looked more like to originate from the cells own plasma membrane. The other lighter circular structures of high abundance seemed not to hold a double membrane as they were only encircled by one darker line. This can be seen on as artefacts possible arising from the sample preparation or from the irradiation damage under the electron beam.

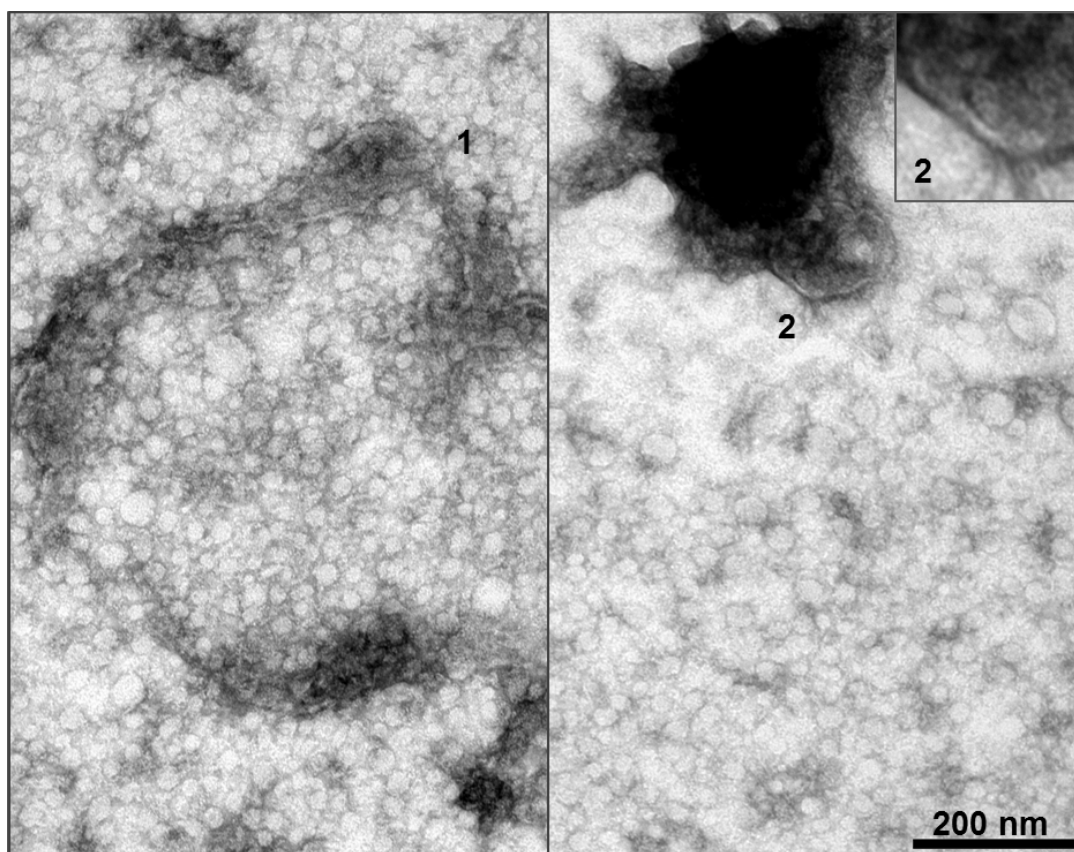


Figure 43: Two images of isolated samples (isolation kit) from MCF-7 cells, with numbers indicating the presence of structures that appear as membrane compounds. Taken with TEM, magnitude of 40 000. The micrographs are cropped and the image at upper right corner was digitally zoomed 50%.

7.2.3 Immunogold labelling optimization with TEM

To determine the presence of double membrane structures related to exosomes, immunogold labelling with a membrane specific protein exosome marker was essential. As bands occurred at the kDa corresponding to CD9 with almost all isolated lysates with WB (**Figure 32**), the membrane protein CD9 was chosen for immunogold labelling. This protein marker has also been used for the same purpose from one of the respective cell lines (MDA-MB-231) in articles written by Melo et al. [30, 141]. Instead of using mouse anti-CD9 (monoclonal) as with WB, rabbit anti-CD9 (polyclonal) was applied because of its higher amount of different epitope-binding sites. This would potentially lead to a higher degree of antibody-antigen bindings and increase the possibility of observing gold labelled membrane structures. As the host was rabbit this would also decrease the sample preparation time. In addition, the PAG could bind directly to the rabbit antibody instead of using a secondary antibody (i.e. bridging antibody).

The grid incubation time on the sample droplet was set to 20 minutes to possibly increase the amount of exosomes adsorbed to the surface. Different concentrations of the antibody

(diluted 1:10 and 1:50) were investigated with samples isolated by both isolation kit and UC samples, however no gold labelled membrane structures were observed (**Figure 44** A, B and **Figure 45** A, B). This could be of several reasons; e.g. the variable region on the antibody did not bind to the epitope of CD9 because they were not sterically accessible and/or because the antibody has lost its function. One other reason could be that the membrane structures observed were not CD9-positive, or the PAG did not bind to the antibody for some reason or/and was not holding a native structure.

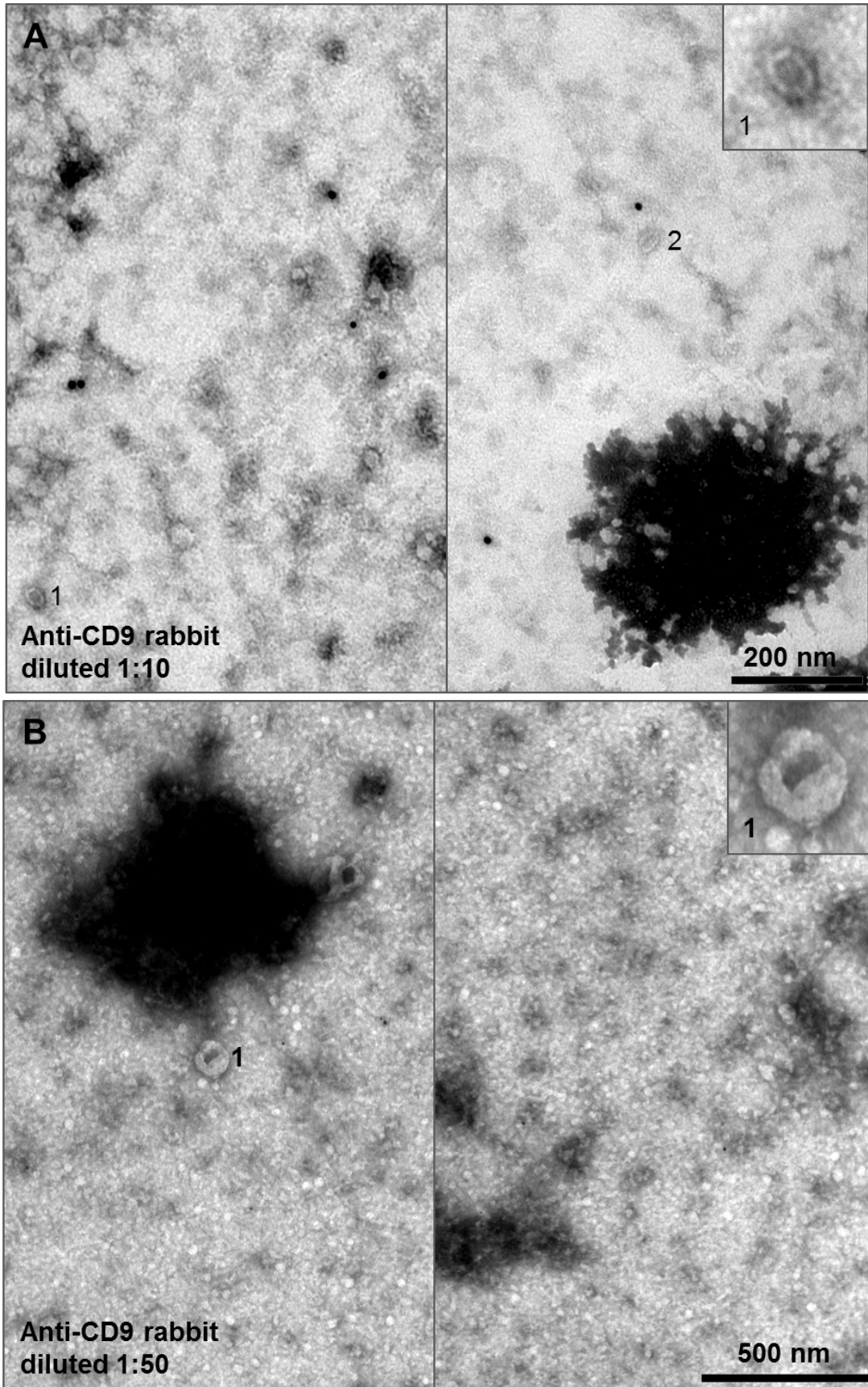


Figure 44: Images of immunogold labelled MCF-7 isolated samples (isolation kit), with numbers indicating the presence of structures that appear as double membrane compounds. Antibody dilution of A) 1:10, with a magnitude of 40 000, and B) 1:50, with a magnitude of 20 000. Gold particles were depicted as black dots. The images are cropped, and the photos at upper right corner were digitally zoomed 50%.

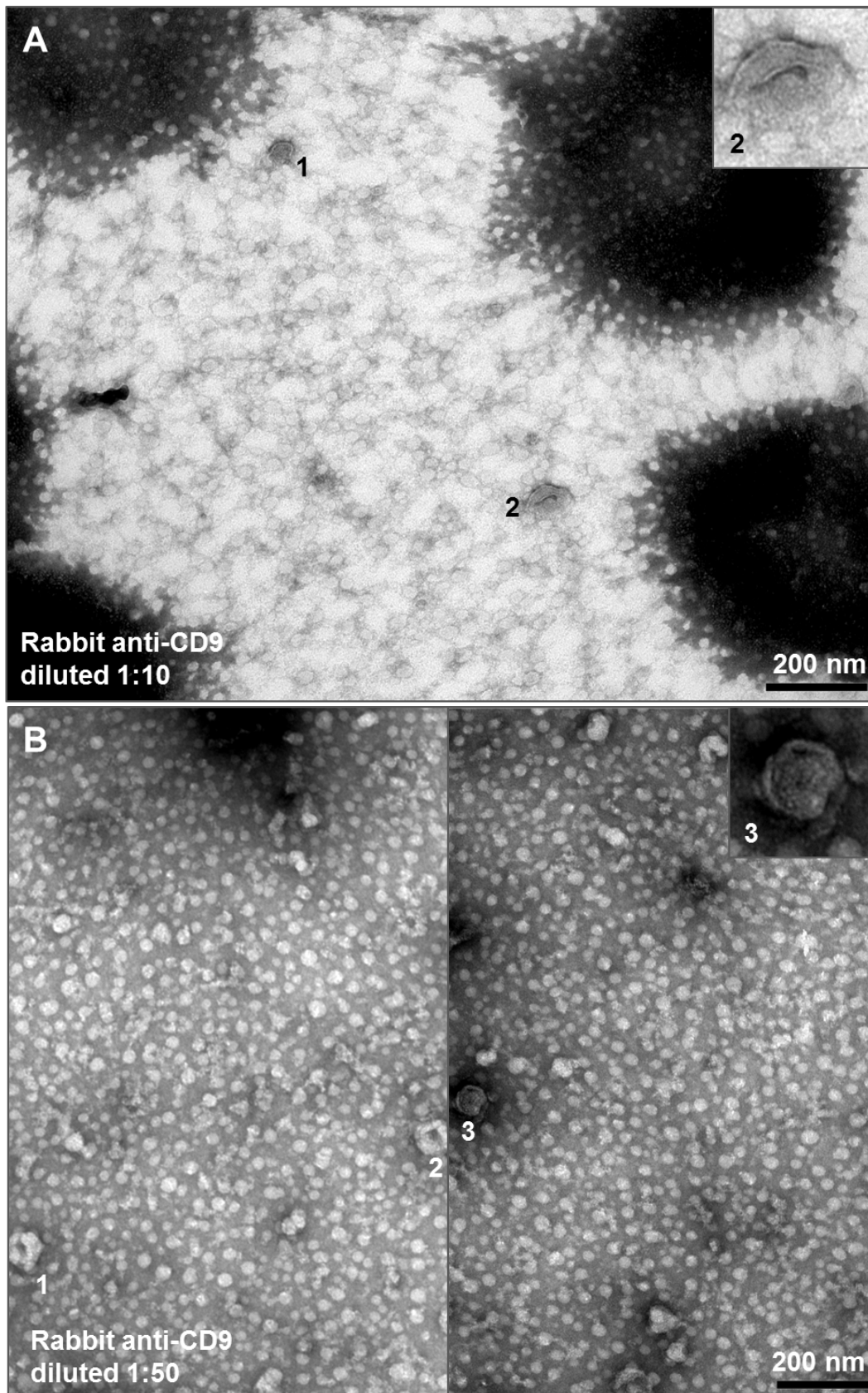


Figure 45: Images of immunogold labelled MCF-7 isolated samples (UC), with numbers indicating the presence of structures that appear as double membrane compounds. Antibody dilution of A) 1:10. and B) 1:50. Gold particles were depicted as black dots. Images were taken with a magnification of 30 000. The images are cropped, and the photos at upper right corner were digitally zoomed approximately 50%.

To investigate if the rabbit antibody was functionally active, exosomes from MCF-7 cells was isolated (isolation kit) and analysed with WB using both mouse- and rabbit antibodies. Both antibodies were functionally active as observed by the presence of a bond of high intensity at the kDa corresponding to CD9 (**Figure 46**). Thus the antibody-binding could be affected by denatured/non-denatured state of the protein.

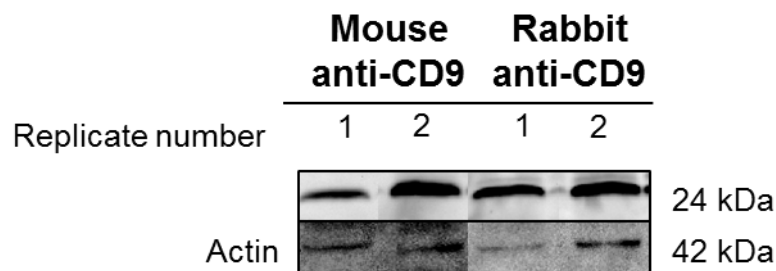


Figure 46: WB of anti-CD9 from mouse and rabbit with loading control (actin) and two replicates isolated from MCF-7 (isolation kit).

To investigate whether the antibody-binding could be affected by denatured/non-denatured of the protein, CD9-positive exosome samples (not isolated, but depleted from cell debris), from the cell line SW480 (colorectal cancer cell line) were received from Thermo Fisher [152].

The SW480 exosome sample showed several membrane compounds (**Figure 47 B**), but still no immunogold labelling was observed. In addition the membrane compounds observed were of size >100 nm, thus it was undefined whether these could be classified as exosomes. As a control, the sample preparation was repeated and the imaging was performed on another instrument (**Figure 47 C**), also with negative presence of PAGs.

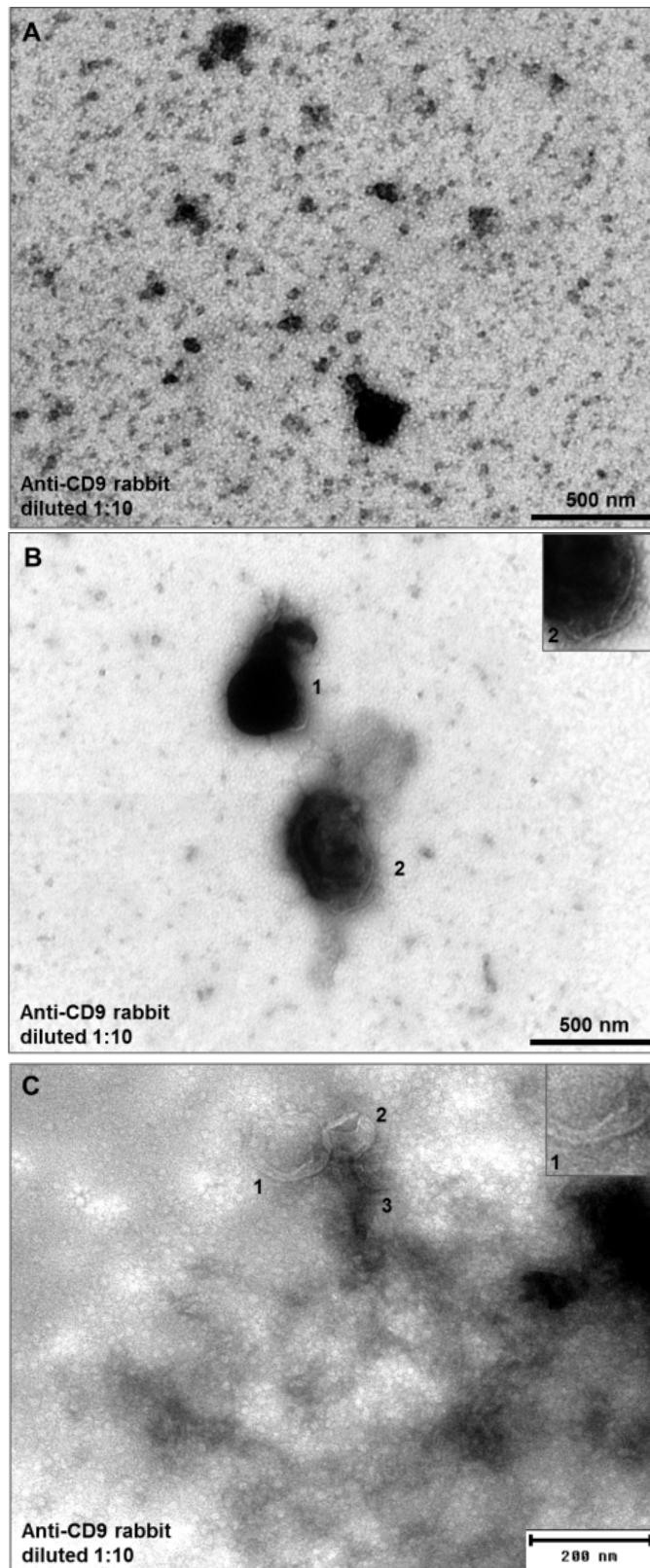


Figure 47: TEM micrographs of immunogold labelled (anti-CD9 rabbit, diluted 1:10) concentrated exosome samples (not isolated) from SW480 cells, with numbers indicating the presence of structures that appear as membrane compounds. A) Sample incubation duration set to 5 minutes yielded in adsorption of too much material. B) Sample incubation duration set to 2 minutes made it possible to observe membrane compounds, but no gold labelling occurred. The membrane compounds observed were of size >100 nm. C) Same sample preparation as in B), imaging was performed with another instrument. Micrographs were taken with a magnification of 20 000 (A and B) and 40 000 (C). The photos at upper right corner were digitally zoomed approximately 50%.

Next, the respective samples were immunogold labelled with mouse anti-CD9 and rabbit anti-mouse as secondary antibody to study if this contributed to labelling of higher specificity. PAGs were distributed around the double membrane compounds (**Figure 48**, 1-4), indicating successful immunogold labelling.

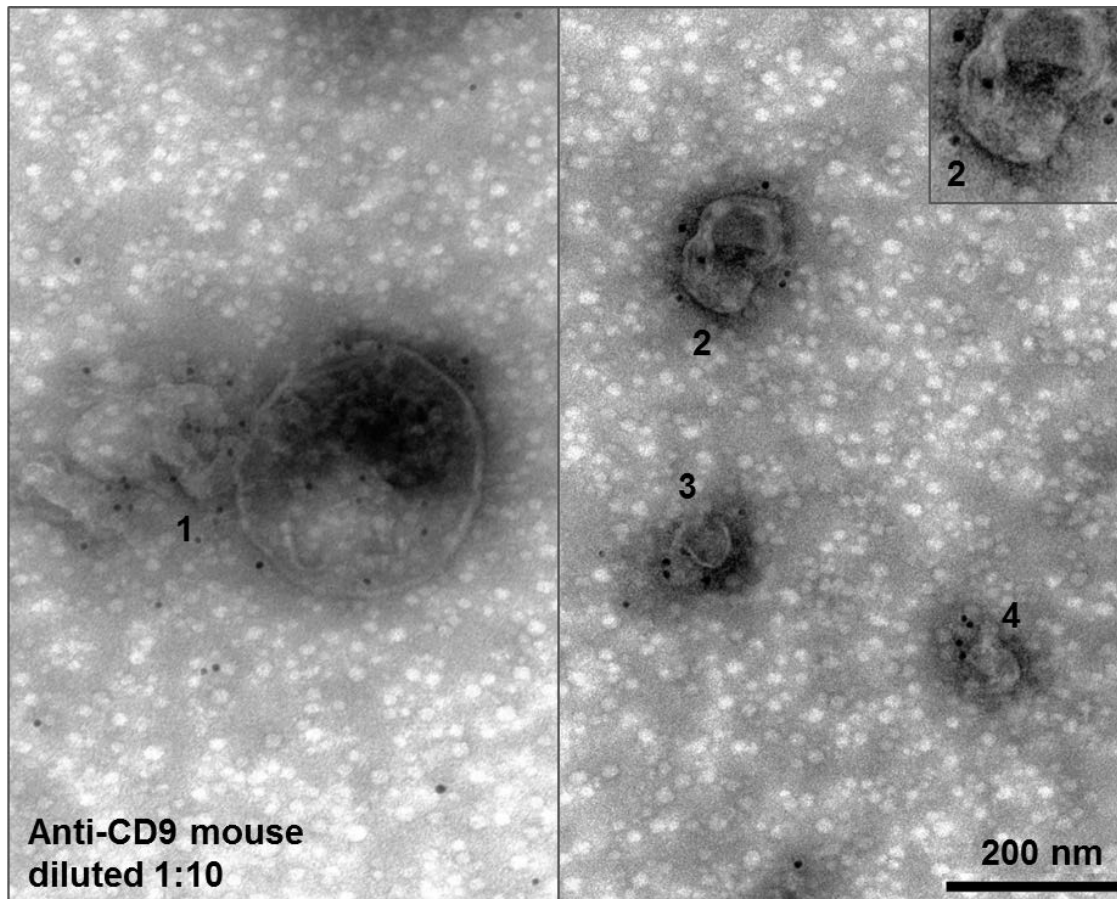
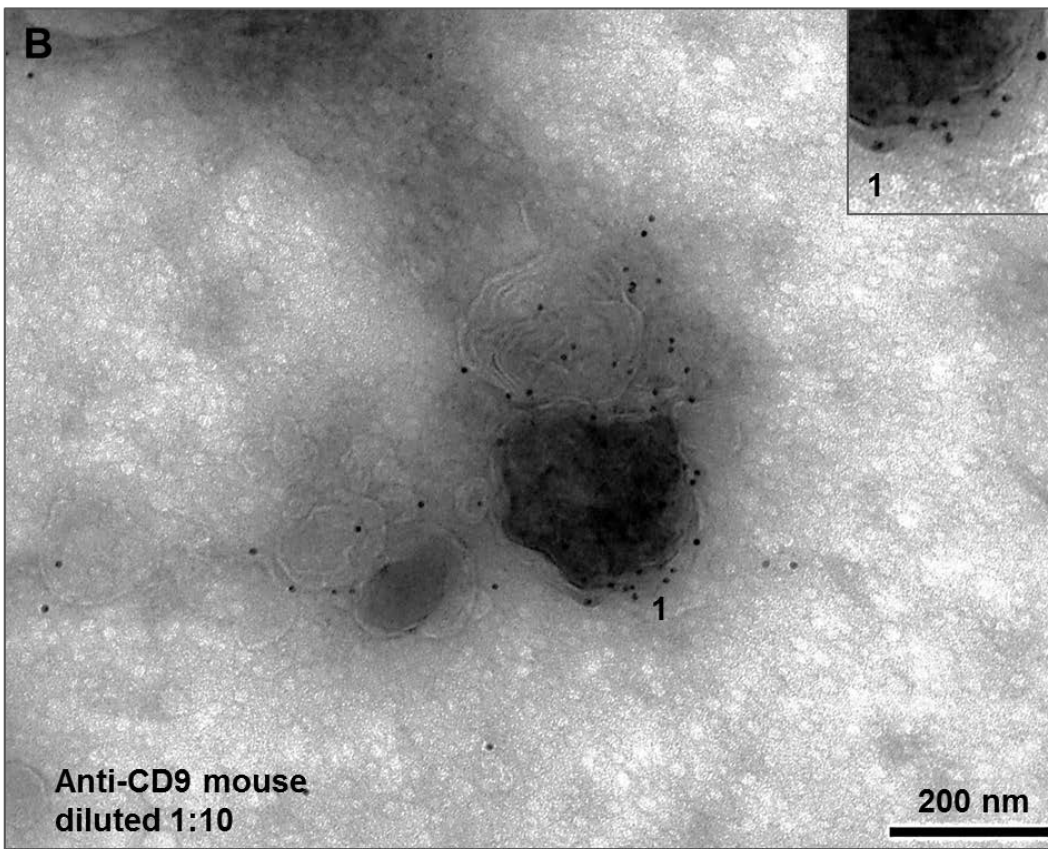
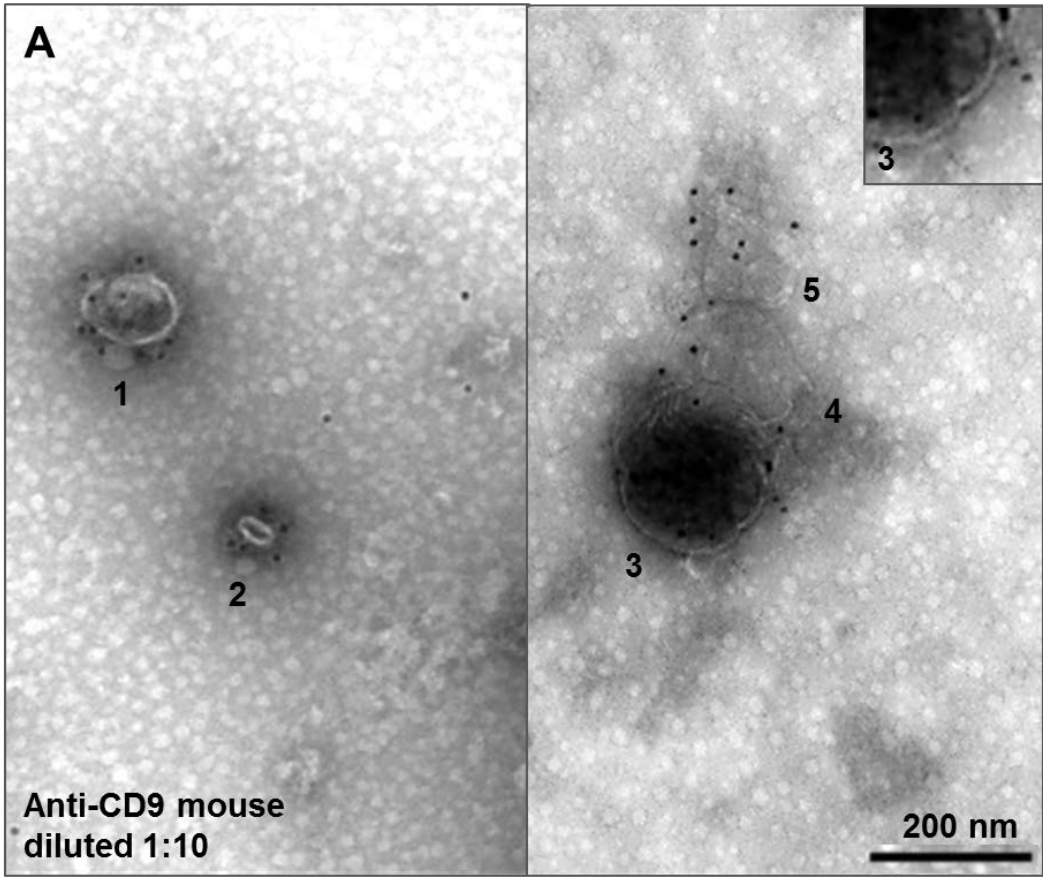


Figure 48: Images of immunogold labelled (mouse anti-CD9) with secondary antibody concentrated exosome samples (not isolated) from SW480 cells, with numbers indicating the presence of structures that appear as double membrane compounds. Gold particles were depicted as black dots. Images were taken with a magnification of 40 000. The images were cropped, and the photo at upper right corner was digitally zoomed approximately 50%.

The same tendencies were observed with SW480 isolated samples with the isolation kit (**Figure 49 A, B and C**). Left picture of **Figure 49 A**, figure B and C was prepared and imaged on the same day, while the right side of figure **Figure 49 A** was prepared and imaged subsequently 12 days. This immunogold labelling showed to be repeatable, thus strengthening the probability of these PAGs to be bound to the epitope of the protein exosome marker CD9. The lack of labelling with rabbit anti-CD9 could most likely be due to the non-binding to the protein in non-denatured state, or rabbit anti-CD9 was specific for a epitope on CD9 sterically less accessible.

Aggregation of double membrane structures was observed in the SW480 isolated samples with the isolation kit (**Figure 49** A, B and C). This can be due to higher concentrations, temperature changes or a result of the water removal during sample preparation. Additionally this can be due to high-speed centrifugation [153]. However this is not uncommonly observed by others (see EM images [65, 154, 155]).



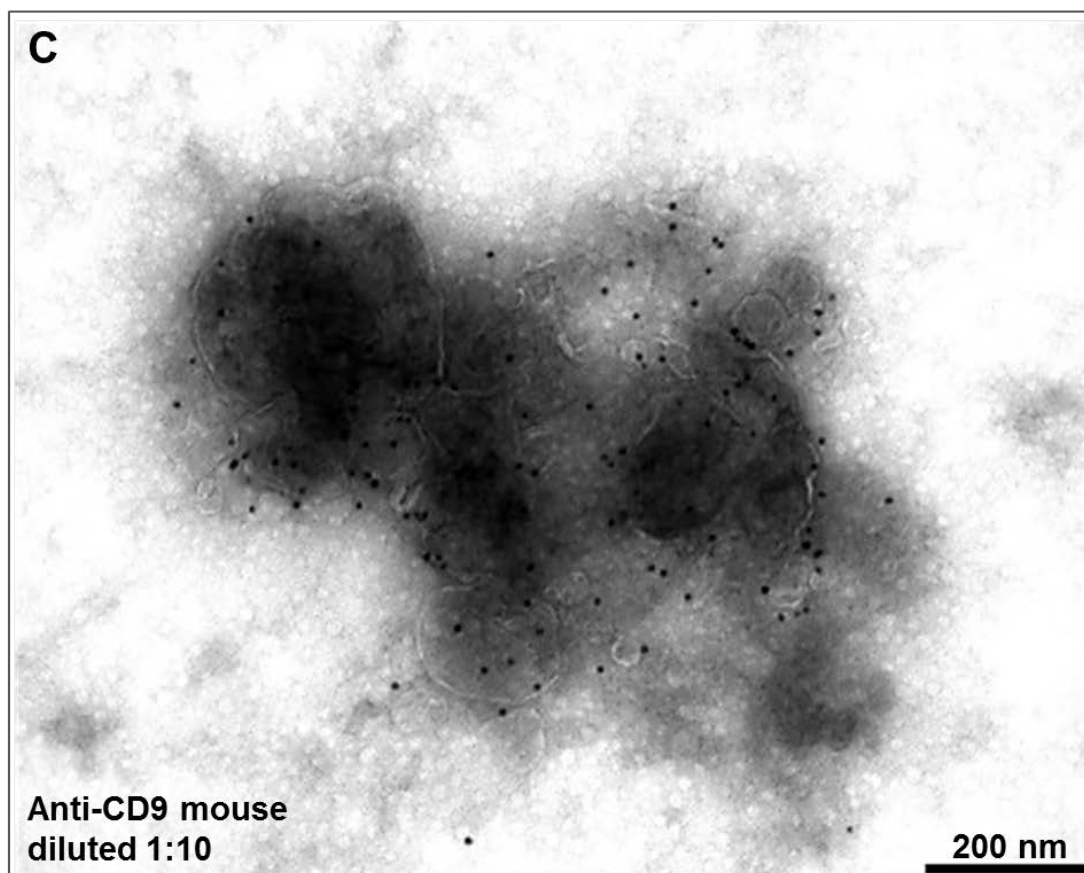


Figure 49: Images of immunogold labelled (mouse anti-CD9 with secondary antibody) SW480 isolated sample with the isolation kit. The numbers are indicating the presence of structures that appear as double membrane compounds. As figure B and C displayed more than 5 membrane compounds, no numbering was performed on the images. Gold particles were depicted as black dots. Images were taken with a magnification of 40 000. Left picture of figure A, figure B and C was prepared and imaged on the same day, while the right side of figure A was prepared and imaged subsequently 12 days. The images are cropped, and the photo at upper right corner (A) was digitally zoomed approximately 50%.

7.2.4 Immunogold labelling of MCF-7 isolated samples (UC), rejected

Specific immunogold labelled fractions was frequently observed (Figure 50 B), which could indicate disruption of the membrane compounds due to increased exposition to high mechanical strength (repeated centrifugation runs). Both unlabelled (Figure 50 A-1) and labelled membrane structures were observed (Figure 50 A-2 and -3); however the zoomed micrograph of Figure 50 A-2 did not display a clear circular membrane structure.

MCF-7 (UC)

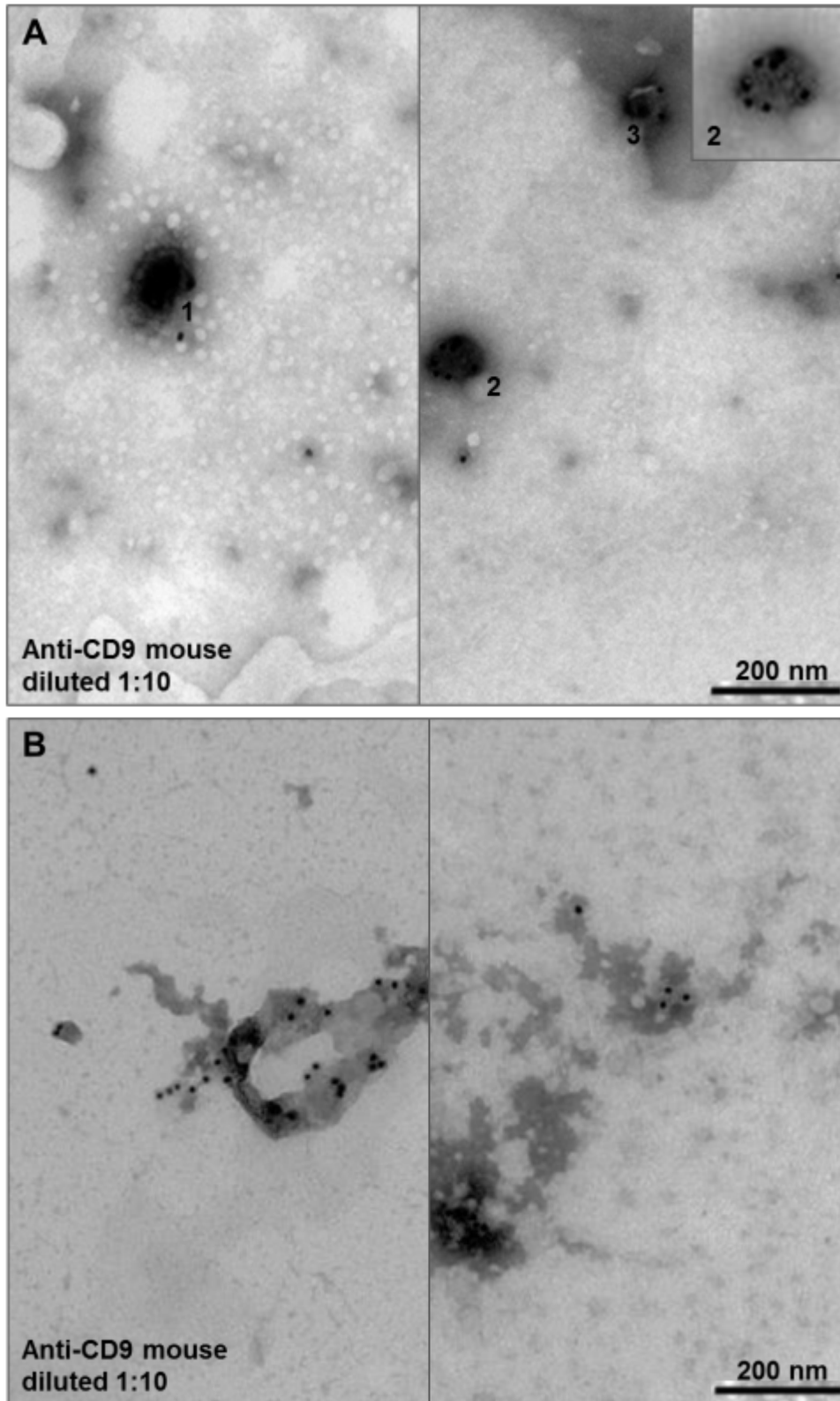


Figure 50: Four TEM micrographs of immunogold labelled (anti-CD9 mouse (1:10) with secondary antibody (1:200)) isolated exosome samples from MCF-7 cells (UC), with numbers indicating the presence of structures that appear as membrane compounds. Gold particles were depicted as 10 nm diameter black dots. Micrographs were taken with a magnification of 40 000. The micrographs are cropped, and the photo at upper right corner (figure A) was digitally zoomed approximately 50%.

7.2.5 Experimental considerations when reproducing the nanoLC-MS/MS protein analyses performed externally

In house, HSA was digested in parallel with the samples as a quality control of the sample preparation and instrumentation. However low protein coverage (%) and poor chromatography were repeatedly observed for the HSA digested samples. In addition, high level of noise in the MS spectra was frequently observed in the m/z range from approximately 400-1000 (charged +1) (**Figure 51**). Delta m/z was of approximately 22, possibly originating from polymers (i.e. PEGs). Exchanging containers from PE to glass did not improve spectral quality, hence detergent buffer added during lysis (NP-40) was suspected as source of contamination. Separation and digestion in-gel are commonly known to remove detergents, thus this was used for the protein samples.

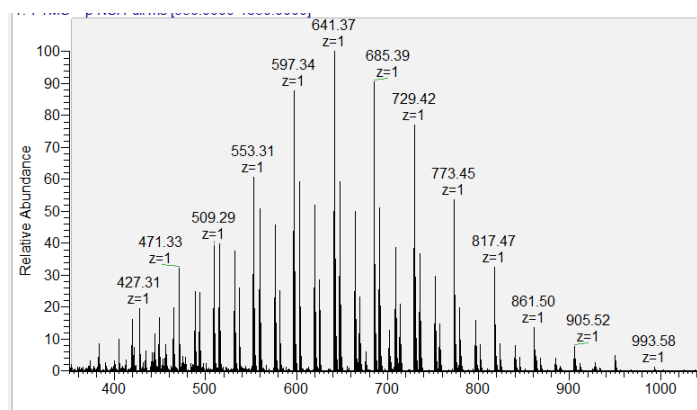


Figure 51: MS-spectrum of contaminating ions of high abundance observed in the m/z range from approximately 400-1000 (charged +1).

The protein samples were separated by SDS-PAGE as contaminants with low molar mass (e.g. NP-40) would not be retained by the gel pores. Additionally, the separation of the proteins would possibly improve the sensitivity of the proteomic profiling. Aliquots of 3 μg protein were used, except one replicate (MCF-7, UC) of 0.6 μg . BSA was digested in parallel. Highest ion sensitivity, protein coverage and peptide fragmentation matches were achieved after a retrypsination of the BSA with newly made trypsin, followed by three protein extractions. Injection of 10 μL sample was chosen, as a 15 μL injection ($n=3$) contributed to a reduced peptide retention window from 28 minutes to 23 minutes (**Figure 52**). In addition monitoring three selected peptides displayed reduced retention time (from 3.0 to 8.2 minutes difference) and chromatography (**Figure 53**) 15 μL injections would possible increase the risk of losing poorly retained peptides.

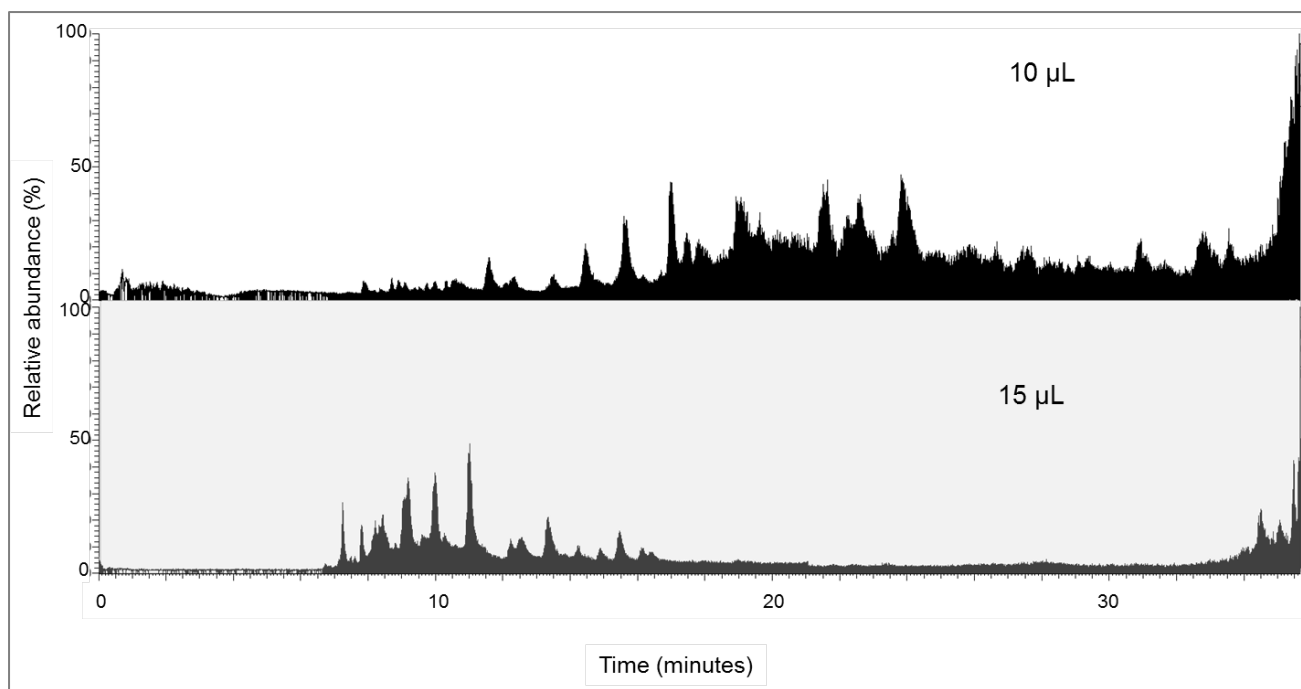


Figure 52: Total ion chromatogram of 10 ng BSA injection of 10 μL (ion intensity of 1.87×10^9) and 15 μL (ion intensity of 1.36×10^9), with relative abundance (%) and retention time (extracted from 0-35 minutes). The gradient elution for the analyses performed in house and external is shown in **Table 5.**

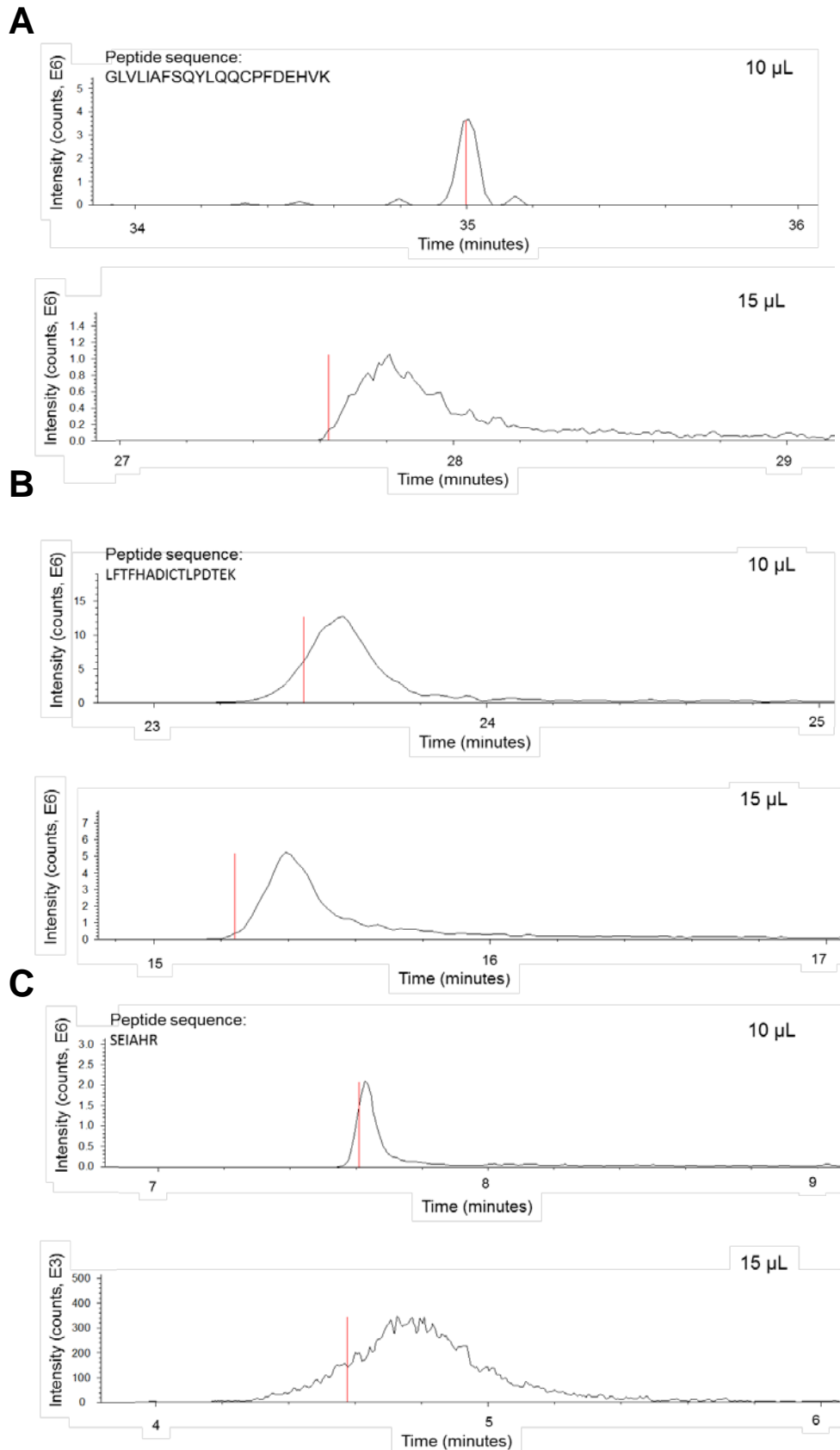


Figure 53: Extracted peptide chromatograms of three peptides when (10 ng BSA) the injection volume was to be tested (10 μ L and 15 μ L). A) showing the peptide GLVLIAFSQYLQQCPFDEHVK, with retention times of 35 minutes (10 μ L) and 27.6 minutes (15 μ L). B) Showing the peptide LFTFHADICTLPDTEK with retention times of 23.5 minutes (10 μ L) and 15.2 minutes (15 μ L). C) Showing the peptide SEIAHR with retention times of 7.6 minutes (10 μ L) and 4.58 minutes (15 μ L). The gradient elution for the analyses performed in house and external is shown in **Table 5.**

7.2.6 Protein identification with MCF-7 isolated exosomes

The protein identifications from the in house analyses of the isolated samples by ultracentrifugation (MCF-7 cell lines) were rejected, as it was suspected to be contaminated with debris from PBS (section 4.2.2).

580 unique proteins were identified in isolated samples (isolation kit) from MCF-7 cell lines (Venn diagram presented in **Figure 54 A**), whereof 239 proteins were unique for the in house analyses and 195 proteins unique in the extern analysis. 146 identified proteins were found in both experiments thus showing the reproducibility.

The greater amount of protein identified by the in house analyses could be of several reasons; 9 mL cell cultured medium was isolated contra 1 mL giving a more heterogeneous mixture of proteins or analysing each gel-fraction yielded in additional identification of the low abundant proteins. Additionally, the absence of a salt removal step during sample preparation (by Zip-Tip) could lead to a decreased sample loss of the peptides from the in house analyses. The greater amount of proteins identified by the in house analyses could simply be due to the different sample batches grown at different stages of the cell cycles and/or passage which would affect the translation diversity of proteins.

By combining data from these four experiments, the protein complexity of the isolated samples from the MCF-7 cell line was prominent (**Figure 54 B**). All experiments uniquely identified 97 proteins. This can explain the diverse responses when analysing the samples with WB; the protein composition of the samples was not identical.

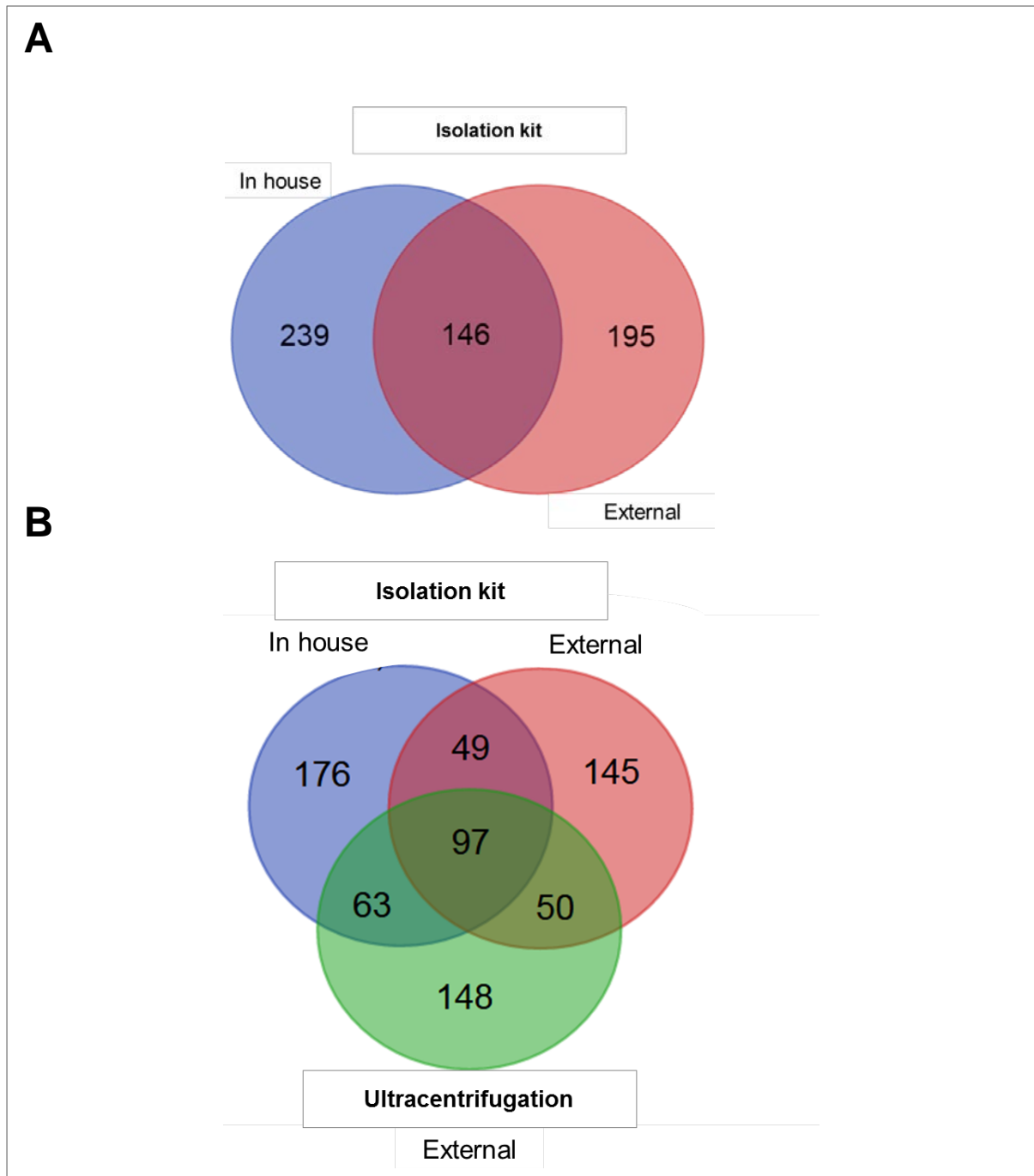


Figure 54: Venn diagrams of proteins identified of isolated exosomes from MCF-7 with analyses in house and external. A) Comparing the proteins identified from isolation kit. B) Comparing the proteins identified in isolated samples by both isolation kit and UC.

7.2.7 Protein identification with MDA-MB-231 isolated exosomes

In samples isolated with the isolation kit from MDA-MB-231 cell cultured media, the in house analyses identified 177 unique proteins while external analysis identified 520 unique proteins (**Figure 55 A**). 246 identified proteins were common for these two analyses. The notable dissimilarity in the number of proteins identified between the samples isolated with the isolation kit was similarly identified with the samples isolated with UC (**Figure 55 B**). 82 proteins were uniquely identified by all four experiments (**Figure 55 C**), also supporting the diverse responses that followed with WB analyses.

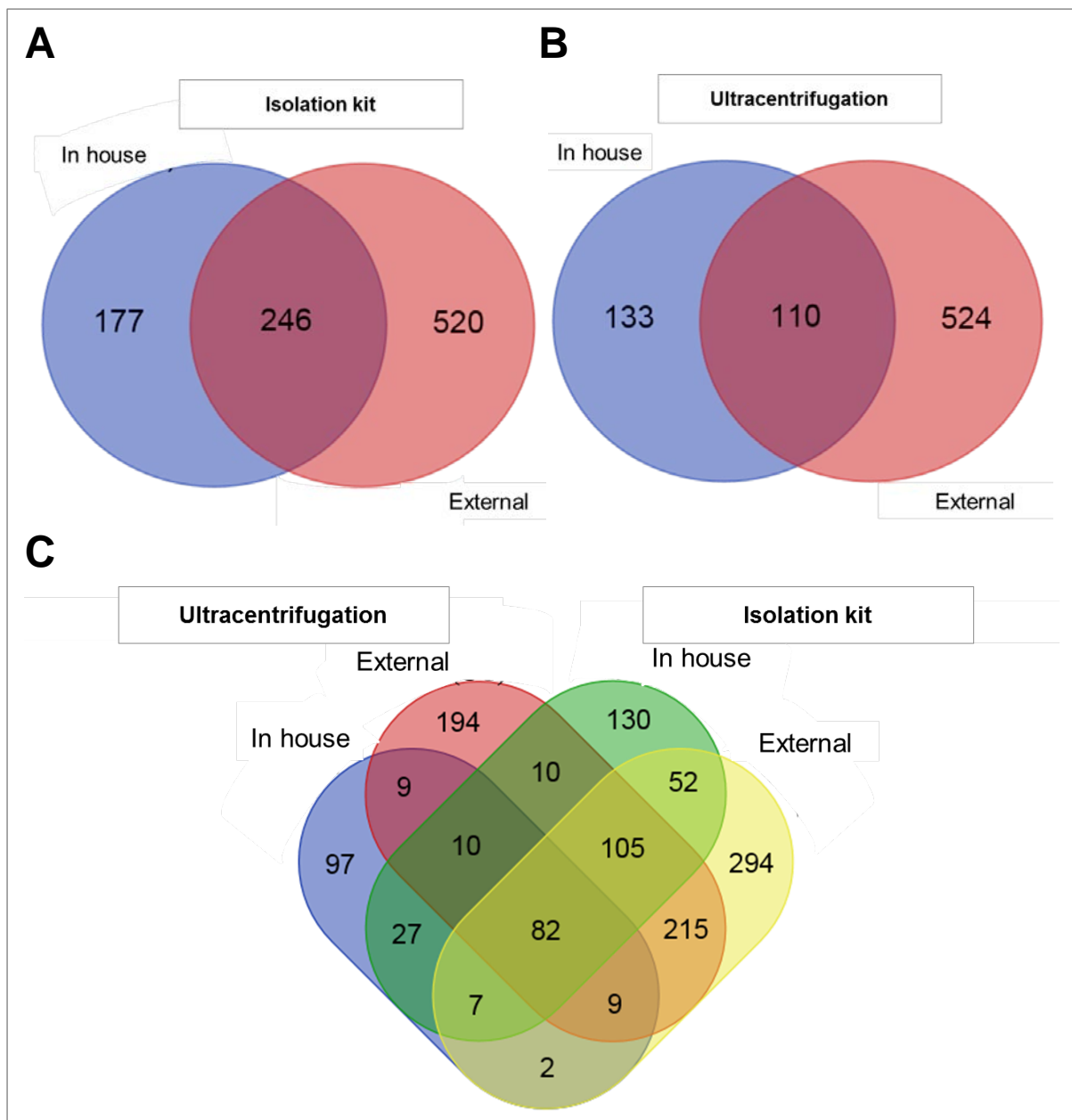


Figure 55: Two Venn diagrams of proteins identified of isolated exosomes from MDA-MB-231 with analyses in house and external. A) Comparing the proteins identified from isolation kit. B) Comparing the proteins identified from ultracentrifugation. C) Comparing the proteins identified in isolated samples by both isolation kit and UC.

7.3 Raw data and calculations (tables)

7.3.1 cell culturing confluency and

The amount of cells measured to yield **Figure 27**, is presented with average (10^6) and standard deviation (10^6) in **Table 12**. The different number of replicates measured is due to different amounts of material available.

Table 11: Overview of the amount of cells ($\times 10^6$) measured after reaching 80-90 % confluency with the average number (\bar{x}) and standard deviation (s) both multiplied with $\times 10^6$.

	Counted amount of cells $\times 10^6$ MCF-7	Counted amount of cells $\times 10^6$ MDA-MB-231
Replicate 1	8.9	44.0
Replicate 2	4.7	22.4
Replicate 3	10.4	15.3
Replicate 4	4.1	9.3
Replicate 5	8.9	5.3
Replicate 6	10.5	24
Replicate 7		19.3
\bar{x} (average counted amount of cells $\times 10^6$)	8.0	19.9
s (Standard deviation of the counted amount of cells $\times 10^6$)	2.6	11.7

7.3.2 UV-measurements

The protein measurements representing **Figure 29** is displayed in **Table 13**. The different number of replicates measured is due to different amounts of material available. The MCF-7 cells measured at the end of the cell culturing prior to exosome isolation with the isolation kit were on average 3 640 500 cells, and 5 361 500 with MDA-MB-231. The MCF-7 cells measured at the end of the cell culturing prior to exosome isolation with the isolation kit were on average 8 312 775 cells, and 15 336 975 with MDA-MB-231.

Table 12: The μg protein / mL isolated cell culture media measured of replicates in exosome samples isolated with the isolation kit and UC, from MCF-7 and MDA-MB-231 cell lines. The average with standard deviation is shown.

	Isolation kit		Ultracentrifugation	
	MCF-7	MDA-MB-231	MCF-7	MDA-MB-231
Replicate 1	57.5	44.9	1.25	0.65
Replicate 2	60.3	46.5	1.48	0.65
Replicate 3	42.9	48.2	1.12	
Replicate 4	72.5	62.7		
Replicate 5	71.6	57.1		
Replicate 6	57.5	50.3		
Replicate 7	150.9	122.4		
x (μg protein / 10^6 cells)	73.3	61.7	1.28	0.65
s (μg protein / 10^6 cells)	35.6	27.5	0.18	0

7.3.3 DLS measurements

Measurement and calculations were performed by Dr. Sara Bekhradnia, Professor Bo Örjan Gunnar Nyströms research group, Department of Chemistry, UiO. The calculated hydrodynamic radius and diameter (with average and standard deviations, nm) presented in **Figure 30**, is shown in **Table 14** and **Table 15**.

Table 13: Measurement and calculation of the hydrodynamic radius (fast)- and diameter in nm, with average, standard deviation and β -value. With samples isolated with the isolation kit and UC, from MCF-7 and MDA-MB-231 cell lines.

Sample	Replicate number	Hydrodynamic radius (fast) nm	Hydrodynamic diameter (fast) nm	Average, nm	Standard deviation, nm	β -value
MCF-7 (isolation kit)	Replicate 1	13.8	27.6	32.5	6.9	0.97
	Replicate 2	18.7	37.4			0.96
MDA-MB-231 (isolation kit)	Replicate 1	13.5	27.0	27.4	0.6	0.94
	Replicate 2	13.9	27.8			0.93
MCF-7 (UC)	Replicate 1	58.5	117.0	148.5	29.3	0.80
	Replicate 2	76.8	153.6			0.81
	Replicate 3	87.5	175.0			0.74
MDA-MB-231 (UC)	Replicate 1	64.1	128.2	137.6	25.3	0.78
	Replicate 2	59.2	118.4			0.78
	Replicate 3	83.1	166.3			0.87
Blank (UC)	Replicate 1	It was not possible to calculate the size				
Blank (Isolation kit)	Replicate 1	33.7	67.3	67.3		

Table 14: Measurement and calculation of the hydrodynamic radius (slow)- and diameter in nm, with average, standard deviation and β -value. With samples isolated with the isolation kit and UC, from MCF-7 and MDA-MB-231 cell lines.

Sample	Replicate number	Hydrodynamic radius (slow) nm	Hydrodynamic diameter (slow) nm	Average, nm	Standard deviation, nm	β -value
MCF-7 (isolation kit)	Replicate 1	48.1	96.2	103.2	9.9	0.89
	Replicate 2	55.1	110.2			0.91
MDA-MB-231 (isolation kit)	Replicate 1	52.1	104.2	95.2	12.7	0.90
	Replicate 2	43.1	86.2			0.91

7.4 WB

7.4.1 WB-raw files

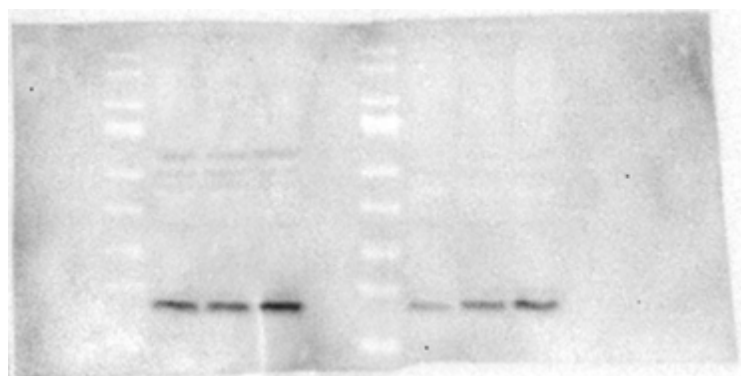


Figure 56: Raw files from the WB of cell lysates (n=3) from MCF-7 (left) and MDA-MB-231 (right) cell lysates, with anti-CD9 (**Figure 35**).

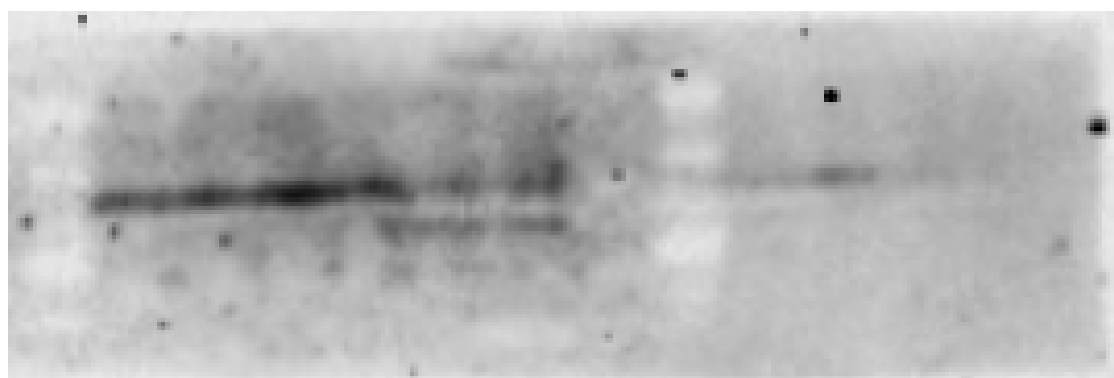


Figure 57: Raw files from the WB with anti-CD81 of cell lysates (n=3) from MCF-7 and MDA-MB-231 cell lysates (left) (**Figure 31**), with exosome isolates from MCF-7 (UC) (n=1) and MDA-MB-231 (UC) (n=2) (**Figure 32**).

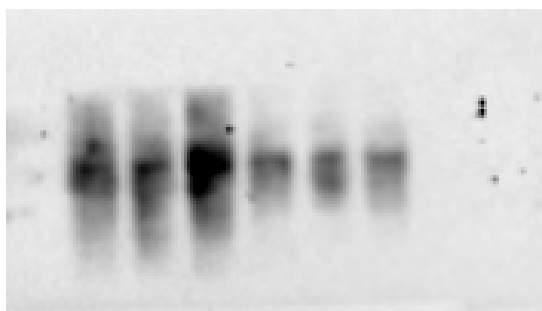


Figure 58: Raw files from the WB of cell lysates (n=3) from MCF-7 (left) and MDA-MB-231 (right) cell lysates, with anti-CD63 (**Figure 31**).

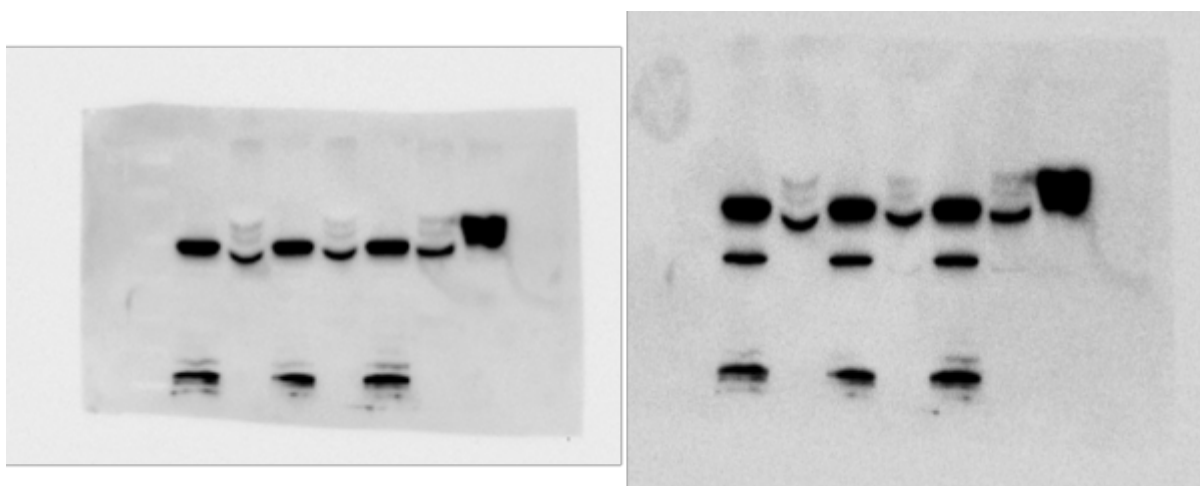


Figure 59: Raw files from the WB of cells and exosomes from the cell line MCF-7. Lane number seven from the left is the blank sample. Antibodies used are anti-TSG101 (left) and anti-GAPDH (right), and they are found in **Figure 31** and **Figure 32**.

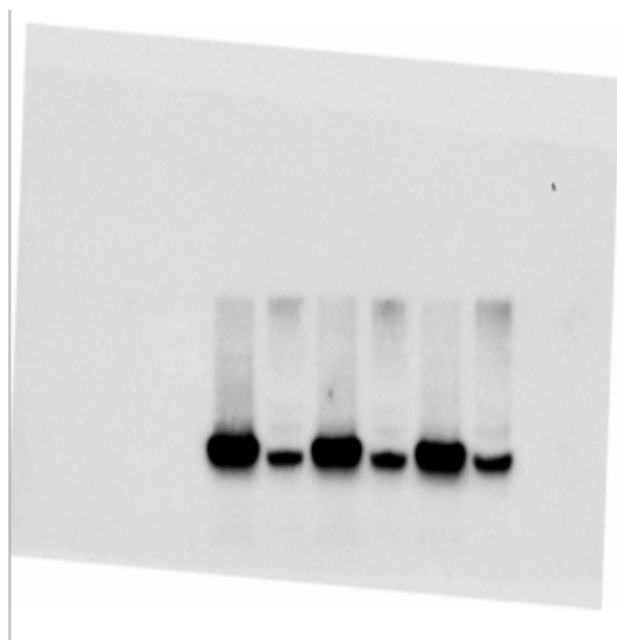


Figure 60: Raw files from the WB of cells(n=3) and exosomes (n=3) from the cell line MDA-MB-231. The antibody used is anti-TSG101, and they are found in **Figure 31** and **Figure 32**.

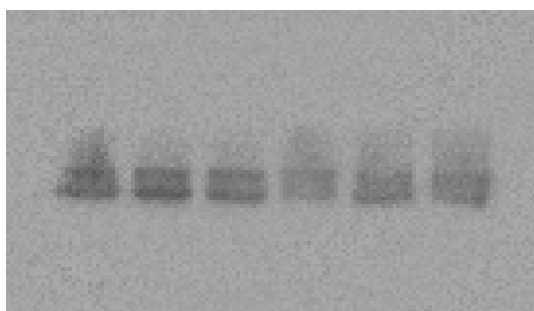


Figure 61: Raw files from the WB of cells from the cell lines MCF-7 (n=3) and MDA-MB-231 (n=3). The antibody used is anti-flotillin-1, and they are found in **Figure 31**.

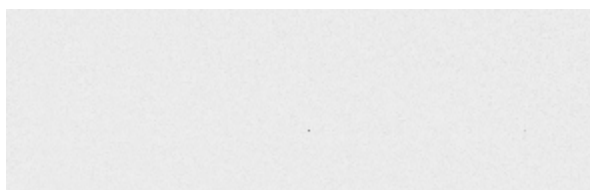


Figure 62: Raw files from the WB of cells from the cell lines MCF-7 (n=3) and MDA-MB-231 (n=3). The antibody used is anti-ALIX, and they are found in **Figure 31**.



Figure 63: Raw files from the WB of cells from the cell lines MCF-7 (n=3) and MDA-MB-231 (n=3). The antibody used is anti-calnexin, and they are found in **Figure 31**.

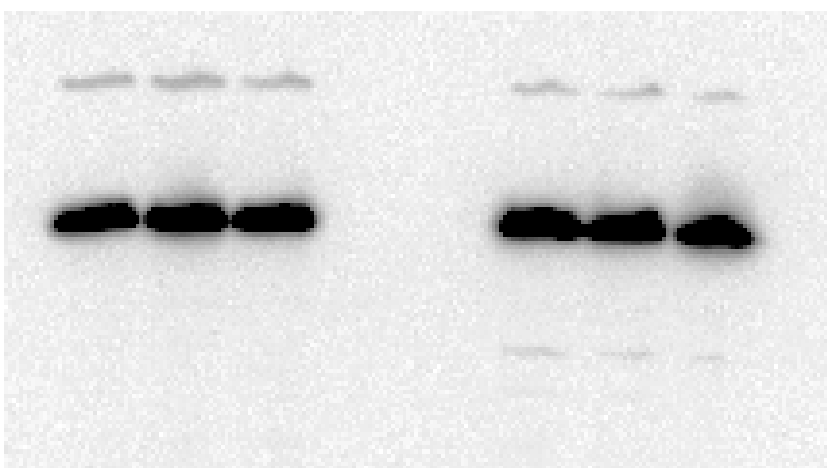


Figure 64: Raw files from the WB of cells from the cell lines MCF-7 (n=3) and MDA-MB-231 (n=3). The antibody used is anti-actin, and they are found in **Figure 31**.

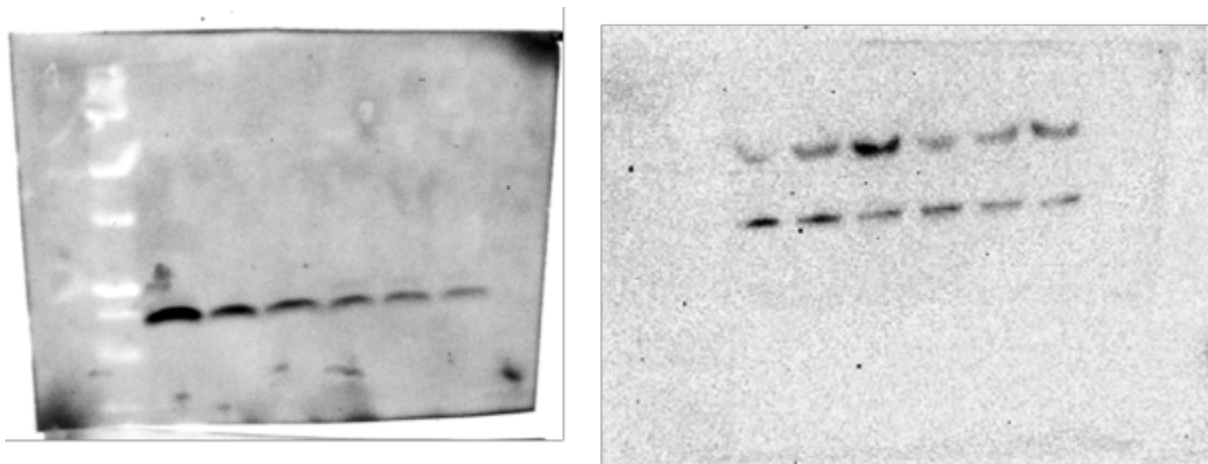


Figure 65: Raw files from the WB of samples isolated with isolation kit, from both cell line MCF-7 (n=3) and MDA-MB-231 (n=3). Antibodies used are anti-CD9 (left) and anti-actin (right), and they are found in **Figure 32**.

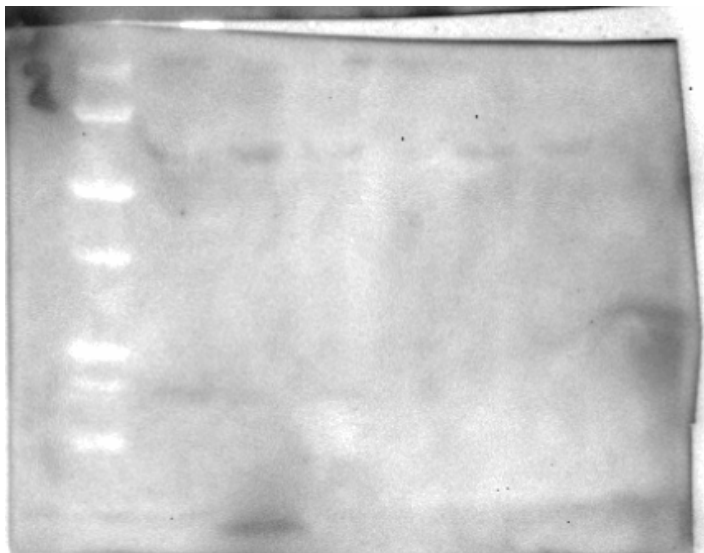


Figure 66: Raw files from the WB of MCF-7 and MDA-MB-231 isolated samples with isolation kit (n=3), with the antibody anti-CD81, **Figure 32**.

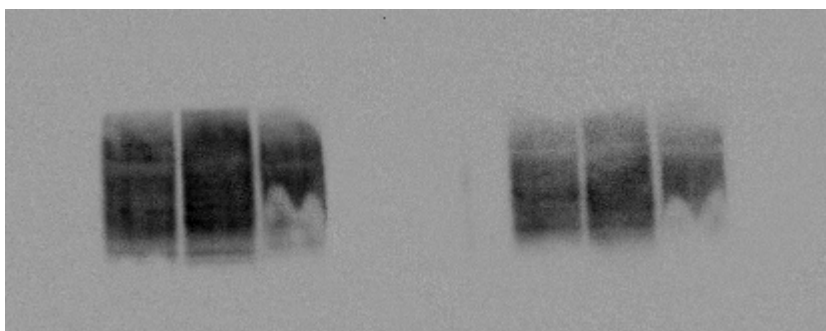


Figure 67: Raw files from the WB of MCF-7 and MDA-MB-231 isolated samples with isolation kit (n=3), with the antibody anti-CD63, **Figure 32**.

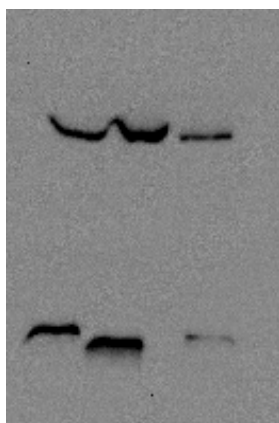


Figure 68: Raw files from the WB of MCF-7 (top) and MDA-MB-231 (bottom) isolated samples with isolation kit (n=3), with the antibody anti-flotillin-1, **Figure 32.**



Figure 69: Raw files from the WB of MCF-7 (left) and MDA-MB-231 (right) isolated samples with isolation kit (n=3), with the antibody anti-ALIX, **Figure 32.**

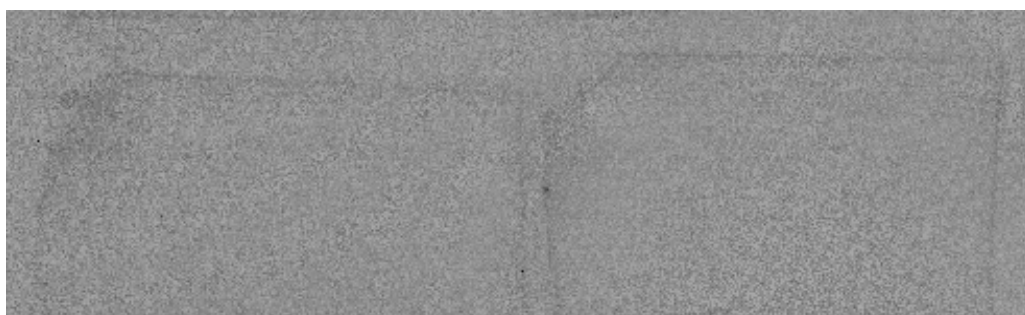


Figure 70: Raw files from the WB of MCF-7 (left) and MDA-MB-231 (right) isolated samples with isolation kit (n=3), with the antibody anti-calnexin, **Figure 32.**

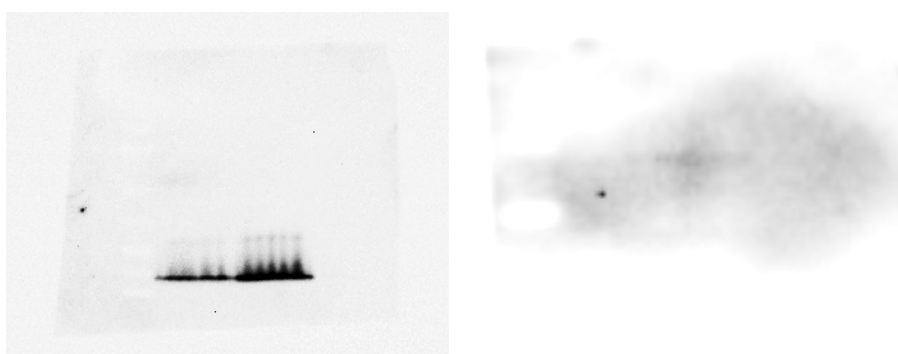


Figure 71: Raw files from the WB of MCF-7 (two replicates at the left side, and one on the right side) and MDA-MB-231 (two replicates on the right side) isolated samples with UC, with the antibody anti-CD9, **Figure 32.**

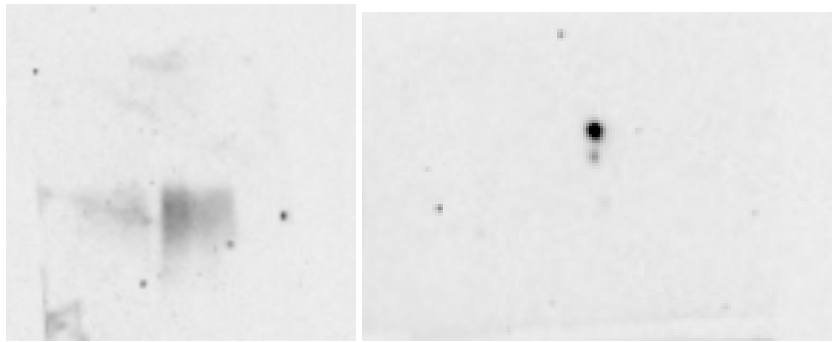


Figure 72: Raw files from the WB of MCF-7 (two replicates at the left side, and one on the right side) and MDA-MB-231 (two replicates on the right side) isolated samples with UC, with the antibody anti-CD63, **Figure 32.**

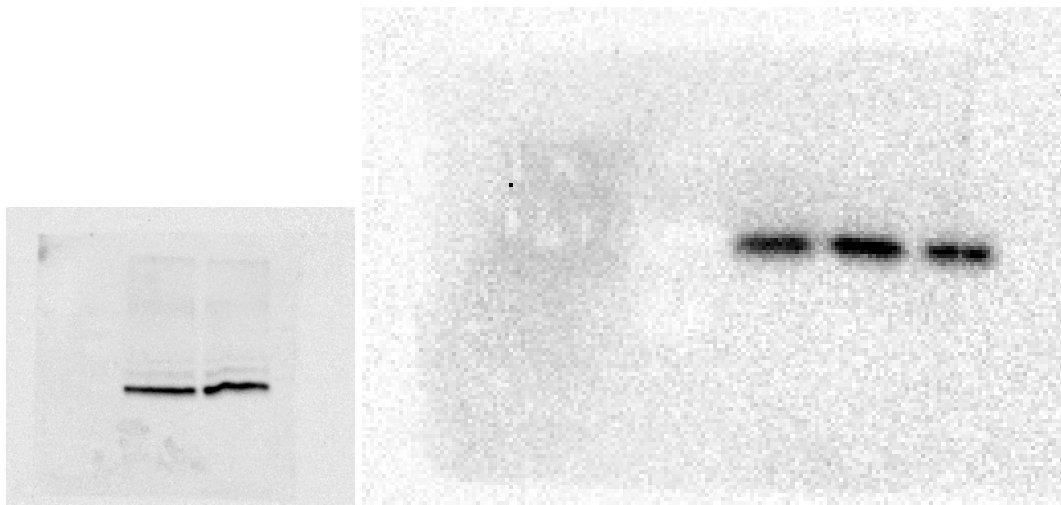


Figure 73: Raw files from the WB of MCF-7 (two replicates at the left side, and one on the right side) and MDA-MB-231 (two replicates on the right side) isolated samples with UC, with the antibody anti-TSG101, **Figure 32.**

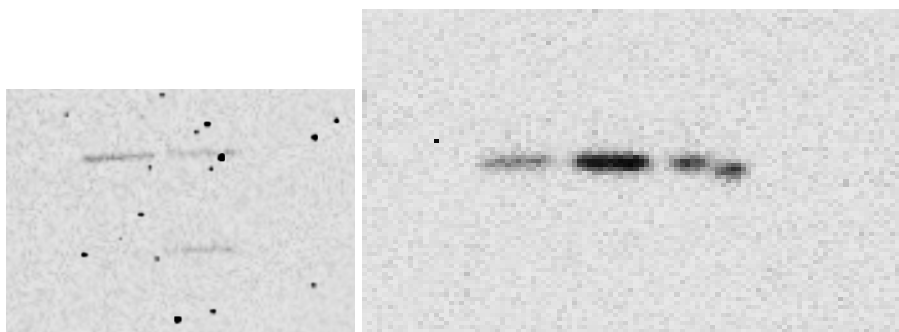


Figure 74: Raw files from the WB of MCF-7 (two replicates at the left side, and one on the right side) and MDA-MB-231 (two replicates on the right side) isolated samples with UC, with the antibody anti-flotillin-1, **Figure 32.**

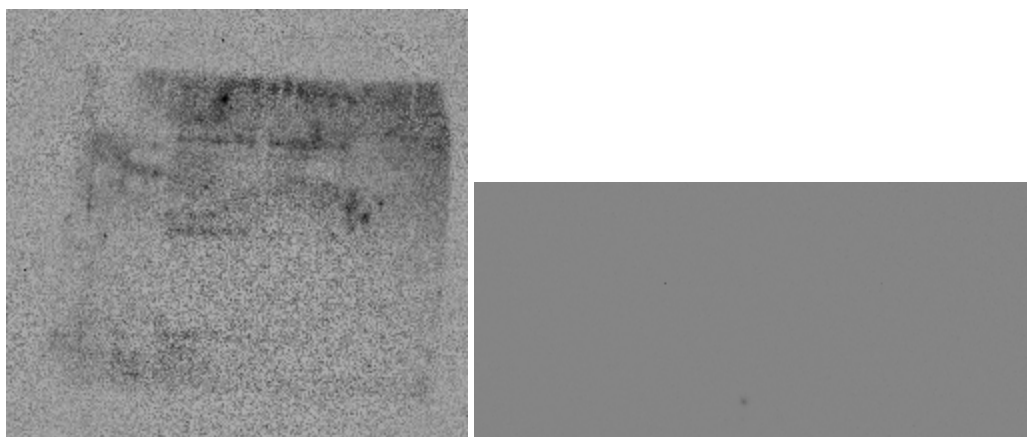


Figure 75: Raw files from the WB of MCF-7 (two replicates at the left side, and one on the right side) and MDA-MB-231 (two replicates on the right side) isolated samples with UC, with the antibody anti-ALIX, **Figure 32.**

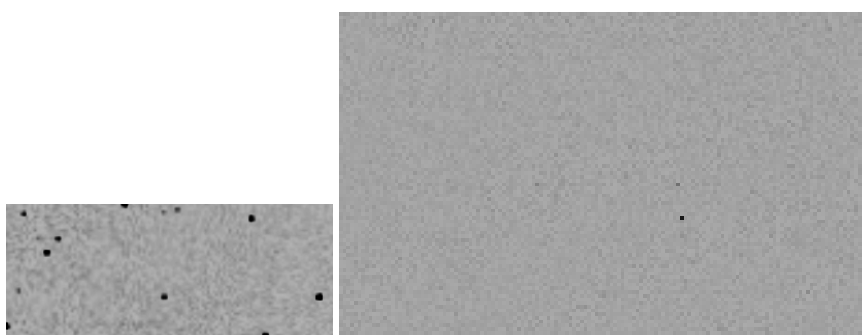


Figure 76: Raw files from the WB of MCF-7 (two replicates at the left side, and one on the right side) and MDA-MB-231 (two replicates on the right side) isolated samples with UC, with the antibody anti-calnexin, **Figure 32.**



Figure 77: Raw files from the WB of MCF-7 (two replicates at the left side, and one on the right side) and MDA-MB-231 (two replicates on the right side) isolated samples with UC, with the antibody anti-GAPDH, **Figure 32.**

7.4.2 TEM raw files

The raw files from WB with anti-CD9 rabbit and mouse seen in **Figure 46**, with raw files shown in **Figure 71**.

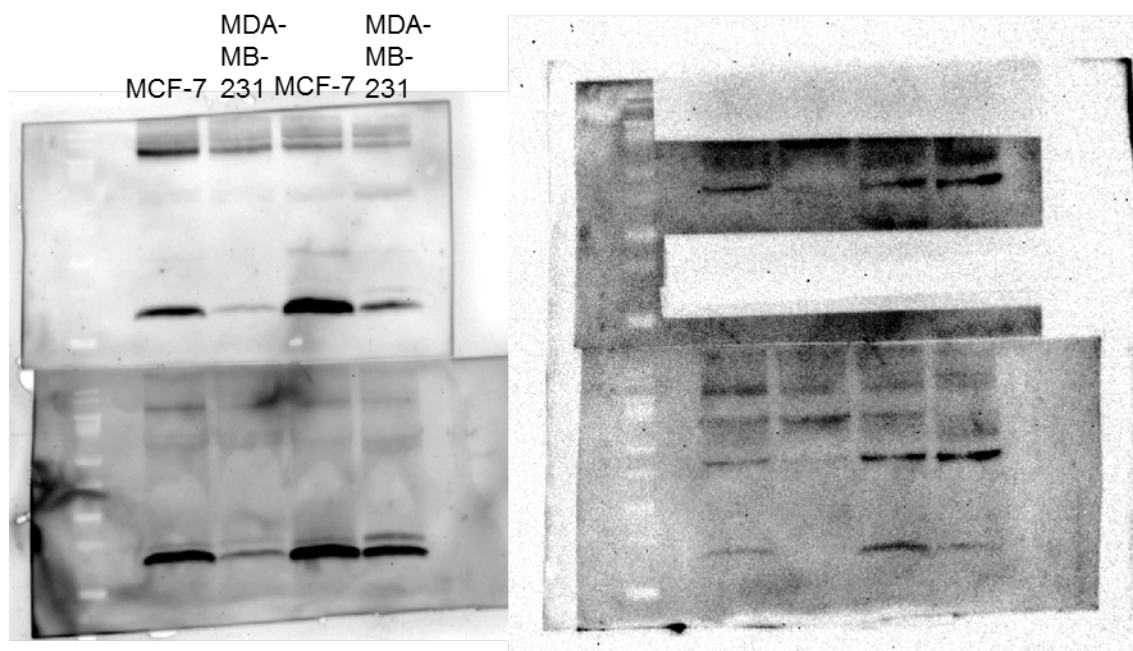


Figure 78: Raw files from the WB of isolated lysates from both cell line MCF-7 and MDA-MB-231. Antibodies used are mouse anti-CD9 (upper left), rabbit anti-CD9 (lower left) with actin (right).

7.5 LC-MS raw files

Table 15: Measured protein concentration (μg) of isolated samples by UC and isolation kit from MCF-7 and MDA-MB-231 cell cultured media.

	Protein concentration, UC (μg)	Protein concentration, isolation kit (μg)
MCF-7	8.3	43.9
MDA-MB-231	14.0	46.9

Table 16: Table of positive -and negative protein exosome markers (coloured gray) with cellular location and accession numbers were identified with coverage (%) of the protein sequence and the sum of peptides identified (including number of unique peptides) with the isolation kit and UC of MCF-7 isolated samples. Proteins identified both in-solution and in-gel were pooled and categorized into different cell types and isolation methods.

Protein name/group	Accession	Isolation kit		UC	
		Coverage (%)	Sum peptides (unique)	Coverage (%)	Sum peptides (unique)
CD9	P21926	21.05	5 (5)	18,42	4 (4)
CD81	P60033	28,39	4 (4)	9,75	1 (1)
CD63	P08962	2,52	1 (1)	-	-
Lactadherin	Q08431	-	-	8,01	2 (2)
Thrombospondin 1	P07996	32,48	31 (31)	13,08	11 (11)
Annexin A2	P07355	63,42		34,81	11 (11)
TSG101	Q99816	-	19 (19)	11.03	3 (3)
Syntenin-1	O00560	25,50	-	35,91	6 (6)
ALIX	Q8WUM4	1.96	3 (3)	19,47	13 (13)
Flotillin-1	O75955	-	-	-	-
Calnexin	P27824	-	-	-4,05	2 (2)
Serine/threonine-protein kinase 26	Q9P289	-	-	-	-
Cytochrome c 1	P08574	-	-	-	-

Table 17: Table of positive- and negative protein exosome markers (coloured gray) with cellular location and accession numbers were identified with coverage (%) of the protein sequence and the sum of peptides identified (including number of unique peptides) with the isolation kit and UC of MDA-MB-231 isolated samples. Proteins identified both in-solution and in-gel were pooled and categorized into different cell types and isolation methods.

Protein name/group	Accession	Isolation kit		UC	
		Coverage (%)	Sum peptides (unique)	Coverage (%)	Sum peptides (unique)
CD9	P21926	18.42	4 (4)	18.42	4 (4)
CD81	P60033	-	-	21.61	3 (3)
CD63	P08962	-	-	17.65	3 (3)
Lactadherin	Q08431	27.91	7 (7)	29.46	7 (7)
Thrombospondin 1	P07996	45.38	53 (53)	4.79	3 (1)
Annexin A2	P07355	74.63	29 (29)	61.65	22 (22)
TSG101	Q99816	-	-	8.72	3 (3)
Syntenin-1	O00560	22.48	3 (3)	45.97	7 (7)
ALIX	Q8WUM4	1.96	1 (1)	16.24	10 (10)
Flotillin-1	O75955	-	-	7.26	2 (2)
Calnexin	P27824	-	-	-	-
Serine/threonine-protein kinase 26	Q9P289	-	-	-	-
Cytochrome c 1	P08574	-	-	-	-

7.5.1 Protein identification

The proteins identified can be viewed with the QR code in **Figure 79** or by using the link; <https://figshare.com/s/36b184ee8756fd0f66b0>



Figure 79: QR code for identified proteins.

7.5.2 GO annotation of proteins

The proteins GO annotated to cellular locations can be viewed with the QR code in **Figure 80**, or by using the link; <https://figshare.com/s/bdc43a301c4437670d52>



Figure 80: QR code for the proteins GO annotated to cellular locations.